

# Suitability of a Commercial Software Defined Radio System for Passive Coherent Location

Aadil Volkwin

A dissertation submitted to the Department of Electrical Engineering,  
University of Cape Town,  
in fulfilment of the requirements for the degree of  
Master of Science in Engineering.

Cape Town, May 2008

*Dedicated to:  
My Parents,  
my Sister and my Wife.*

# Declaration

I declare that this work done is my own, unaided work. This dissertation is being submitted to the Department of Electrical Engineering, University of Cape Town, in fulfilment of the requirements for the degree of Master of Science in Engineering. It has not been submitted for any degree or examination in any other university.

.....  
Signature of Author

Cape Town

2008

# Abstract

This dissertation provides a comprehensive discussion around bistatic radar with specific reference to PCL, highlighting existing literature and work, examining the various performance metrics. In particular the performance of commercial FM radio broadcasts as the radar waveform is examined by implementation of the ambiguity function.

The FM signals show desirable characteristics in the context of our application, the average range resolution obtained is 5.98km, with range and doppler peak sidelobe levels measured at -25.98dB and -33.14dB respectively.

Furthermore, the SDR paradigm and technology is examined, with discussion around the design considerations. The USRP, the TVRx daughterboard and GNURadio are examined further as a potential receiver and development environment, in this light.

The system meets the low cost ambitions costing just over US\$1000.00 for the USRP motherboard and a single daughterboard. Furthermore it performs well, displaying desirable characteristics, The receiver's frontend provides a bandwidth of 6MHz and a tunable range between 50MHz and 800MHz, with a tuning step size as low as 31.25kHz. The noise characterisation of the receiver reveals a NF of 10dB, a sensitivity of -105dB and a dynamic range of 62dB.

Finally, the investigation into the stability of the daughterboard frontend oscillators due to ageing effects is shown to be steady with acceptable levels of variation, showing a fractional frequency variation from 2.3 to 0.8 parts per 10 million and a maximum frequency drift of 4Hz.

# Acknowledgements

All praises and thanks to the almighty for all the blessings and abilities that have been afforded to me.

Further gratitude is expressed to:

My supervisor, Prof. M.R. Inggs for his advice, support and encouragement.

Dr. Yoann Paichard, for invaluable technical advice in developing and interpreting various aspects of the research.

To the RRSg, in particular Regine Lord for administrative support, Lance Williams, Jonathan Ward and Gunther Lange for various hardware assistance.

To members of the GNURadio mailing list, in particular Matt Ettus and Firas Abbas.

Finally, to my family and friends for their encouragement, support and patience .

# Contents

Declaration.....	3
Abstract.....	4
Acknowledgements.....	5
Contents.....	6
List of Figures.....	8
List of Tables.....	10
Nomenclature.....	11
Chapter 1.....	13
Introduction.....	13
1.1 Background.....	13
1.2 Plan of Development.....	14
Chapter 2.....	20
Passive Coherent Location.....	20
2.1 System level description of PCL.....	20
2.2 Advantages and Disadvantages of PCL Systems.....	25
2.3 History and Examples of PCL Systems.....	26
2.4 Applications of PCL.....	28
2.5 Typical Illuminators.....	28
2.6 Relevant Equations .....	30
2.7 Summary .....	40
Chapter 3.....	41
USRP and GNURadio.....	41
3.1 Introduction .....	41
3.2 Software Defined Radio .....	41
3.3 Anatomy of a SDR Receiver.....	43
3.4 Universal Software Radio Peripheral.....	44
3.5 GNURadio.....	52
3.6 Summary.....	55
Chapter 4.....	57
Receiver Characterisation.....	57
4.1 Introduction .....	57
4.2 Test System Overview .....	57
4.3 Receiver Bandwidth.....	58
4.4 Gain Range and Control.....	59
4.5 Multiplexer Usage and Data Interleaving.....	61
4.6 Frequency Range and Control.....	62
4.7 Spurious Artifact .....	63
4.8 Receiver Noise Figure .....	64
4.9 Sensitivity.....	66
4.10 Dynamic Range, Minimum Detectable Signal and Gain Compression.....	67
4.11 Summary.....	71

Chapter 5.....	73
Ambiguity Plot Analysis.....	73
5.1 Introduction .....	73
5.2 System Overview.....	73
5.3 Algorithm Concept.....	75
5.4 Results.....	76
5.5 Summary.....	82
Chapter 6.....	84
Oscillator Stability.....	84
6.1 Introduction .....	84
6.2 Quartz Crystal Oscillators .....	85
6.3 Characterisation of stability .....	86
6.4 System Overview .....	92
6.5 Results .....	94
6.6 Summary.....	95
Chapter 7.....	96
Conclusions and Recommendations.....	96
Bibliography .....	98
Appendix A .....	100
Ambiguity Analysis and Results.....	100
Appendix B .....	116
Datasheet and Sentech Table.....	116

# List of Figures

Figure 1.1: PCL block diagram.....	15
Figure 1.2: Software Radio block diagram.....	15
Figure 1.3: Experimental setup of the USRP for the characterisation tests.....	16
Figure 1.4: USRP with two TVRx boards, reference channel and target channel.....	18
Figure 2.1: PCL system diagram.....	22
Figure 2.2: Variation of RCS and angular width of a forward scatter target against frequency...	32
Figure 2.3: A target echo detected after the transmission of the second pulse results in ambiguous ranges at B and C.....	36
Figure 3.1: USRP and daughterboard block diagram.....	45
Figure 3.2: USRP and daughterboards.....	46
Figure 3.3: AD9862 ADC block Diagram.....	47
Figure 3.4: USRP and FPGA block Diagram.....	48
Figure 3.5: DDC block Diagram.....	49
Figure 3.6: USRP transmit chain block Diagram.....	50
Figure 3.7: Signal flow from a single TVRx daughterboard to DDC0.....	51
Figure 3.8: GNURadio application structure.....	53
Figure 4.1: Experimental setup used in characterisation tests.....	58
Figure 4.2: Block diagram showing TVRx gain stages.....	59
Figure 4.3: Variation of voltage applied to RF AGC against RF Gain.....	60
Figure 4.4: Variation of voltage applied to IF AGC against IF Gain.....	60
Figure 4.5: multiplexer setup for two TVRx to DDC0 and DDC1.....	61
Figure 4.6: Spurious signal generated by USRP on startup.....	63
Figure 4.7: closer look at the spurious signal generated by USRP on startup.....	64
Figure 4.8: Cascaded components.....	65
Figure 4.9: Variation of receiver sensitivity.....	67
Figure 4.10: MDS, 1 dB compression point and dynamic range.....	68
Figure 4.11: Spurious Free Dynamic Range.....	69
Figure 4.12: Input power against output power, showing receiver dynamic range.....	70
Figure 4.13: TVRx and ADC dynamic range comparison.....	71
Figure 5.1: Experiment setup to capture signals for ambiguity function analysis.....	74
Figure 5.2: Block Diagram of experimental setup.....	74
Figure 5.3: Signal processing algorithm.....	75
Figure 5.4: Ambiguity plot of Rad5 transmission.....	77
Figure 5.4a: Zero doppler cut through ambiguity plot.....	77
Figure 5.4b: Zero delay cut through ambiguity plot.....	78
Figure 5.5a: Variation of signal range resolution with time.....	81
Figure 5.5b: Variation of signal range resolution with time.....	82
Figure 6.1: Determining the fractional frequency.....	88
Figure 6.2: Dependence of stability measurement on time window.....	89

Figure 6.3: measurement process.....	91
Figure 6.4: Block diagram of experimental setup.....	92
Figure 6.5: Experiment setup for stability tests.....	93
Figure 6.6: Fractional frequency variation of the daughterboards.....	94
Figure 6.7: Allan Variance of the fractional frequencies.....	95
Figure A.1: Ambiguity plot of Radio 2000 transmission.....	100
Figure A.1 a: Zero doppler cut through ambiguity plot.....	101
Figure A.1 b: Zero delay cut through ambiguity plot.....	101
Figure A.2: Ambiguity plot of Classic FM transmission.....	103
Figure A.2a: Zero doppler cut through ambiguity plot.....	103
Figure A.2b: Zero delay cut through ambiguity plot.....	104
Figure A.3: Ambiguity plot of UmhloboFM transmission.....	105
Figure A.3a: Zero doppler cut through ambiguity plot.....	106
Figure A.3b: Zero delay cut through ambiguity plot.....	106
Figure A.4: Ambiguity plot for RGHP transmission.....	108
Figure A.4a: Zero doppler cut through ambiguity plot.....	108
Figure A.4b: Zero delay cut through ambiguity plot.....	109
Figure A.5: Ambiguity plot of RSGR transmission.....	110
Figure A.5a: Zero doppler cut through ambiguity plot.....	111
Figure A.5b: Zero delay cut through ambiguity plot.....	111
Figure A.6: Ambiguity plot of SAFM transmission.....	113
Figure A.6a: Zero doppler cut through ambiguity plot.....	114
Figure A.6b: Zero delay cut through ambiguity plot.....	114

# List of Tables

Table 5.1: Bandwidth Variation of RAD5 waveform.....	78
Table 5.2: Summary of waveform ambiguity function performances.....	83
Table A.1: Bandwidth variation of Radio 2000 waveform.....	102
Table A.2: Bandwidth variation of Classic FM waveform.....	104
Table A.3: Bandwidth variation of Umhlobo FM waveform.....	107
Table A.4: Bandwidth variation of RGHP waveform.....	109
Table A.5: Bandwidth variation of RSFR waveform.....	112
Table A.6: Bandwidth variation of SAFM waveform.....	115

# Nomenclature

<b>AGC</b>	<b>Automatic Gain Control</b>
<b>ADBF</b>	<b>Adaptive Beamformer</b>
<b>CFAR</b>	<b>Constant False Alarm Rate</b>
<b>CIC</b>	<b>Cascaded Integrator Comb Filter</b>
<b>CW</b>	<b>Continuous Wave</b>
<b>DBS</b>	<b>Direct Broadcast by Satellite</b>
<b>DDC</b>	<b>Digital Down Converter</b>
<b>DOA</b>	<b>Direction Of Arrival</b>
<b>DPI</b>	<b>Direct Path Interference</b>
<b>DSP</b>	<b>Digital Signal Processors</b>
<b>FPGA</b>	<b>Field Programmable Gate Arrays</b>
<b>FSF</b>	<b>Free Software Foundation</b>
<b>GNU</b>	<b>GNU Not Unix</b>
<b>GPIF</b>	<b>General Purpose Interface</b>
<b>GPS</b>	<b>Global Positioning System</b>
<b>GSM</b>	<b>Global System for Mobile</b>
<b>IP3</b>	<b>Third Order Intercept Point</b>
<b>LO</b>	<b>Local Oscillator</b>
<b>MDS</b>	<b>Minimum Detectable Signal</b>
<b>MTI</b>	<b>Moving Target Indicator</b>
<b>NCO</b>	<b>Numerically Controlled Oscillator</b>
<b>PCL</b>	<b>Passive Coherent Location radar</b>
<b>PGA</b>	<b>Programmable Gain Amplifier</b>
<b>PPM</b>	<b>Part Per Million</b>
<b>RCS</b>	<b>Radar Cross Section</b>
<b>SAR</b>	<b>Synthetic Aperture Radar</b>
<b>SDR</b>	<b>Software Defined Radio</b>
<b>SFDR</b>	<b>Spurious Free Dynamic Range</b>

**SINAD**

**Signal to Noise and Distortion ratio**

**SIR**

**Signal to Interference Ratio**

**SNR**

**Signal to Noise Ratio**

**USRP**

**Universal Software Radio Peripheral**

# Chapter 1

## Introduction

The University of Cape Town (UCT) Radar Remote Sensing Group (RRSG) is currently engaged in the research and development of an air traffic control system that utilises *passive coherent location* (PCL) radar.

Thus the purpose of this dissertation is to investigate the performance of the *Universal Software Radio Peripheral* (USRP) and the *GNU Not Unix* (GNU) *Radio* software radio development environment as a low cost PCL receiver and additionally to investigate and comment on the performance of analogue FM radio broadcast signals as the radar waveform.

### 1.1 Background

The first radar systems built were bistatic in nature, with transmitter and receiver in separate locations. An example of this is the *Klein Heidelberg*, developed by the Germans during the second world war, that used the British Chain Home radars as illuminators. Technological developments in the form of the duplexer in 1936 allowed the transmitter and receiver to share a common antenna and therefore the same site [34].

This provided the means for simplicity of operation as well as savings on cost and space and hence monostatic radar dominated radar research and design.

Bistatic radar does have advantages over monostatic radar, however, their disadvantages; in particular the complexity of transmitter/receiver synchronisation and antenna beam pointing had previously outweighed their advantages and hampered the advancement of bistatic radar.

Technological improvements in the shape of high speed digital signal processors (DSP), phased array antennas and the deployment of *global positioning system* (GPS) satellite navigation systems, which can be used for synchronisation, have provided the means to mitigate the complexities of bistatic radar and thus fuelling the current wave of interest in bistatic radar systems.

Interest in bistatic radar varies on a period of fifteen years, currently we are at a peak of that cycle; with particular interest in PCL techniques [35], using 'illuminators of opportunity' such as existing radar transmissions and broadcast and communication signals.

Of the illuminators of opportunity available in the environment, broadcast transmitters present themselves as the most attractive for surveillance purposes, owing to their inherent properties of high powers of transmission and widespread coverage.

If such signals are to be used on the basis of PCL, it is necessary to know their behaviour in terms of their ambiguity function [36] i.e. resolution and sidelobe levels in range and doppler, and the effect of range and doppler ambiguities.

Over the last ten years the enhancement of semiconductor technologies in performance capability and cost has led to the emergence of *Software Defined Radio* (SDR) as a mainstream technology. SDR is defined as a collection of hardware and software technologies that enable reconfigurable system architectures for wireless networks and user terminals. SDR provides an efficient and comparatively inexpensive solution to the problem of building multi-mode, multi-band, multi-functional wireless devices that can be adapted, upgraded or enhanced by using software upgrades [31].

The obvious flexibility and costs benefits offered by SDR systems provide the impetus for the choice to explore the USRP and GNURadio as a radar receiver in a bistatic PCL context.

## 1.2 Plan of Development

Chapter 1:

This chapter, which provides a brief background to the subject of the dissertation and motivation for the research pursued.

Chapter 2:

This chapter reviews the published material on PCL radar techniques to provide the background information to the techniques used within the research. This chapter begins by defining PCL radar and its uses. The discussion then evolves describing the various advantages and disadvantages for the system. Thereafter, the history of bistatic radars is discussed, ranging from the first use of these systems to modern day systems. The discussion progresses further to highlight previous work in the development of a PCL radar system and examines the characteristics that motivate the choice of commercial FM radio broadcasts as a potential radar waveform. Various applications of PCL radars were described, both for military uses as well as non military uses. These applications were presented to show how bistatic radars have been of use to society. Some of the enhanced techniques of bistatic and PCL systems are also discussed with regards to the performance of these systems. The literature reviewed provides the necessary background understanding and sets up the context in which this research finds purpose.

The following image depicts the geometrical setup of a PCL system.

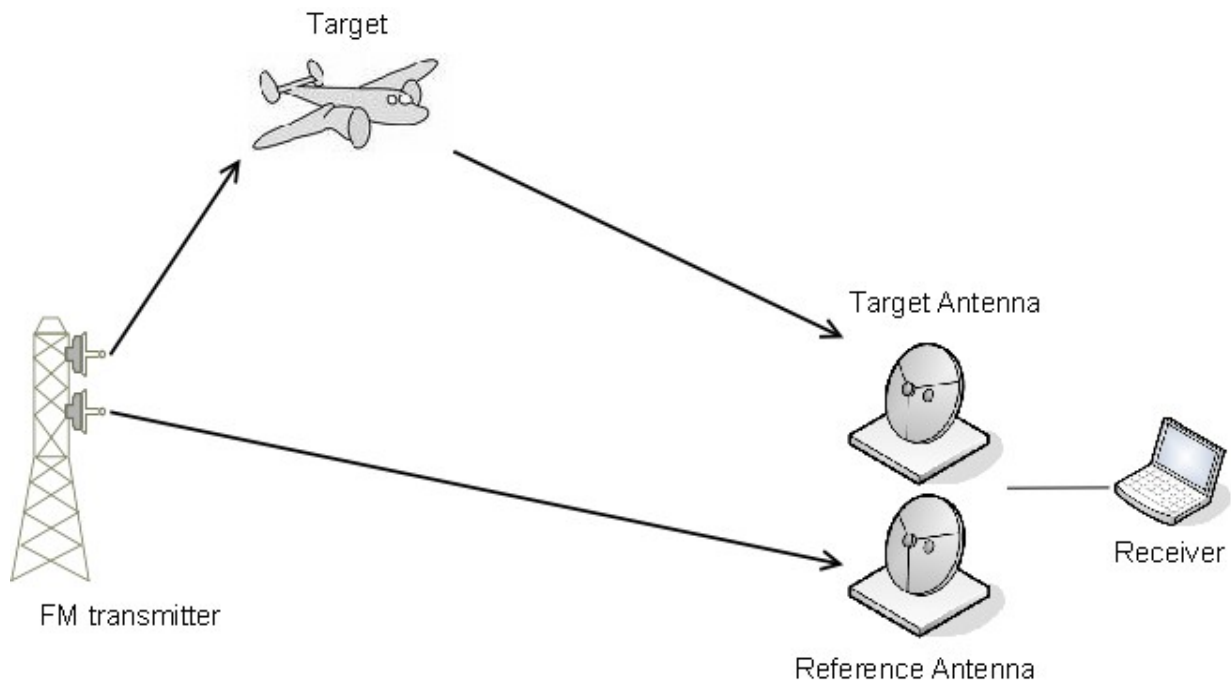


Figure 1.1: PCL block diagram

### Chapter 3:

Software radio is a system which turns radio hardware problems into software problems. The fundamental characteristic of software radio is that software defines the transmitted waveforms and software demodulates the received waveforms. Thus a software radio can tune to any frequency band and receive any modulation across a large frequency spectrum. A block diagram of the basic SDR structure is shown below.

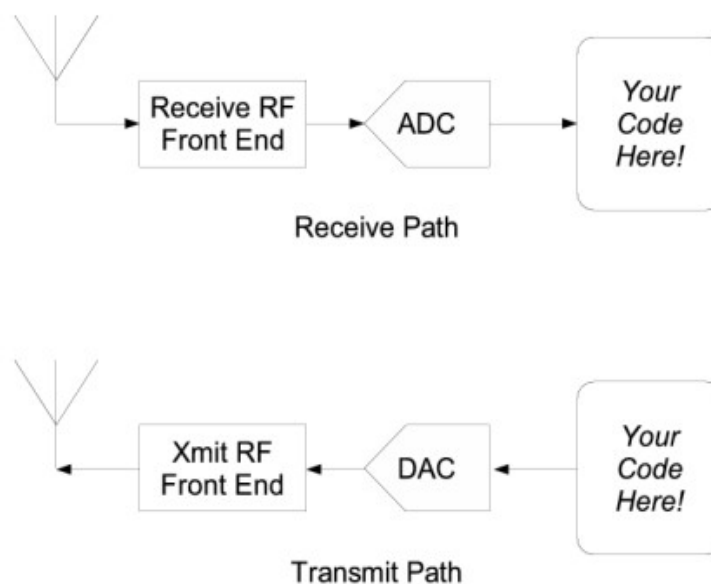


Figure 1.2: Software Radio block diagram

Additionally, performing a significant amount of the signal processing on reprogrammable hardware permits the radios to receive and transmit a new form of radio protocol simply by running an alternative configuration of the hardware. This is unlike most radios in which the processing is done with either analogue circuitry alone or combined with digital chips.

The chapter explores the USRP and GNURadio as development tools of this technology, in the light of this. Through this it is found that the USRP provides a flexible and powerful FPGA, the Altera cyclone, as the processing unit, which implements a great deal of the signal processing in the receive and transmit chains. Furthermore, the USRP hosts two Analog Devices AD9862 chips, each providing a two ADCs sampling at a rate of 64 Msamples/second with 12 bits of resolution and two DACs operating at 128 Msamples/second with 14 bits of resolution. Moreover, the AD9862 chips provide two auxiliary ADCs and three auxiliary DACs which can provide further flexibility in computation and control of external daughterboard components. These daughterboards provide front end flexibility allowing for the down-conversion and thus manipulation of the radio spectrum.

GNURadio is seen to be a powerful toolkit that implements numerous complex signal processing elements and additionally interfaces with the USRP. Thus, GNURadio and the USRP combine to provide a powerful and widely versatile toolset for the development of a variety of radio devices.

#### Chapter 4:

Often the most critical component of a wireless system is its receiver, the purpose of which is to extract, reliably, the desired signal from the various sources of signals, interference and noise. This chapter presents the results of experiments that examine and characterise the performance of the USRP, TVRx daughterboard, which is a complete VHF and UHF receiver system based on a TV tuner module and GNURadio as a PCL receiver.

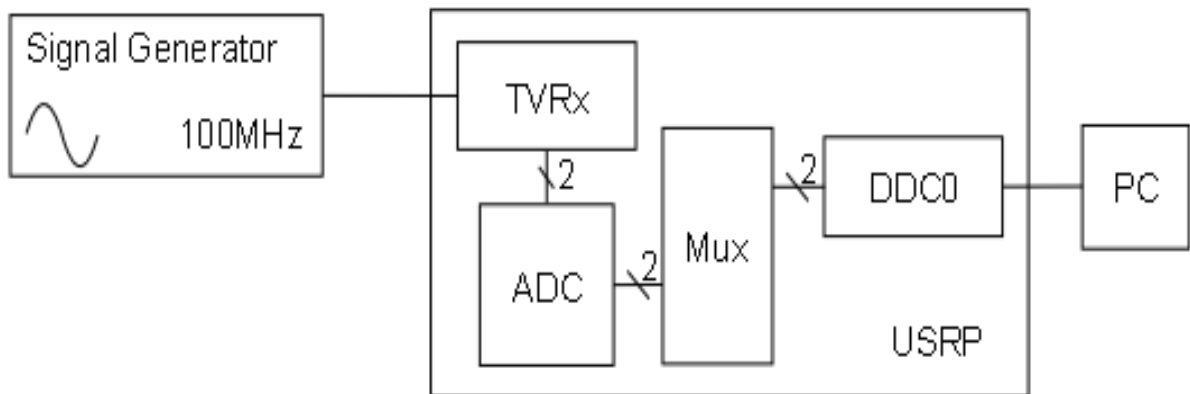


Figure 1.3: Experimental setup of the USRP for the characterisation tests

A number of the TVRx and USRP receiver system parameters as well as the GNURadio interface to the controllable aspects are examined. The receiver's frontend provides a bandwidth of 6MHz, which far exceeds the performance requirements of our application. and a tunable range between 50MHz and 800MHz, with a tuning step size as low as 31.25kHz. This is sufficient for the manipulation of FM Broadcast signals as the radar waveform and provides further functionality and versatility to incorporate additional areas of the frequency spectrum if desired, i.e. the television video and sound carriers.

The multiplexer implemented in the FPGA and the ability to directly control its operation through GNURadio further extends the receiver's flexibility in its digital manipulation of signals through it. The noise characterisation of the receiver reveals a NF of 10dB, a sensitivity of -105dB and a dynamic range of 62dB. Furthermore, it is observed that when the GNURadio application is started, when the USRP is setup as a source and includes the occasion when the application is stopped and restarted, a spurious spike occurs at the beginning of the data set. This phenomenon is unexplained but noted by the USRP developers. The effects of this are mitigated by simply cutting out that part of the data set.

Thus the USRP with the TVRx and GNURadio show performance characteristics suitable for our application.

## Chapter 5:

This chapter presents the measurements of the ambiguity functions of off-air signals that will be considered for the PCL system and comments on their form and usefulness by demonstrating the waveform variability and its effect on range and doppler resolution in addition to detection performance.

From the results it is evident that the measured FM Broadcast signals due to the randomness in their modulation, exhibit noise like characteristics and behaviour. This is observed as the ambiguity function plots can be approximated by the ideal thumbtack ambiguity function, therefore providing the radar with unambiguous range and doppler information. However, it is additionally clear that the ambiguity function depends largely on the modulating format.

Thus there is a variation in performance between the pop music and dance music channels and the rock and classical music channels which exhibit a slightly degraded performance. Speech content shows the poorest performance though, as the performance does vary significantly with time, especially during pauses in words due to the low spectral content. This variation in performance does have a significant impact on the radar's potential detection ability and will be one that does vary with time, as seen from Equation 2.6 and Table A.6, this variation translates to a change in processing gain of 15dB.

Table 5.2 summarises the ambiguity function performance of the measured signals.

Table 5.2: Summary of waveform ambiguity function performances

Signal	Range Resolution (km)	Effective Bandwidth (kHz)	Peak range Sidelobe level (dB)	Peak doppler Sidelobe level (dB)
RAD5	3.38	44.3	- 30	- 27
Radio 2000	7.94	18.9	- 18	- 34
Classic FM	7.98	18.8	- 30	- 33
Umhlobe	3.33	45.0	- 31	- 25
RGHP	2.36	63.6	- 30	- 37
RSGR	9.32	16.1	- 18	- 36
SAFM	7.54	19.9	- 20	- 40
Average	5.98	32.37	-25.29	-33.14

## Chapter 6:

A limiting factor in the performance of radar applications is the ability of the radar's frequency reference to maintain timing accuracy. Chapter 6 thus is a presentation of experimental measurements aimed at determining the stability of the local oscillators present in the TVRx frontend daughterboards of the USRP and hence the PCL receiver.



Figure 1.4: USRP with two TVRx boards, reference channel and target channel

The local oscillator in the TVRx daughterboard of the USRP is a 4MHz quartz crystal oscillator. It is for this reason that the properties of crystal oscillators and the associated performance parameters of interest were investigated. These parameters include accuracy, reproducibility and stability. It was found that crystal oscillators provide good performance at a reasonable price and dominate the field of frequency sources [19].

Furthermore, the techniques associated with the specification of stability were presented, including measurement of the frequency deviation and the Allan variance. These tests concluded that the crystal ageing effect is reduced over the measurement period of thirty minutes, showing a variation from 2.3 to 0.8 parts per 10 million. In order to qualify the results of this chapter a 5% error in the calculated doppler shift is set as the maximum acceptable limit of frequency shift. Thus a frequency drift of no greater than 5Hz is set as the requirement of the system.

## Chapter 7:

This chapter presents the conclusions and recommendations of future work.

In particular the ambiguity function is examined and the performance of commercial FM radio broadcasts as the radar waveform is determined and summarised by Table 5.2, reproduced here.

Table 5.2: Summary of waveform ambiguity function

Signal	Range Resolution (km)	Effective Bandwidth (kHz)	Peak range Sidelobe level (dB)	Peak doppler Sidelobe level (dB)
RAD5	3.38	44.3	- 30	- 27
Radio 2000	7.94	18.9	- 18	- 34
Classic FM	7.98	18.8	- 30	- 33
Umhlobe	3.33	45.0	- 31	- 25
RGHP	2.36	63.6	- 30	- 37
RSGR	9.32	16.1	- 18	- 36
SAFM	7.54	19.9	- 20	- 40
Average	5.98	32.37	-25.29	-33.14

The analysis of the FM broadcast signal ambiguity plots reveal the attractive performance of the signals as they in general tend toward the idealised thumbtack. However, this is greatly dependant upon the instantaneous modulating content, revealing highly degraded performance in the case of a signal with low spectral content such as speech with many pauses and breaks.

Furthermore, the SDR paradigm and technology is examined, with discussion around the design considerations. The USRP, the TVRx daughterboard and GNURadio are examined further as a potential receiver and development environment, in this light.

GNURadio, is found to be a powerful toolkit that implements numerous complex signal processing elements and additionally interfaces with the USRP that provides flexible and powerful computing capabilities. Thus combining to provide a powerful and widely versatile toolset for the development of a variety of radio devices.

The system meets the low cost ambitions costing just over US\$500.00 for the USRP motherboard and a single daughterboard. The receiver's frontend provides a static bandwidth of 6MHz and a tunable range between 50MHz and 800MHz. The noise characterisation of the receiver reveals a NF of 10dB, a sensitivity of -105dB and a dynamic range of 62dB.

Finally, the investigation into the stability of the daughterboard frontend oscillators due to ageing effects is shown to be steady through examination of the fractional frequency variation as well as the Allan variance, showing a fractional frequency variation from 2.3 to 0.8 parts per 10 million and a frequency drift no greater than 4Hz. This falls within the maximum allowance of 5Hz, calculated in section 6.1.

Appendix A:

Ambiguity Analysis Results.

Appendix B:

Relevant datasheets and Sentech transmission table.

Bibliography

## Chapter 2

# Passive Coherent Location

Conventional (dedicated) radar systems are comprised of a dedicated transmitter and receiver.

In a passive radar system, however, there is no dedicated transmitter. Instead the receiver uses third-party non cooperative transmitters in the environment. PCL systems are bistatic in nature and thus measure the difference in time of arrival between the signal directly from the transmitter and the signal reflected off the target. This allows the bistatic range of the object to be determined. In addition to the bistatic range, in order for the the location, direction and velocity of the target to be calculated the bistatic doppler shift of the reflected signal and its direction of arrival is determined.

Clearly, in a dedicated radar system, the the transmitter and its location are directly under the control of the radar engineer, hence timing information related to the transmission of the pulse and the form of the transmitted waveform are exactly known. This allows the target range to be easily calculated and for a matched filter to be used to achieve an optimal *signal to noise ratio* (SNR) in the receiver.

A passive radar however, does not have control over the transmitter, its location, the nature of the transmitted waveform or timing information related to the transmission and therefore must use a dedicated receiver “reference channel” to monitor each transmitter being exploited.

## 2.1 System level description of PCL

The purpose of this section is to provide the reader with insight into the workings and implementation of the overall system, without providing an overwhelming detail of theory. This will enable the reader to understand the context within which the later sections fit.

A passive radar would typically consist of the following processing steps:[33]. This is illustrated in Figure 2.1

- Reception of the direct signal from the transmitter(s) and from the surveillance region on dedicated low-noise, linear, digital receivers.
- Digital beam forming to determine the DOA of signals and spatial rejection of strong in-band interference.
- Adaptive filtering to cancel any unwanted direct signal returns in the surveillance channel(s).
- Transmitter-specific signal conditioning.
- Cross-correlation of Doppler-shifted copies of the reference channel with the surveillance channel(s) to determine target bistatic range and Doppler.
- Detection using a *constant false alarm rate* (CFAR) scheme.
- Association and tracking of object returns in range/doppler space, known as “trajectory tracking” typically employing a Kalman filter.
- Association and fusion of line tracks from each transmitter to form the final estimate of an object’s location, heading and speed.

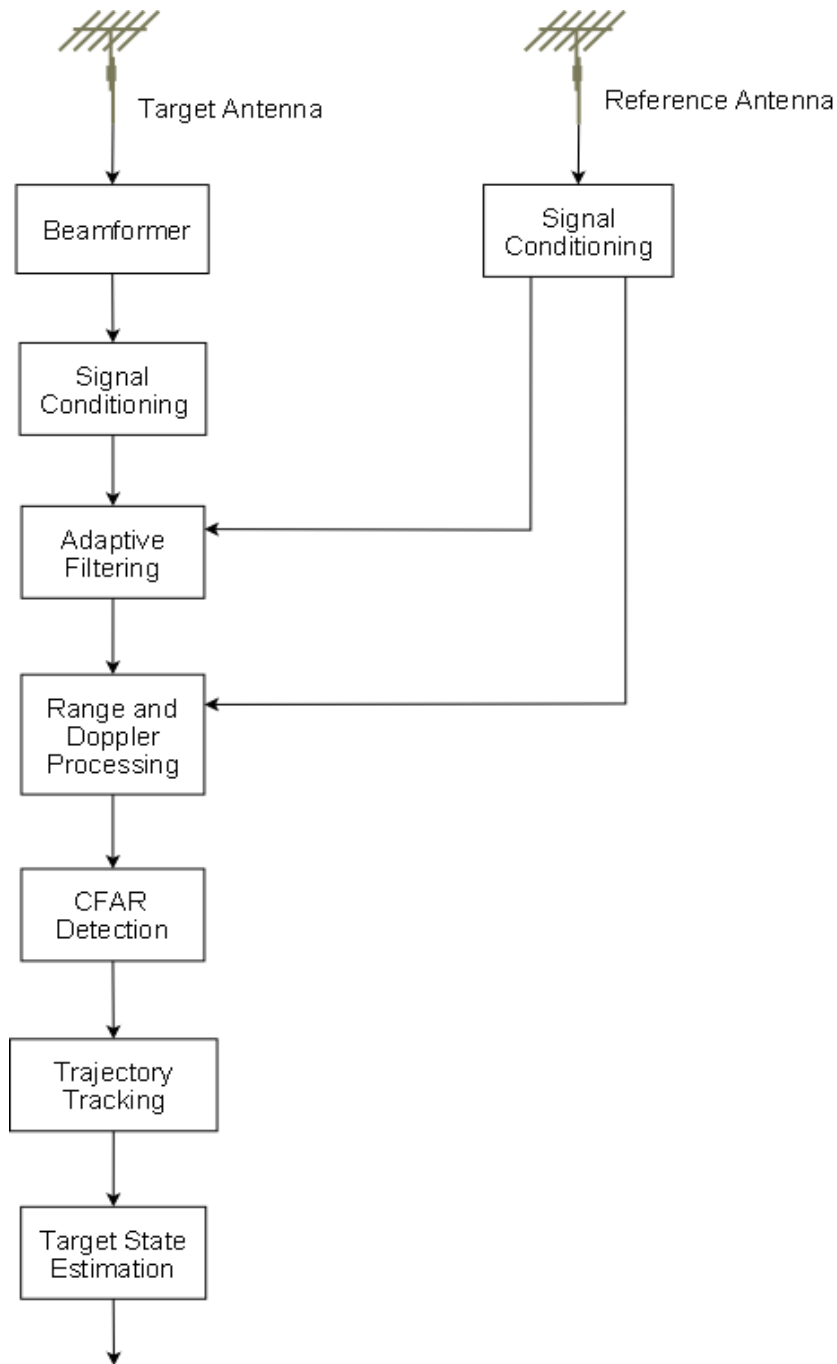


Figure 2.1: PCL system diagram [33]

### 2.1.1 Receiver system

It is essential that the PCL receiver should have a low noise figure, high dynamic range and high linearity. This is as a result of the nature of PCL systems using illuminators of opportunity with continuous wave signals, wherein they must detect very small target returns in the presence of continuous and significant interference.

In order to achieve the processing gain necessary to detect these weak target returns in a background of noise and interference it is necessary to achieve an equivalent to the optimal matched filter processing used in conventional radar systems.

Passing target echoes through a matched filter is equivalent to the correlation of the radar echo with a delayed replica of the transmitted signal which is obtained via the reference channel mentioned earlier.

The greatest source of interference and hence limitation on the system performance is the *Direct Path Interference* (DPI) received from the transmitter being used to detect aircraft. This unwanted DPI signal correlates perfectly with the reference signal and produces range and doppler sidelobes that are several orders of magnitude greater than the echoes that are sought [18].

To detect anything but the closest of targets, it is necessary to remove this signal, by both angular nulling with the antenna and adaptive echo cancellation in the receiver. These strategies are further elucidated in the sections to follow.

However, eventually the dynamic range of the receiver limits the cancellation and so the principal limitation on system performance lies with the *analogue to digital converter* (ADC) technology [16].

Further interference is due co-channel interference coming from other transmissions operating at the same frequency within a single frequency network. This has a similar effect to the DPI.

In addition, the signal is always received against a background of reflections from the surface, i.e. clutter, and could be buried under these interferences. Their power density at the radar antenna, in addition to correlation between the desired signal and the interferences, further influences the system's performance.

These effects highlight the importance of conducting a characterisation of the USRP receiver.

A more thorough treatment of these interferences and the methods used to mitigate them are discussed in [18] [12] [13].

## 2.1.2 Digital beamforming

Passive radar systems use antenna arrays with several antenna elements and element-level digitisation. This allows the direction of arrival of echoes to be calculated using standard radar beamforming techniques, such as amplitude monopulse using a series of fixed, overlapping beams or more sophisticated adaptive beamforming. Alternatively, some research systems have used only a pair of antenna elements and the phase-difference of arrival to calculate the direction of arrival of the echoes (known as phase interferometry) [15] [40].

## 2.1.3 Signal conditioning

Adaptive nulling is spatial filtering through an *adaptive beamformer* (ADBFB), to null the interference. To null the interference, the output power of the beamformer along the direction of the interference must be minimized, whereas the output power along the desired signal's direction must be maximized. This may include high quality analogue bandpass filtering of the signal, channel equalization to improve the quality of the reference signal, removal of unwanted structures in digital signals to improve the radar ambiguity function or even complete reconstruction of the reference signal from the received digital signal [18] [33].

## 2.1.4 Adaptive filtering

The principal limitation in detection range for most passive radar systems is the *signal to interference ratio* (SIR), due to the large and constant direct signal received from the transmitter. To remove this, an adaptive filter can be used to remove the direct signal in a process similar to active noise control. This step is essential to ensure that the range/doppler sidelobes of the direct signal do not mask the smaller echoes in the subsequent cross-correlation stage.

In a few specific cases, the direct interference is not a limiting factor, due to the transmitter being beyond the horizon or obscured by terrain (such as with the Manastash Ridge Radar), but this is the exception rather than the rule, as the transmitter must normally be within line-of-sight of the receiver to ensure good low-level coverage [33].

## 2.1.5 Cross-correlation processing

The key processing step in a passive radar is cross-correlation. This step acts as the matched filter to provide the necessary processing gain thereby maximising the SNR. The response to this matched filter with respect to time and doppler shift of the carrier frequency from a normalized version of the transmitted waveform is known as the ambiguity function.

This topic is treated with greater detail in section 2.6 of this chapter.

Most analogue and digital broadcast signals are noise-like in nature, and as a consequence they tend to only correlate with themselves. This presents a problem with moving targets, as the doppler shift imposed on the echo means that it will not correlate with the direct signal from the transmitter. As a result, the cross-correlation processing must implement a bank of matched filters, each matched to a different target doppler shift.

## 2.1.6 Target detection

Targets are detected on the cross-correlation surface by applying an adaptive threshold, and declaring all returns above this surface to be targets. A standard cell-averaging CFAR algorithm is typically used and determines the range and doppler of each target.

## 2.1.7 Trajectory tracking

At this stage in the processing the system has determined the range and doppler of a number of targets. In order to further process the data it is necessary to associate this plot data with individual targets and this is performed using a conventional Kalman filter. Most false alarms are rejected during this stage of the processing.

## 2.1.8 Track association and state estimation

After having associated plots-to-targets, the range and doppler data for each target are processed by a non-linear estimator to determine the target's location, speed and heading. Use of a non-linear estimator allows optimum use of the doppler information in this tracking process.

## 2.1.9 Narrow band and CW illumination sources

The above description assumes that the waveform of the transmitter being exploited possesses a usable radar ambiguity function and hence cross-correlation yields a useful result. Some broadcast signals, such as analogue television, contain a structure in the time domain that yields a highly ambiguous or inaccurate result when cross-correlated. In this case, the processing described above is ineffective.

If the signal contains a *continuous wave* (CW) component, however, such as a strong carrier tone, then it is possible to detect and track targets in an alternative way. Over time, moving targets will impose a changing doppler shift and direction of arrival on the CW tone that is characteristic of the location, speed and heading of the target. It is therefore possible to use a non-linear estimator to estimate the state of the target from the time history of the doppler and bearing measurements.

The vision carrier of analogue TV signals has been shown to have successfully achieved this [15]. However, target track initiation is slow and difficult, and so the use of narrow band signals i.e. FM radio broadcasts is probably best considered as an ancillary to the use of illuminators with better ambiguity surfaces. Later sections examine the merits of such a choice in greater detail.

## 2.2 Advantages and Disadvantages of PCL Systems

PCL systems operate in bistatic and multistatic configurations, thus inherit all the associated advantages and disadvantages.

Further additional advantages include:

- Low procurement costs as they do not have any transmitter hardware.
- Lower costs of operation and maintenance due to lack of transmitter and moving parts.
- Covert operation, including no need for frequency allocations.
- Physically small and hence easily deployed in places where conventional radars cannot be.
- Rapid updates, typically once a second [33].

Disadvantages:

- Lack of control over the form, nature and origin of the transmitters and signal waveform.
- Performance limitations and complexity of deployment due to direct path interference, co-channel interference, etc.

## 2.3 History and Examples of PCL Systems

Much of the early work published on PCL systems was conducted at University College London (UCL) and was undertaken in the late 1970s.

A number of experimental bistatic systems have been built and evaluated by Schoenenberger who designed and built a system using a UHF Air Traffic Control radar at Heathrow airport as an illuminator, and investigated particularly the problems of synchronization between receiver and transmitter [28]. A real-time co-ordinate correction scheme was also developed for this system. Further developments included a digital beamforming array for pulse chasing experiments and a coherent MTI system using clutter from stable local echoes as a phase reference [4].

Subsequent work at UCL attempted to use UHF television transmissions as illuminators of opportunity, to detect aircraft targets landing and taking off from Heathrow airport.

This work made use of the pulsed-like nature of parts of the television waveform for bistatic use and showed the ability to receive clutter from the surrounding buildings. By implementing a two pulse MTI canceller, off line, they were able to “track” moving targets. This system was impractical in the sense that they required a special transmission waveform and only has a range resolution of 1800m and range ambiguity of 9600m.

In attempt to improve the system performance, the use of a multi burst test pattern was investigated. This once again yielded positive results for static objects, yet failed to resolve moving targets.

This work illustrated that terrestrial television, in the time domain, was not suitable for use in a bistatic configuration and that the use of a pulse radar transmitter is the best case, however when the transmitter is not radar like, then the autocorrelation function of the transmitted waveform is of paramount importance [15].

In addition to this, the transmit power should be proportionate to the coverage required. In the case of complex modulation functions such as television, the calculation is made on the basis of the power of that part of the spectrum used by the radar. Moreover, the radiation pattern of the transmitter should be either omnidirectional or pencil-beam. Finally, the modulation bandwidth must be commensurable with the required range resolution [12].

Further work on television in the time domain using sophisticated correlation techniques which were applied to *Direct Broadcast by Satellite* (DBS) TV signal was still not able to detect moving targets at useful range. Thus suggesting that the problems associated with useful target detection using DBS TV prevent it from being a practical approach to detecting airborne targets[8].

Howland [15] developed a UHF forward scatter system based on television transmissions. A forward scatter system is not able to provide range information, due to the nature of the bistatic geometry, Thus a different approach was adopted, measuring *direction of arrival* (DOA) by phase interferometry and doppler shift of the vision carrier of the television signal. The angle of arrival of a target echo is related to the phase difference of the received signal at the surveillance antennas by:

$$\Phi = \frac{2\pi d}{\lambda} \sin(\Theta) \quad (2.1)$$

where:

- $\Phi$  is the angle of arrival of a target echo
- $\Theta$  is the phase difference of the received signal
- $\lambda$  is the wavelength of the signal
- $d$  is the distance between the dipoles

This work focused on developing signal processing techniques used for target tracking by means of an extended Kalman filter algorithm and assumes that there is only one receiver system, and one remotely located television transmitter. On its own the information extracted from a single measurement of doppler shift and DOA of the target echo, is not useful. Therefore, a series of measurements for doppler and DOA with respect to time were taken.

This choice was due to the unique association of the target echo's change in doppler shift and DOA with its course and velocity. Howland's research bore similarity to the work done at UCL, with the exception that his work was done in the frequency domain and exploited DOA and was able to demonstrate tracking of aircraft targets at ranges in excess of 100km from the receiver.

Further work by Howland [16] investigated the use of FM radio broadcast transmissions, which closely resembles his previous work based on television transmissions, employing doppler, range and bearing data. Adaptive filtering was applied to two surveillance channels to reject the direct transmitter signal interference. A conventional CFAR detection scheme was applied to range and doppler information resulting from the matched filtering to determine the range and doppler of each target. With only two surveillance channels the direction finding system again uses phase interferometry to estimate the target bearing.

Target tracking was employed by implementation of a Kalman filter and nonlinear estimation to determine the target's location, speed and heading. Use of a nonlinear estimator allowed optimum use of the doppler information in this tracking process. Via this approach Howland was able to demonstrate tracking of aircraft at ranges in excess of 150km from the receiver.

The Manastash Ridge Radar is a system conceived and built by John Sahr of the University of Washington, Seattle, for studies of the ionosphere [26]. It uses a single VHF radio transmitter as illuminator, and a receiver separated from the transmitter by a large mountain range (Mt.Rainier). The receiving system is based on a standard digitizer card and PC, and is extremely simple and cheap, approximately US\$15 000. Synchronization is achieved by GPS, giving uncertainties of 100ns in timing which equates to 15 m in range and 0.01 Hz in doppler. Although the purpose of the system is for ionospheric studies, it does detect aircraft targets at ranges up to about 100km. Their system vividly demonstrates that high performance can be achieved from simple and inexpensive PCL systems.

Silent Sentry developed by the Lockheed Martin company, based on multiple VHF FM radio and television transmissions. It has demonstrated tracking of aircraft and space targets renewing tracking targets can be completed eight times in a second. The database of the system has stored in it, about 55,000 correlative FM broadcast and digital audio broadcast parameters and is advertised as being applicable to: air surveillance and tracking in areas of limited coverage; capable of tracking low flying, non-cooperative, slow moving targets; continuous total volume surveillance of air breathing and ballistic objects; low acquisition and operations cost, unattended remotely managed.

## 2.4 Applications of PCL

Reported applications of PCL include:[10]

- air-space surveillance
- maritime surveillance
- atmospheric studies and ionospheric studies
- oceanography
- mapping lightning channels in thunderstorms
- monitoring radioactive pollution

There are also reports of algorithm development for interferometry, target tracking and target classification [10]. This panoramic diversity of systems and applications is indicative of the increasing importance of PCL systems.

## 2.5 Typical Illuminators

A wide variety of RF emissions in the form of TV and radio broadcasts in addition to terrestrial and space based communications has resulted in a wide range of signal types available for exploitation by passive radar. Furthermore, many such transmissions are at VHF and UHF frequencies, which allows these parts of the spectrum not normally available for radar use, and at which stealth treatment of targets may be less effective, to be used.

Typical broadcast service sources include:

- Analogue TV signals
- FM broadcast radio signals
- *Global System for Mobile* (GSM) base stations
- Digital audio broadcasts
- Digital video broadcasts
- Terrestrial HDTV

### So Why FM radio?

Of all the transmitters of opportunity available in the environment, the typical broadcast service sources represent some of the most attractive for surveillance purposes, owing to their inherent attractive properties of very broad coverage and relatively high transmitter powers.

Satellite signals have generally been found to be inadequate for passive radar use [33]. This is as a result of their transmission powers being too low, or because the orbits of the satellites are such that illumination is too infrequent. However, exceptions to this include the exploitation of satellite based radar and satellite radio systems.

Digital audio transmitters emit signals at a much higher frequency than FM broadcast transmissions, however FM broadcast transmissions are comparatively higher in their power. Thus, the maximum detection ranges offered by FM broadcast transmissions are greater than that of Digital audio [10]. Furthermore, the coverage of Digital audio is generally poor, although the transmitter networks are expanding elsewhere, they are currently non-existent in South Africa.

Cellular phone base stations transmit at a rather low power and would seem therefore to be limited in their performance and application. However, there is an extensive network and targets could be tracked through such a network and hence the coverage may be extended greatly. This however comes at the cost of increased system complexity. Furthermore, base stations deliberately concentrate their emissions towards the ground and may not necessarily have good coverage of higher altitude aircraft.

Analogue television transmitters, with high radiated powers and a pulse like waveform structure present themselves as an obvious choice of illuminator. However, in spite of these instant points of appeal, it has been shown that the waveform is far from suited for radar usage when used in a conventional radar matched filtering approach [12]. In an alternative approach however, making use of doppler and bearing information in echoes of the television video carrier it is possible to track aircraft at ranges of up to 260km from the receiver and 150km from the transmitter [15].

This approach is referred to as narrow band processing as only a few kilohertz and thus small percentage of the 5.5MHz television waveform bandwidth is processed to determine the target doppler shifts. The disadvantages of this stem from the relatively low information content in the doppler measurements and the system must observe the target's doppler history for an extended time before there is sufficient information to locate the target.

Moreover, the use of non-linear estimation techniques to calculate the target's trajectory mean that a good estimate of the target's location must be initially available. In the case of a forward scatter radar the unique geometry can be manipulated in order to determine an expression of the target's location [2].

In the general bistatic problem it is necessary employ global optimisation schemes [15]. The former approach is limited in its operational applications and the latter is neither robust nor computationally efficient.

FM broadcast transmissions have been used to probe the ionosphere [26] and therefore might be expected to have useful height surveillance. Their high powers and good coverage make FM broadcast radio transmissions particularly well suited to air target detection for both civil and military applications. Moreover, they could be used for marine navigation in coastal waters although clutter will be a more significant problem.

In PCL systems wideband processing is defined as the use of a receiver that has a bandwidth that is comparable to that of the waveform being processed. A typical FM radio broadcast occupies a bandwidth of approximately 100kHz, thus offering a potential range resolution of up to 1500m. It is clear that the signal offers useful target ranging information. However, as a result of this lower bandwidth available, range and bearing are a factor of ten or so worse than a conventional microwave radar.

Doppler, on the other hand, is two or three orders of magnitude more accurate. This is due to the extended integration times that are potentially achieved by passive radar. The doppler information can be used to provide a resolution comparable to conventional radars and by simultaneously using multiple transmitters the system can achieve target location accuracies that may be even better.

However, the suitability of a signal for target location is governed by more than its bandwidth. Of greater value and importance is the ability of the radar receiver to locate the target unambiguously. For this we must compute its ambiguity function.

## 2.6 Relevant Equations

### 2.6.1 The Bistatic Radar equation

The starting point of an analysis of the performance of a system is the radar equation. The radar equation for a bistatic system is derived in the same way as for monostatic systems.

$$\frac{P_r}{P_n} = \frac{P_t G_t}{4\pi r_1^2} \cdot \sigma_b \cdot \frac{1}{4\pi r_2^2} \cdot \frac{G_r \lambda^2}{4\pi} \cdot \frac{1}{k T_0 B F} \cdot L \quad (2.2)$$

where: [10]

$P_r$	is the received signal power
$P_n$	is the receiver noise power
$P_t$	is the transmit power
$G_t$	is the transmit antenna gain
$G_r$	is the receive antenna gain
$r_1$	is the transmitter to target range
$r_2$	is the target to receiver range
$\sigma_b$	is the bistatic radar cross section
$\lambda$	is the signal wavelength
$k$	is Boltzmann's constant
$T_0$	is the noise reference temperature, 290 K (standard room temperature)
$B$	is the receiver effective bandwidth
$F$	is the receiver effective noise figure
$L (\leq 1)$	are system losses

setting the values:

- $\sigma_b = \sigma_m$
- $r_1 = r_2 = r_m$

where:

$\sigma_m$  is the monostatic radar cross section

$r_m$  is the radar to target range

allows for the reduction of the bistatic range equation to the monostatic case.

In order to use the radar range equation appropriately and correctly to predict performance of a radar system it is necessary to understand the correct value of each parameter to be used.

The transmit power  $P_t$  of the various illuminators of opportunity exploited in PCL is high. This is due to the fact that the intended receivers often have inefficient antennas and poor noise figures, with the transmission paths far from line of sight. Thus the substantial transmit power is necessary to overcome the inefficiencies. However, for example, the analogue TV broadcast has pronounced ambiguities every  $64 \mu s$  and thus does not exhibit favourable ambiguity properties and a more attractive ambiguity may be realised by using a portion of the signal spectrum, at the expense of reduced power. Therefore, when employing the radar equation it is necessary to consider only the portion of the signal spectrum that is used for the radar purposes. This may not necessarily be the same as the power of the entire signal spectrum.

## 2.6.2 Bistatic Radar Cross Section

The likelihood of target detection and location is dependant on the spatially influenced bistatic RCS and target dynamics, in addition to the radar design parameters. The use of conventional processing techniques will result in the detection of targets in range, doppler and angle. Relatively little has been published regarding the bistatic RCS of targets and this remains an area for future research. However, early work, that resulted in the formulation of the bistatic equivalence theorem, states that that the bistatic RCS is equal to the monostatic RCS at the bisector of the bistatic angle  $\beta$ , reduced in frequency by the factor  $\cos(\beta/2)$ [9].

This theorem however, is valid typically, for small angles, when the bistatic angle,  $\beta$ , is  $5^\circ$  or less. Therefore, above  $5^\circ$  the target bistatic RCS will not in general be the same as the monostatic RCS, although will be comparable for targets that have a low monostatic RCS and due to shadowing that occurs in the monostatic geometry but not the bistatic geometry. In a monostatic radar, phase interference from two or more targets causes a distortion of the echo signal. This in turn results in the apparent phase centre of the radar reflection swinging between the targets. This random movement of radar reflecting centres, leads to jittered angle tracking, known as target glint [14]. The effect of target glint is reduced in the bistatic RCS region, thus the bistatic RCS has the advantage of glint reduction.

As the bistatic angle is increased to  $180^\circ$  the forward scatter region is encountered where the target lies on the transmitter-receiver baseline. Within this region, the bistatic RCS can be many times greater than that of the monostatic RCS. The magnitude of the target's forward scatter return does not depend on the material composition, therefore irregular shaped targets, and radar absorbent materials used on targets are still able to be detected.

Any target illuminated by the transmitter on the baseline, when the targets dimensions are larger than the transmitted wavelength, produces a shadow. This shadow region occurs on the opposite side of the target from the transmitter. This maybe understood with reference to Babinet's Principle. Babinet's principle is an approximation according to which the amplitude of near forward scattering by an opaque, planar object is the same as that of an aperture of the same shape and size in a perfectly conducting screen [10].

The forward scatter cross-section of a target with cross sectional area A is given by:

$$\sigma_b = \frac{4\pi A^2}{\lambda^2} \quad (2.3)$$

Where the radiation wavelength,  $\lambda$  is assumed small compared to the target dimension.

The angular width of the scattered signal in the horizontal or vertical plane is given by:

$$\theta_b = \frac{\lambda}{d} \quad (2.4)$$

where:

$d$  is the target linear dimension.

The dependence of  $\sigma_b$  and  $\theta_b$  for a target of the size of a typical aircraft, is shown below.

Where  $A = 10\text{m}^2$  and  $d = 20\text{m}$ .

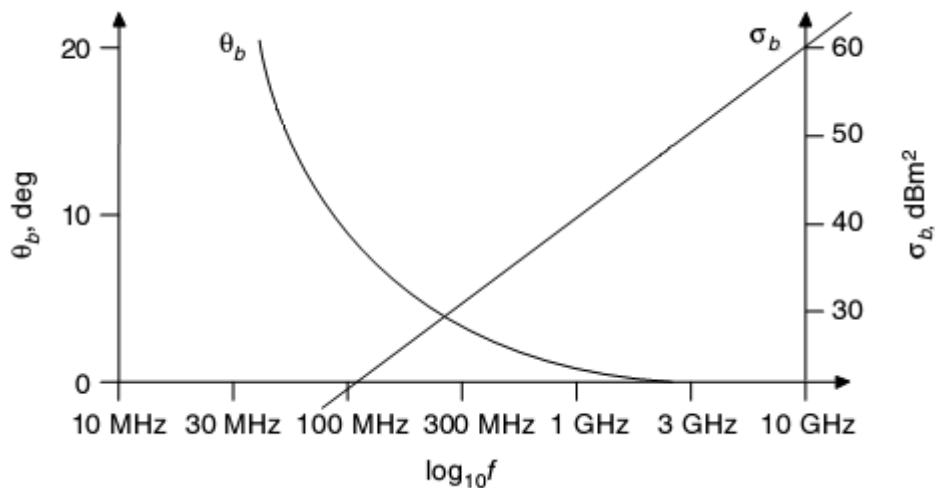


Figure 2.2: Variation of RCS and angular width of a forward scatter target against frequency [10]

Angular width decreases with an increase in frequency. Thus the forward scatter illumination is focused into an increasingly narrower beam. This implies that frequencies around VHF and UHF are more likely to be optimum for exploiting forward scatter as target detection may be achieved over an adequately wide angular range. Taking advantage of the forward scatter configuration, however, comes at the expense of target doppler and position information. However, target location can be estimated using a combination of doppler and bearing as explained in [15].

### 2.6.3 Bistatic Clutter

The received signal at any location is the vector RF sum of the direct signal and of the multipath propagation [12]. Most of these multipath signal energies would result from reflection off fixed objects, such as, buildings, other large objects, other aircraft, etc. This multipath propagation is defined as clutter. Clutter, in general, is a cause of degradation in radar system performance, as the target returns must compete with the clutter returns at the receiver. More often than not clutter RCS are larger than target RCS [4].

Bistatic clutter is subject to greater variability than the monostatic case, because there are more variables associated with the geometry [34], in addition to frequency and surface composition.

Relatively little work has been done in developing models for bistatic clutter and available experimental data from the intended receiver location at UCT is minimal, and thus remains an area worthy of future research.

It is important to know the clutter power returns at the receiver, in order to prevent the receiver from saturating. Thus the work to be presented in chapter 4, characterising the receiver, will provide the reader with an indication of the expected performance in this regard.

### 2.6.4 Integration Gain

Radar signals are considered to be coherent when the relative phases of the signals have a known relationship, even though they may be separated in time. To improve the SNR a combination of coherent and incoherent integration may be implemented. Coherent integration is performed by correlating the target echo with the reference signal and in essence, is the addition of a sequence of  $M$  coherent radar signals where the signals are summed vectorially and is regarded as a single waveform. Through this process the SNR will increase by a factor  $M$ , as given by Equation 2.5, a derivation of this can be found in [24].

$$SNR_m = M \times SNR_1 \quad (2.5)$$

Where:

$M$  is the number of coherent radar signals.

$SNR_m$  Is the the SNR of the average of  $M$  signals.

In the case of incoherent integration, these  $M$  pulses will not add in phase and will not improve the SNR. Instead the signals are processed separately and the separate observations are then combined, usually by means of averaging.

The relative roles of coherent and incoherent integration will be a function of the coherency of the target echo and of competing noise and clutter signals. The maximum signal processing gain achievable is given by:

$$G_p = BT_{max} \quad (2.6)$$

Where:

$B$  is the waveform bandwidth.

$T_{max}$  Is the maximum integration dwell time.

The effective waveform bandwidth of an FM radio transmission is known to vary with time, clearly this will translate to a variation in signal processing gain.

A rule of thumb determining the maximum value for the integration dwell time or maximum coherent processing time is given by:

$$T_{max} = \left\{ \frac{\lambda}{A_R} \right\}^{1/2} \quad (2.7)$$

where:

$A_R$  is the radial component of the target acceleration.

The integration dwell time is the length of time taken to make an observation with a radar set, the integration dwell time is dependant on the waveform coherence and target dynamics, namely target velocity and manoeuvrability.

$T_{max}$  consequently, is additionally a time varying entity and care will need to be observed in its choice.

## 2.6.5 Range Resolution and Maximum Unambiguous Range

The minimum distance necessary to separate two targets in order to distinguish between them defines the range resolution.

For both monostatic and bistatic cases, adequate separation between the two target echoes at the receiver is taken to be:

$$\frac{c \cdot \tau}{2} \quad (2.8)$$

where:

$\tau$  is the compressed radar pulse width.

Furthermore, (2.9)

$$\tau = \frac{1}{B}$$

and thus, Equation 2.8 can be restated as: (2.10)

$$\frac{c}{2B}$$

If the time delay between the echoes from two targets is  $>$  the pulse width  $\tau$  then the two echoes are resolvable. However, if the targets are closer than  $\tau$  their echoes merge and are unresolvable.

In order to generate this separation at a bistatic receiver, two-point targets must lie on a bistatic isorange contour with a separation  $R_B$ . In the monostatic case, the distance between the two circles are constant, unlike the bistatic case.

The equation for a monostatic system resolution is given by the equation:

$$\Delta R_M = \frac{c \cdot \tau}{2} \tag{2.11}$$

For a bistatic radar, separation between the ellipses depend on the bistatic angles. As the bistatic angle increases, so does the distance between the isorange contours, and vice versa. Eventually on an extended baseline, or long ranges, they become equispaced, and start to represent a monostatic case. An approximation for  $R_B$  is:[40]

$$\begin{aligned} \Delta R_B &= \frac{\Delta R_M}{\cos(\frac{\beta}{2})} & (2.12) \\ &= \frac{c \cdot \tau}{2 \cos(\frac{\beta}{2})} \end{aligned}$$

The above equation is based on the monostatic case, reduced by a factor of  $\cos(\frac{\beta}{2})$ . This relationship is common in additional bistatic properties. For example bistatic doppler is reduced by the factor  $\cos(\frac{\beta}{2})$  and when beta is small the bistatic RCS is equal to the monostatic RCS reduced by the factor  $\cos(\frac{\beta}{2})$ .

In general any measurement made with a basic resolution of M, will have a root mean square (RMS) error  $\delta M$  given by:[24]

$$\delta M \simeq \frac{M}{\sqrt{(2 \cdot SNR)}} \tag{2.13}$$

Thus for the range resolution, the range error is given by:[24]

$$\delta R \simeq \frac{c}{2B \sqrt{(2 \cdot SNR)}} \tag{2.14}$$

Thus the range accuracy is limited by the pulse effective bandwidth and SNR.

It is clear from the above that the resolution and its accuracy is improved by using shorter pulses, i.e. Large pulse bandwidths. However, there's a lower limit to pulse duration. Depending on various parameters a minimum signal energy is required in order to detect a target echo.

The energy carried by the pulse is a product of transmitter power and pulse duration. Therefore, cutting pulse duration in half, for instance, would necessitate doubling transmitter power in order to keep the signal's energy constant. The problem with that is that transmitter power cannot be increased at will because of cost and other constraints. Increasing the rate at which pulses are transmitted by the radar will increase the mean power radiated and thus the energy radiated. However, radars are designed so that a range counter starts at the transmission of the pulse, is read out when an echo is detected, and is reset upon transmission of the next pulse. Thus when pulses are transmitted so frequently that a pulse is transmitted before the previous pulse has completed the round trip to the target and back. The resulting effect is an uncertainty in determining the correct relationship between the transmitted and the echo pulses and the target range becomes ambiguous. As depicted in Figure 2.3.

The range beyond which targets appear as second time around echoes is called the maximum unambiguous range [29], which is given by:

$$(R_M)_u = \frac{c}{2 \cdot PRF} \quad (2.15)$$

where:

PRF is the Pulse Repetition Frequency and is the rate at which pulses are transmitted

The corresponding bistatic unambiguous range is given by:

$$(R_T + R_R)_u = \frac{c}{PRF} \quad (2.16)$$

which lies on an isorange contour, of major axis length equal to equation (B.1). Further details on unambiguous bistatic PRF can be found in [34] [24] [17].

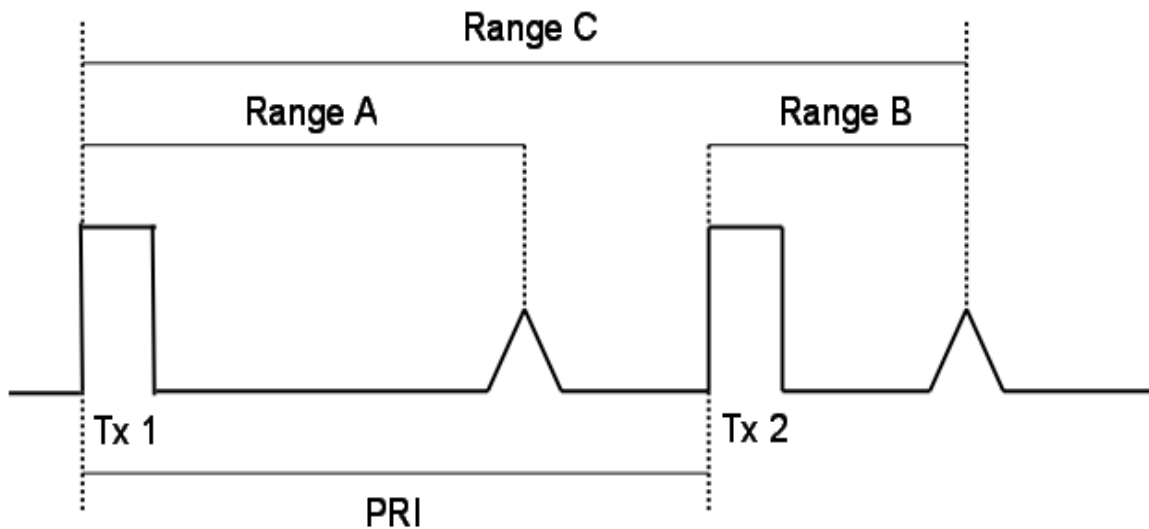


Figure 2.3: A target echo detected after the transmission of the second pulse results in ambiguous ranges at B and C.

## 2.6.6 Doppler Resolution

In order to accurately measure the speed of the target the doppler shift will be used. This is the change in radio frequency of the signal, caused by the relative motions of the target and receiver.

With the target in motion, the radar to target range as well as the phase of the radar signal are continuously changing.

This change in phase with respect to time is related to the doppler angular frequency and can be further shown [29] that the doppler frequency shift is given by:

$$f_d = \frac{2v_r}{\lambda} = \frac{2v_r f_0}{c} \quad (2.17)$$

where:

$f_d$  is the doppler frequency shift

$f_0$  is the transmitted frequency

$v_r$  is the radial velocity of the target with respect to the radar

The definition of the bistatic doppler frequency shift is different to the monostatic case, above. The change in radio frequency is a result of the rate of change of the total path length travelled by the signal. In the monostatic case this change in path length is equal to a change in the targets range. For a bistatic system the doppler shift is given by:

$$f_d = -\frac{1}{\lambda} \frac{d(R_T + R_R)}{dt} \quad (2.18)$$

The expression indicates a decrease in doppler frequency for an increasing path length [24].

The doppler frequency shift provides the means to distinguish between stationary and moving targets. However, is not a measure of the radial velocity of the target with respect to the radar as with the monostatic case.

The velocity resolution, which is the ability to separate two targets separated in doppler is synonymous with the doppler resolution and can be expressed by:

$$\Delta f_d = \frac{1}{PRI} \quad (2.19)$$

The longer the duration of the signal, the finer the resolution will be and the more accurately the doppler frequency shift can be determined.

From equation (2.19) above, the accuracy of the doppler resolution is given by:

$$\delta f_d \simeq \frac{1}{PRI \cdot \sqrt{(2 \cdot SNR)}} \quad (2.20)$$

Thus it is noted that the requirement for velocity resolution and accuracy implies long duration waveforms whereas for range resolution and accuracy implies short waveforms. This paradox must be considered during the signal processing and waveform design.

## 2.6.7 Ambiguity Function

The radar system's resolution, detection, measurement accuracy and ambiguity are defined by the radar waveform [29]. The effect of the waveform on these parameters maybe determined upon examination of the receiver output, which is optimum when designed on the matched filter among others [29] [24] [22]. Should a target be present where it is expected to be, the receiver output will peak to a maximum, in the absence of noise.

Thus the probability of detection is independent of the shape of the waveform and depends on the ratio of the energy in the signal to the noise power per cycle of bandwidth. Range and doppler accuracies are additionally dependant on this ratio, as previously discussed, additionally are affected by the shape of the radar waveform as are ambiguity and resolution.

Ambiguity occurs when more than one choice for a particular parameter is available but only one choice is expected. With respect to the matched filter receiver output, ambiguities arise when peaks occur at values other than the expected value.

The effect of the transmitted waveform on the doppler and range can be produced upon extension of the matched filter or autocorrelation function of the received signal. A three dimensional plot of echo turn around time, doppler frequency and the output of the function results in the *ambiguity diagram* which graphically presents the accuracy and ambiguity afforded by the transmitted radar waveform. Additionally, to examine the waveform's potential to resolve two targets of equal amplitude with different doppler and range [29].

The ambiguity plot is determined by the ambiguity function and as is given by:

$$\left| \psi(R_R, f_d) \right|^2 = \left| \int_{-\infty}^{\infty} s_t(t) s_t^*(t - R_R) \exp[j 2\pi f_d t] dt \right|^2 \quad (2.21)$$

where:

$R_R$  is the time delay (or range)

$f_d$  is the signal doppler shift

$\psi(R_R, f_d)$  is the ambiguity response at  $R_R$  and  $f_d$

The ideal ambiguity diagram, also know as the thumbtack surface, would consist of a single peak with a minuscule thickness at the origin and zero elsewhere [29]. This single spike prevents ambiguities and permits the frequency and echo delay time to be determined simultaneously to a high degree of accuracy. Furthermore, no matter their position, any two targets are resolvable.

However, the fundamental properties of the ambiguity function prevent this type of behaviour. The main restrictions affecting the performance are that the maximum height of the function, and therefore the peak at the origin are of a fixed height. In addition to this, the volume enclosed by the function is fixed and finite.

Typically, the function will be spread about the origin and the maximum peak height will be no greater than the fixed maximum amount thus the remaining energy is spread through the remainder of the diagram which may result in one or more additional peaks, perhaps as high as the one at the origin. The ambiguity diagram is centred at the origin, thus the response at  $\psi(R_R, 0)$  is the response to reflections at a different range but at the same doppler as the target.  $\psi(0, f_d)$  is the response to reflections at the same range as the target but at different doppler shifts.

In PCL radar, there are two factors which affect the ambiguity function. These are the geometry of the system and the instantaneous modulation of the reference signal.

The dependence of the ambiguity function of a bistatic radar on geometry has been evaluated by Tsao et al [40] [9] [17] [11]. They show that in the bistatic arrangement, time delay is no longer a linear function of target range and doppler is no longer a linear function of target velocity. Thus, the form of the ambiguity function depends on the position and direction of motion of the target.

Thus the bistatic ambiguity function of the signal  $s(t)$  is given by:

$$\left| \psi(R_{RH}, R_{Ra}, V_H, V_a, \theta_R, L) \right|^2 = \quad (2.22)$$

$$\left| \int_{-\infty}^{\infty} s_t(t - \tau_a(R_{Ra}, \theta_R, L)) s_t^*(t - \tau_H(R_{RH}, \theta_R, L)) \exp[j(2\pi f_{dH}(R_{RH}, V_H, \theta_R, L) - 2\pi f_{da}(R_{Ra}, V_a, \theta_R, L))t] dt \right|^2$$

where:

- $R_{RH}$  is the hypothesised range from the receiver to the target
- $R_{Ra}$  is the actual range from the receiver to the target
- $V_H$  is the hypothesised radial velocity of the target with respect to the receiver
- $V_a$  is the actual radial velocity of the target with respect to the receiver
- $f_{dH}$  is the hypothesised doppler frequency
- $f_{da}$  is the actual doppler frequency
- $\theta_R$  is the angle from the receiver to the target with respect to North
- $L$  is the length of the baseline formed by the transmitter and receiver

The reference point of the geometry is assumed to be the receiver. The important difference between this form of the ambiguity function and the form presented in Equation 2.21, is that the geometrical layout and relationship between the transmitter, receiver and target have been factored in. This can have a significant effect on the form of the ambiguity function and the resulting range and doppler resolutions.

It is important to know the properties of these ambiguity functions with time, as the variation in the form of the ambiguity function would determine the radar's performance.

Thus investigation into the dependence of the ambiguity function on the instantaneous modulation or programme content of the particular signal being broadcast forms, in part, the objective of this dissertation.

## 2.7 Summary

This chapter introduces and explores the concept of PCL and notes that fundamentally, PCL systems are bistatic in nature and thus measure the difference in time of arrival between the signal directly from the transmitter and the signal reflected off the target. Furthermore, PCL systems make use non-co-operative transmitters using 'illuminators of opportunity' such as existing radar transmissions and broadcast and communication signals.

Some of the unique advantages and disadvantages that arise as a result of the geometry and the use of illuminators of opportunity are listed. Although the performance of the bistatic arrangement does not rival that of the monostatic geometry, there are some distinct applications within the bistatic system which cannot be implemented by monostatic radars. An example whereby bistatic systems are a major advantage, is using such a system to detect stealthy aircraft and complete systems can be built on an extremely low budget.

The history and progression of development and research in PCL systems is explored and thus highlighting the techniques developed by Howland, that express the viability with regards to the tracking accuracy, as well as the distance at which targets were detected. Furthermore, work presented by Baker and Griffiths examines the performance of a variety of potential waveforms as the radar signal.

Of the illuminators of opportunity available in the environment, broadcast transmitters present themselves as the most attractive for surveillance purposes, owing to their inherent properties of high powers of transmission and widespread coverage.

If such signals are to be used on the basis of PCL, it is necessary to know their behaviour in terms of their ambiguity function [36] i.e. resolution and sidelobe levels in range and doppler, and the effect of range and doppler ambiguities. These signal processing techniques are outlined at the end of the chapter, furthermore, the theory begins to highlight the purpose of work done in measuring the the radar's frequency reference to maintain timing accuracy.

# Chapter 3

## USRP and GNURadio

### 3.1 Introduction

The continuum of innovation in semiconductor technology has led to the development of new radio technologies. One such technology is software defined radio. Thus far, no standard definition of software radio has been generated. This can be largely attributed to the nature of the flexibility that software defined radios offer.

As the interest and proliferation of this technology pushes ever widening frontiers, the Free Software Foundation (FSF) has developed and is maintaining a Software Defined Radio project called GNURadio. This GNU project is a collection of software tools that can be used to implement signal processing and radio applications on a PC using external USB based hardware, known as the *Universal Software Radio Peripheral* (USRP) also developed as part of GNURadio.

This chapter presents the research into the SDR paradigm and the associated design considerations, thus providing the natural backdrop against which the performance of the USRP and GNURadio are examined.

### 3.2 Software Defined Radio

However, SDRs do have characteristics that make them unique in comparison to other types of radios. SDRs have the ability to be transformed through the use of software and redefinable logic. This is achieved with general purpose *digital signal processors* (DSPs) or *field programmable gate arrays* (FPGAs). Thus SDRs have the ability to go beyond simple single channel, single mode transceiver technology with the ability to change modes arbitrarily because the channel bandwidth, rate, and modulation are all flexibly determined through software. This is unlike most radios in which the processing is done with either analogue circuitry or analogue circuitry combined with digital chips.

As an example, a European GSM SDR device may load a codec to process American GSM signals on detecting a change in the underlying service network, continuing to demodulate GSM signalling with no change in the physical hardware [20].

In order to make full use of this concept, SDRs keep the signal in the digital domain for as much of the signal chain as possible, digitizing and reconstructing close to the antenna, thereby allowing digital techniques to perform functions done by analogue components as well as the additional functions that are not possible in the analogue domain. To achieve this digitisation, ADCs, in the receive chain and DACs, in the transmit chain, are employed. However, connecting these components directly to the antenna introduces concerns regarding selectivity and sensitivity.

Thus the need for a flexible analogue front end capable of translating a wide range of frequencies and bands to that which the data converters are able to adequately process [25]. Some of the typical dynamic characteristics of an SDR include:

- Channel Bandwidth
- Data rates
- Modulation type
- Conversion Gain

This is exemplified in multiband radio systems, these systems are capable of operating on two or more frequency bands sequentially or simultaneously. Typically multiple radios would be required, each limited to operation in a specified band. In addition to this, multicarrier or multichannel radios have the ability to simultaneously operate on more than one frequency at a time, whether or not they fall in the same frequency band.

Multimode systems process several different kinds of standards and can be continuously reprogrammed. Examples of such standards include AM, FM, GMSK, and CDMA. Furthermore, a traditional radio determines the channel bandwidth with a fixed analogue filter. However, a SDR determines the channel bandwidth using digital filters that can be altered. This provides SDRs with the resources to vary the bandwidth dynamically, additionally, digital filters have the potential to implement filters not possible in the analogue domain and are able to compensate for transmission path distortion [7]. These features are complex to implement using analogue filters.

### 3.2.1 Applications of Software Radio

Software Radio is finding use in an ever broadening spectrum of applications. Software radio enable rapid prototyping and deployment of sophisticated wireless systems, making it ideal for a plethora of research and development applications in academia, industry and defence.

To name just a few, software radio systems have been deployed in:

- Public Safety and mine/underground communications
- Battlefield, survivable and ad-hoc networks
- Passive Coherent Radar
- Cognitive Radio
- Radio Astronomy

## 3.2.2 Software Radio development Tools and Frameworks

Several Software Radio environments are available. The common and favoured solutions include:

- C/C++
- Matlab/Simulink/LabView
- JTRS
- OSSIE
- GNURadio

This dissertation focuses its investigation on GNURadio.

## 3.3 Anatomy of a SDR Receiver

The first element in the receiver chain is the antenna. In a fully developed SDR the antenna is additionally a programmable component. The antenna generally tends to be the weakest element of the receiver. This is primarily so as the antenna has a bandwidth that is a small percentage of the centre frequency and therefore, multiband operation is difficult. However, in instances where single bands of operation are used, this is not a problem.

In the ideal scenario, the SDR would have its ADC connected directly to the antenna of the receiver, this is in order to facilitate the implementation of as much of the system components in the digital domain. This, however, is not a practical solution and some form of an analogue front end must be used before the ADC in the receive path in order to conduct the appropriate frequency translation.

The most common of these architectures is the super heterodyne architecture. In this instance the midrange IF produced by the receiver allows the use of sharper cut off filters for improved selectivity. Additionally higher IF gains are achieved through the use of IF amplifiers, improving the sensitivity. The super heterodyne receiver uses two stages of conversion and is useful at microwave frequencies in avoiding problems associated with *Local Oscillator* (LO) instability.

The super heterodyne receiver offers this performance over a range of frequencies, thus, by combining wideband analogue techniques and multiple front ends facilitates the operation of the receiver across different RF bands.

The direct conversion architecture, which converts the RF signal directly to an IF frequency of zero, in less demanding applications, is seeing an increase in popularity. This architecture has the advantage of being simpler to implement and less costly to build. This is so as they have no IF amplifier, IF bandpass filter or IF LO required for the final down-conversion. Additionally, the direct conversion approach does not generate any image frequencies as the mixer difference frequency is effectively zero, while the sum frequency is easily filtered out.

However, this architecture has a major drawback in that the LO must have a very high degree of precision and stability to avoid drifting of the received signal frequency. Currently, direct conversion is found in user terminals for cellular communication [23]. Additionally, direct conversion receivers are susceptible to various noise sources at DC, which create a DC offset which may be larger than the signal itself and will degrade the SNR of the signal [1].

Band select filters are made use of in order to limit the range of input frequencies presented to the high gain stage. This is in aid of minimising the effects of intermodulation distortion. In addition, where intermodulation is not a problem, it is still possible that strong out of band signals could limit the amount of potential gain in the following stages, resulting in limited sensitivity. If all the signals input are of interest and filtering of the stronger signals is not possible, it becomes necessary for the receiver to have a large dynamic range.

Mixers are used to translate the RF spectrum to a suitable IF frequency. Receivers may use a number of mixer stages, each successively generating a lower frequency, as was described in the super heterodyne architecture. In order to eliminate undesired images as well as other undesired signals, filtering is made use of at each stage. The filtering should also be appropriate for the application. For example a traditional single carrier receiver would generally apply channel filtering through the mixer stages to help control the IP3 requirements of each stage [7].

A quadrature demodulator in addition to, or instead of, a mixer is employed in some receiver architectures. This is in order to separate the I and Q components which undergo separate signal conditioning. Due to the digital nature of the receiver this is not a problem. However, in the analogue domain the signal paths must be perfectly matched, or I/Q imbalances will be introduced, potentially limiting the suitability of the system.

An IF amplifier is often made use of in the form of an *Automatic Gain Control* (AGC). The goal of the AGC is to use the maximum gain possible without saturating the the signal chain. If the dynamic range in the receiver, which is a function of the ADC performance, is insufficient, reduction in gain from a strong signal may cause weaker signals to be lost in the noise floor of the receiver.

The ADC is used to convert the IF signal or signals into digital format for processing. The ADC capabilities define the performance of the the SDR receiver. It is common place for the ADCs in SDR receivers to be over specified as their applications are unknown prior to their selection and the best available ADC is selected.

A number of options are available to implement the digital preprocessor. For very high sample and data rates, this is usually implemented as a FPGA, which by nature are flexible in their functions and range of parameters. An FPGA can, of course, be programmed for any function desired. Typically, an FPGA would be programmed to perform the quadrature demodulation and tuning, channel filtering, and data rate reduction among others. The FPGA is capable of implementing and performing most signal processing tasks and control all of the features in the other elements.

## 3.4 Universal Software Radio Peripheral

The USRP is a hardware platform that encompasses the software radio paradigm. It has been designed to interface primarily with the GNURadio software, thereby providing a cheap, flexible and high speed software radio prototyping test bed. The USRP is comprised of the motherboard, which houses a FPGA for high speed signal processing, and interchangeable daughterboards that cover different frequency ranges. The average cost of the USRP motherboard and a single daughterboard is US\$1000.00

The USRP provides several functions; digitization of the input signal, digital tuning within the IF band, and sample rate reduction before sending the digitized baseband data to the computing platform via the USB interface. It provides the opposite processing functions for the transmit path.

Figure 3.1 below shows the high level block diagram of the USRP board with daughterboards and Figure 3.2 shows an image of the USRP with the basic daughterboards plugged in.

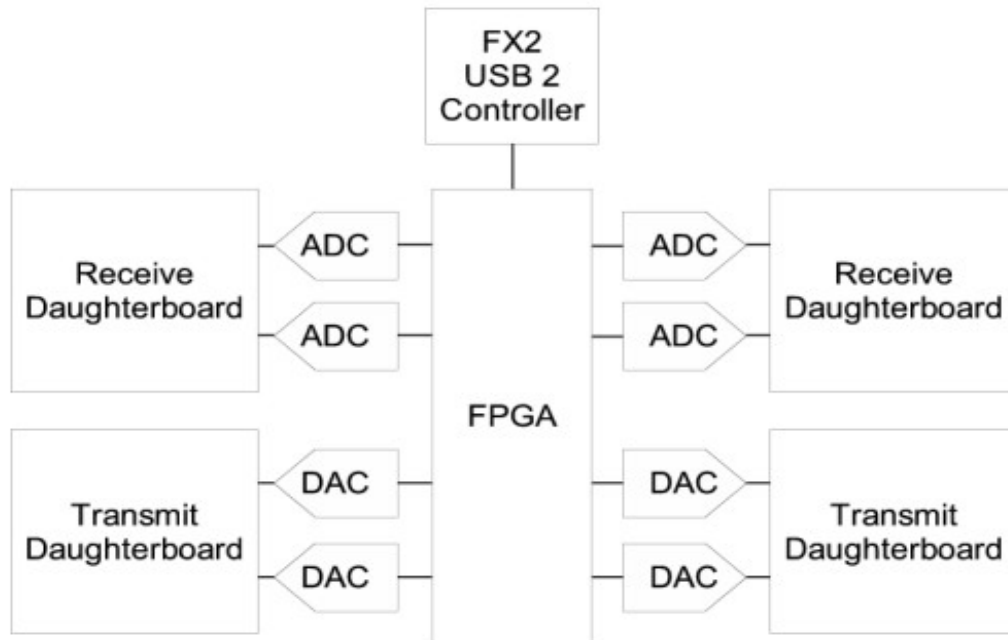


Figure 3.1: USRP and daughterboard block diagram [5]

### 3.4.1 FX2 USB 2 Controller

The FX2 microcontroller contains an embedded USB 2.0 transceiver and handles all USB transfers with the upstream USB host. It presents a data bus to the FPGA, with generic control signals which can be programmed to behave in a custom manner. This interface is called the *General Purpose Interface* (GPIF).

The FX2 also handles all USB control requests, which all USB enabled devices must support to fully comply with the USB standard. These include responses to device capability interrogations and standard setup requests [32].

### 3.4.2 ADCs and DACs

The analogue interface portion houses the Analog Devices, AD9862. The AD9862 provides several functions. Each receive section contains two ADCs. The ADCs operate at 64 Msamples/second with 12 bits of resolution and with reference to the Nyquist criterion the ADCs are capable of digitising a band 32MHz wide.

Positioned ahead of the ADCs there are *programmable gain amplifiers* (PGA) with 20dB of gain available to adjust the input signal level in order to maximise use of the ADCs dynamic range which evaluates to approximately 72dB of dynamic range. The full range on the ADCs is 2V peak to peak, and the input is 200 ohms differential. This is equates to 5mW, or 7dBm.

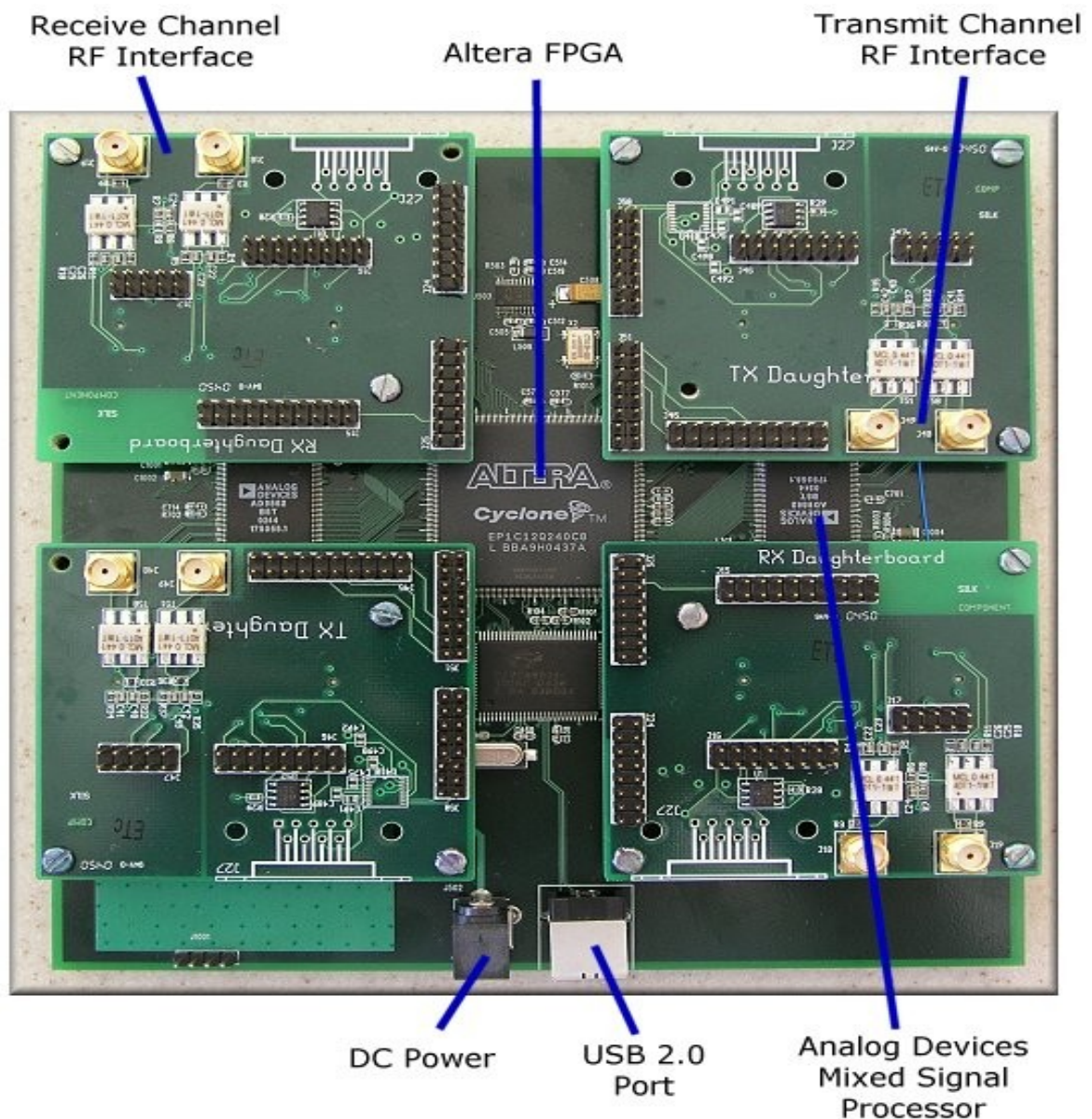


Figure 3.2: USRP and daughterboards [39]

The transmit path provides an interpolater and upconverter to match the output sample rate to the DAC sample rate and convert the baseband input to a low IF output. There are PGAs after the DACs. The DACs operate at 128 Msamples/second with 14 bits of resolution and can supply a 50 ohm differential load, with 10mW or 10dBm. There is also PGA used after the DAC, providing up to 20dB gain.

This is shown in the ADC block diagram, in Figure 3.3.

In any digitisation process, the faster that the signal is sampled, results in an effective gain of received SNR.

Furthermore, the relationship between the SNR and sampling rate in the signal bandwidth is given by:

$$SNR = 6.02 N + 1.76\text{dB} + 10 \log\left(\frac{f_s}{2B}\right) \tag{3.1}$$

where:

- $N$  is the number of bits of resolution of the ADC
- $f_s$  is the sampling rate of the ADC
- $B$  is the Bandwidth of the signal

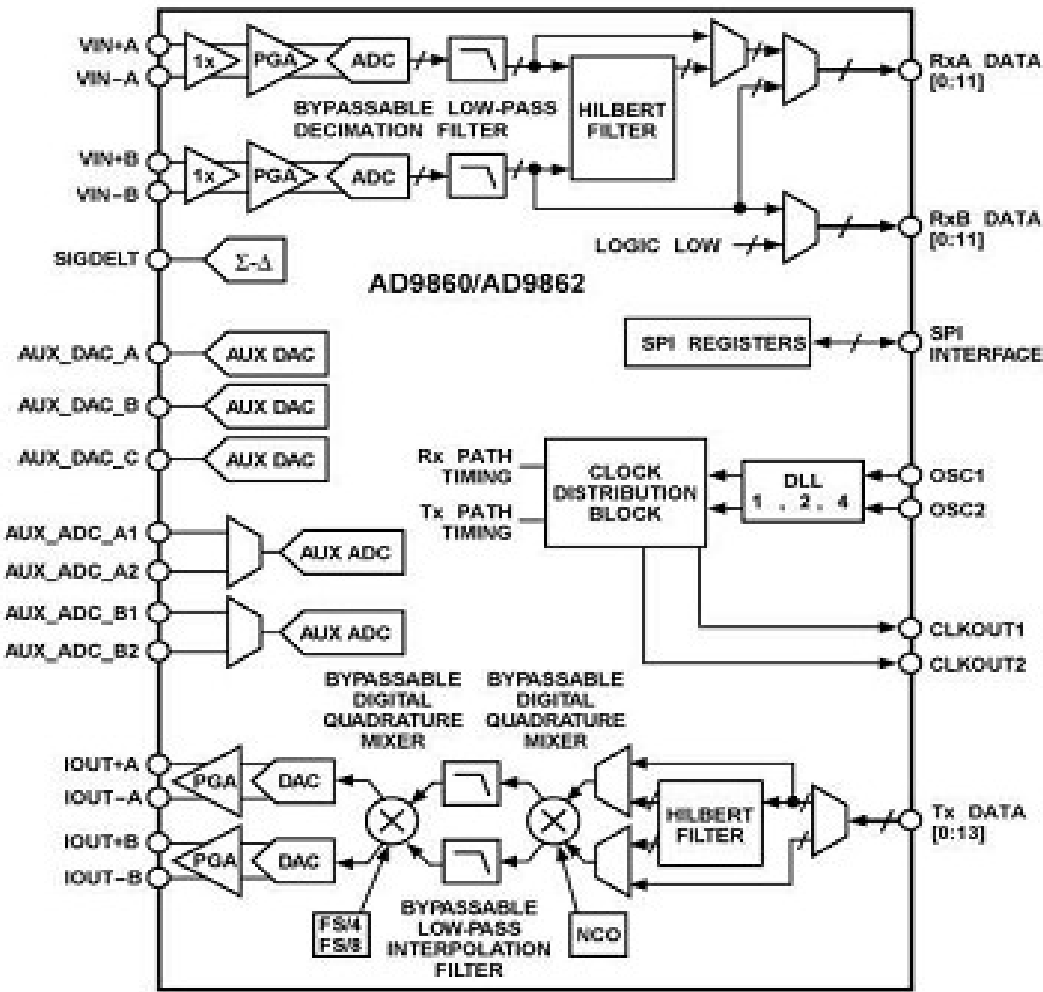


Figure 3.3: AD9862 ADC block Diagram [38]

### 3.4.3 FPGA

The FPGA employed by the USRP is the Altera Cyclone and performs the high speed signal processing. Furthermore, the FPGA manages the signal including reducing the data rates to facilitate their transport over the USB2 interface chip, the Cypress FX2, to the host PC where less intensive processing takes place. The FPGA and the FX2 chip are programmed over the USB2 bus.

The clock provided by the USRP drives the ADCs at 64 Msp/s. If needed the AD9862 may divide this clock by two to reduce the sample rate. This only affects the clock rate of the ADCs, most of the sample rate conversion is done in the FPGA and is referred to as decimation in this case.

The block diagram of the USRP board and the high level FPGA signal processing blocks is shown in the image below.

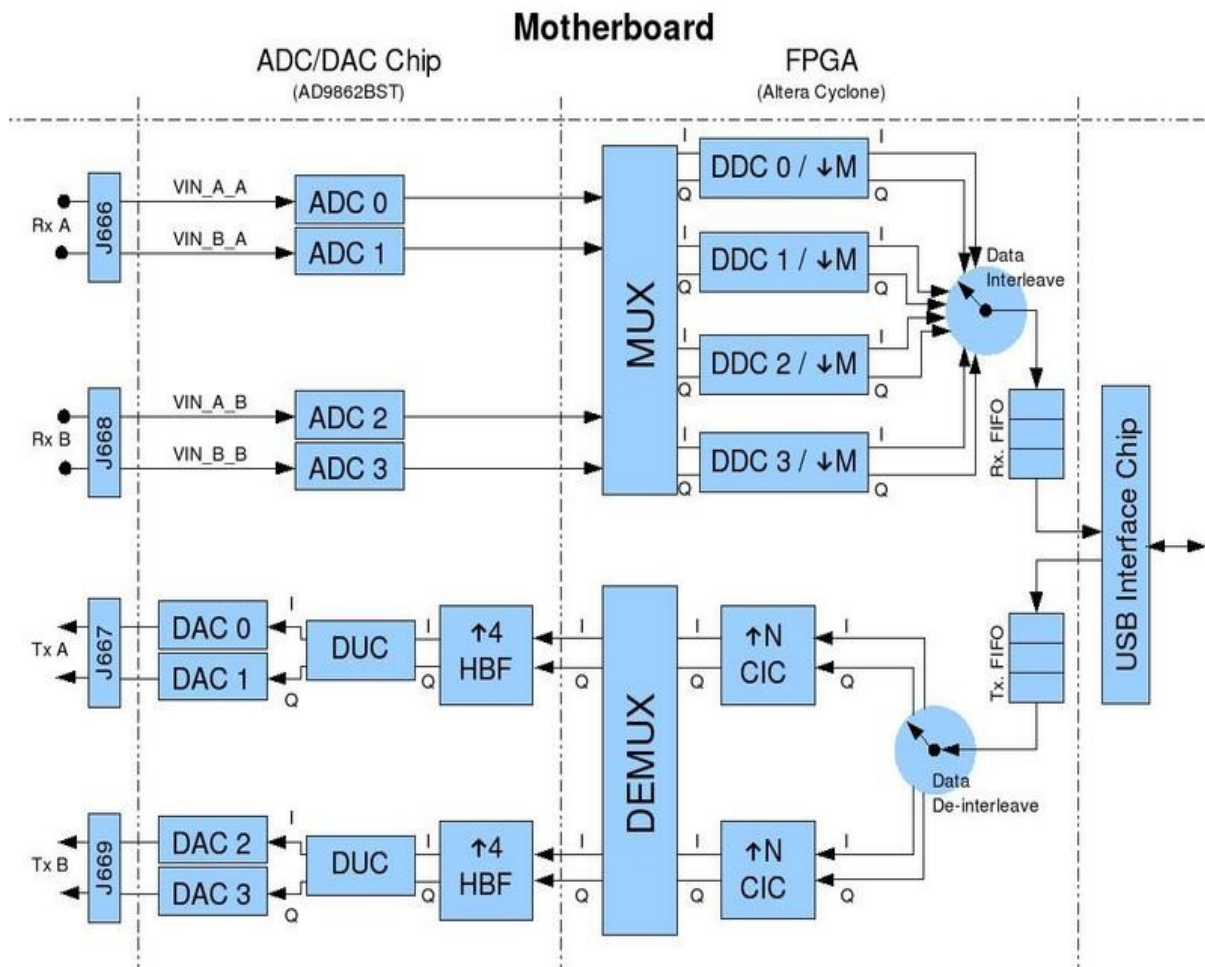


Figure 3.4: USRP and FPGA block Diagram [39]

Following the signals digitisation, the data is sent to the FPGA. The standard FPGA firmware provides two Digital Downconverters (DDC), a second FPGA implementation however provides an additional two DDCs. The FPGA uses a multiplexer to connect the input streams from each of the ADCs to the inputs of the DDCs.

The multiplexer allows the USRP to support both real and complex input signals and allows for having multiple channels selected out of the same ADC sample stream. The DDCs operate as real downconverters using the data from one ADC fed into the real channel or as complex DDCs where the data from one ADC is fed to the real channel and the data from another ADC is fed to the complex channel via the multiplexer.

The DDC consists of a *numerically controlled oscillator* (NCO), a digital mixer, and a cascaded integrator comb (CIC) filter. These components downconvert the desired channel from the IF to baseband, reduce the sample rate and provide low pass filtering. The effect of the NCO and multiplier are implemented using the CORDIC algorithm.

This shown in Figure 3.5.

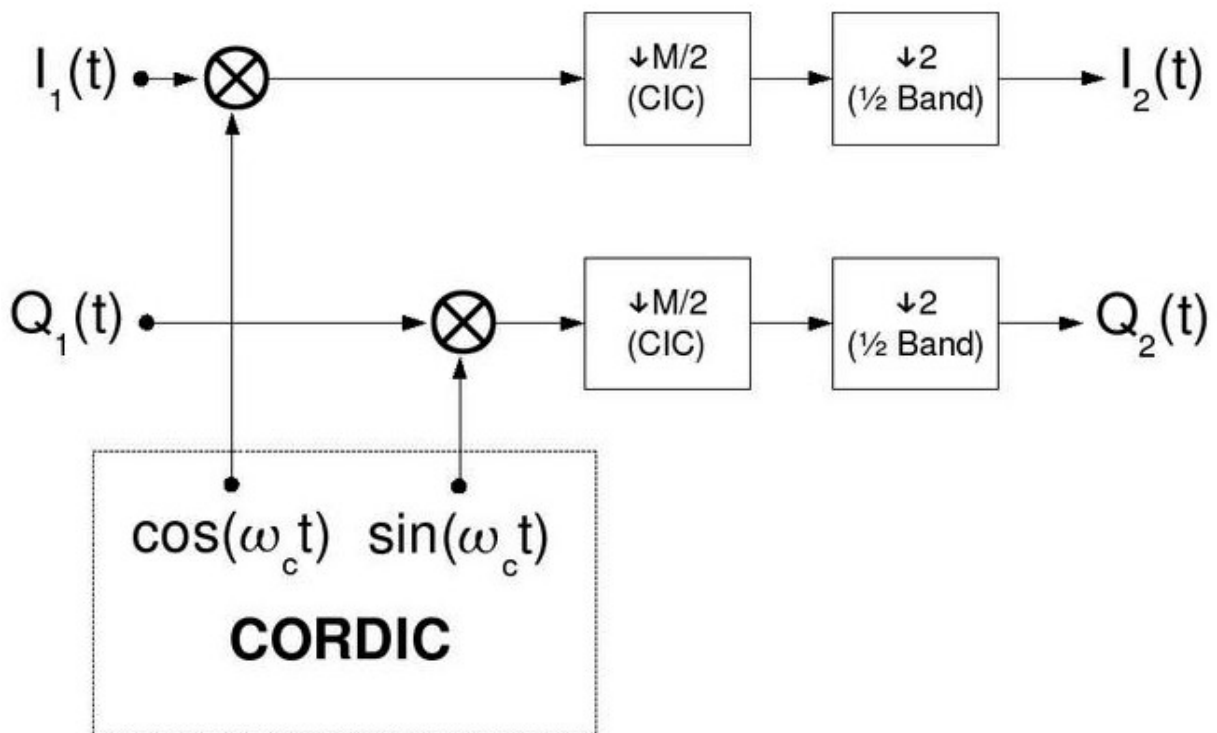


Figure 3.5: DDC block Diagram [39]

Since the USB bus operates at a maximum rate of 480 Mbps the FPGA must reduce the sample rate in the receive path. The decimator can be treated as a low pass filter followed by a downsampler. Suppose the decimation factor is  $D$ . If we look at the digital spectrum, the low pass filter selects out the band  $[-\pi/D, \pi/D]$  and then the downsampler spreads the spectrum to  $[-\pi, \pi]$ . So in fact, we have narrowed the bandwidth of the digital signal of interest by a factor of  $D$ .

The transmit path for the USRP is similar to the receive path, however there are differences. Since the sample rate the DACs operate at 128 Msps, it is necessary to increase the sample rate in order to match the sample rates between the high speed data converter and the lower speeds supported by the USB connection, this process is called interpolation and an interpolater running on the FPGA increases the data rate. The AD9862 also provides a further data rate increase by a factor of four. The transmit portion of the AD9862 provides the mixer and NCO required to set the IF frequency of the transmitted signal, the FPGA performs this function in the receive path.

This is shown in Figure 3.6.

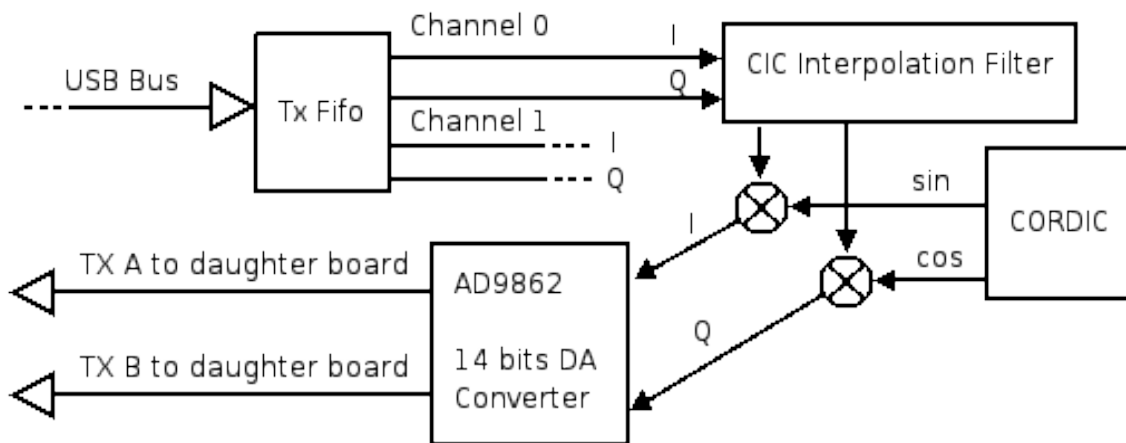


Figure 3.6: USRP transmit chain block Diagram [39]

### 3.4.4 The Daughterboards

On the motherboard there are four slots into which you can plug in up to 2 RX daughterboards and 2 TX daughterboards. The daughterboards are used to hold the the RF receiver interface or tuner and the RF transmitter.

There are slots for 2 TX daughterboards, labelled TXA and TXB, and 2 corresponding RX daughterboards, RXA and RXB. Each daughterboard slot has access to 2 of the 4 high-speed AD/DA converters (DAC outputs for TX, ADC inputs for RX). This allows each daughterboard which uses real (not IQ) sampling to have 2 independent RF sections, and 2 antennas (4 total for the system). If complex IQ sampling is used, each board can support a single RF section, for a total of 2 for the whole system.

A variety of daughterboards are available, including [6]:

#### Basic Tx and Rx Boards

The BasicTX and BasicRX are designed for use with external RF frontends as an IF interface. The ADC inputs and DAC outputs are directly transformer-coupled to SMA connectors 50 Ohm impedance with no mixers, filters, or amplifiers.

The BasicTX and BasicRX operate in the 1MHz to 250MHz range and give direct access to all of the signals on the daughterboard interface including 16 bits of high-speed digital I/O, SPI and I2C buses, and the low-speed ADCs and DACs, and as such are useful for developing custom daughterboards or FPGA designs.

#### LFTX and LFRX Boards

The LFTX and LFRX are very similar to the BasicTX and BasicRX, respectively, with 2 main differences. Because the LFTX and LFRX use differential amplifiers instead of transformers, their frequency response extends down to DC. The LFTX and LFRX also have 30 MHz low pass filters for anti aliasing.

## DBSRX

The DBSRX is a complete receiver system for 800 MHz to 2.4 GHz with a 3-5 dB noise figure. The DBSRX features a software controllable channel filter which can be made as narrow as 1 MHz, or as wide as 60 MHz.

The DBSRX frequency range covers many bands of interest, including all GPS and Galileo bands, the 902-928 MHz ISM band, cellular and PCS, the Hydrogen and Hydroxyl radio astronomy bands, DECT, and others. The DBSRX is MIMO capable, and can power an active antenna via the coax.

## RFX

The RFX family of daughterboards turns a USRP motherboard into a complete RF transceiver system. An antenna is necessary in order to achieve two-way, high bandwidth communications in many popular frequency bands. The family of RFX daughterboards cover a frequency range from 400MHz to 2.9GHz. The boards have many features which facilitate their integration into more complex systems, such as digital control lines and the option for split transmit and receive ports.

## TVRX

The TVRX daughterboard is a complete VHF and UHF receiver system based on a TV tuner module. It operates over a 6 MHz wide block of spectrum from anywhere in the 50-860 MHz range. All tuning and AGC functions can be controlled from software.

Different tuner modules have been used for the TVRx. They differ in the frequency of the IF output and whether or not they perform a single-conversion or a second down-conversion. In this dissertation the module using a single-conversion approach to 43.75MHz has been used. The alternative module offers a second conversion to 5.75MHz.

This board will be used as the front end for the PCL system and thus is used in all the receiver tests conducted and forms the subject of the receiver characterisation presented in this dissertation.

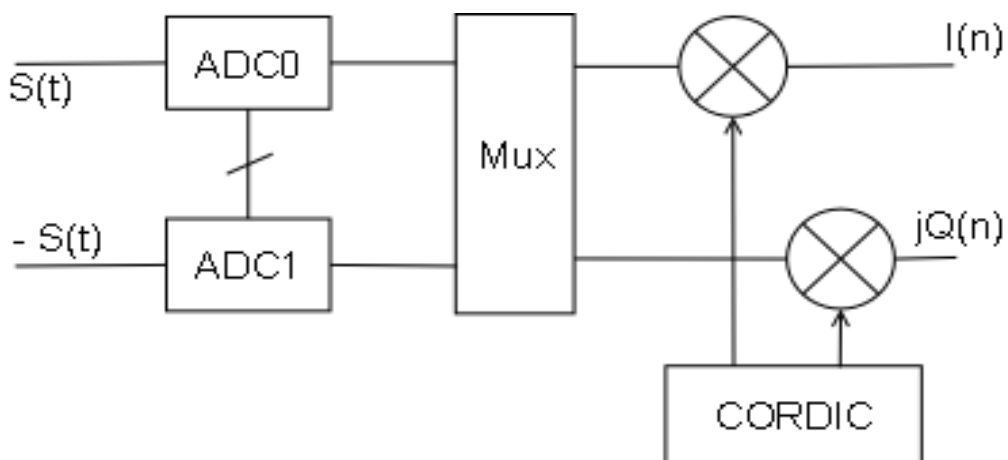


Figure 3.7: Signal flow from a single TVRx daughterboard to DDC0

The block diagram in Figure 3.7 is representative of the flow path of the TVRx signal. The daughterboard produces a differential pair as output, shown as the signal  $S(t)$  and  $-S(t)$ . These signals, after they have been digitised, are routed via the multiplexer to the inputs of the DDC0. It is at this stage that the complex signal  $I(n) + jQ(n)$  is produced. In the instances where the second TVRx daughterboard is used, a second differential pair is produced, digitised at ADC2 and ADC3 respectively and routed to DDC1 through the multiplexer. Thus two IQ pairs are sent from the USRP to the PC via the USB for further processing.

## 3.5 GNURadio

GNURadio is an open source, software defined, radio platform for building and deploying software radios. It has a large worldwide community of developers and users that have contributed to a substantial code base and provided many practical applications for the hardware and software.

It provides a complete development environment to create software radios, handling all of the hardware interfacing, multi threading and portability issues. GNU Radio has libraries for all common software radio needs, including;

various modulations:

- GMSK
- PSK
- OFDM

error-correcting codes:

- Reed-Solomon
- Viterbi
- Turbo Codes

signal processing constructs

- optimized filters
- FFTs
- equalizers
- timing recovery
- Scheduling

It is a very flexible system, it is user expandable and it allows applications to be developed in C++ or Python.

### 3.5.1 The GNURadio Architecture

GNU Radio is organised using a two-tier structure that provides a data flow abstraction. It builds applications using python code for high level organisation, policy, GUI and other non performance critical functions, by employing the concept of a graph containing signal processing blocks and connections for data flow between them.

The signal processing blocks are implemented and correspond to some sophisticated functions or class methods in C++.

Many processing blocks currently exist within the GNURadio framework and include filters, demodulators and other signal manipulation elements.

A graph can be thought of as a framework upon which all the necessary elements are placed and then connected. Using a schematic diagram as an analogy for a graph, the elements placed on the schematic include the resistors, amplifiers, etc. These components are then “wired” up for current to flow between them. Thus in GNU Radio, the circuit parts are replaced by signal sources, sinks and the signal processing blocks.

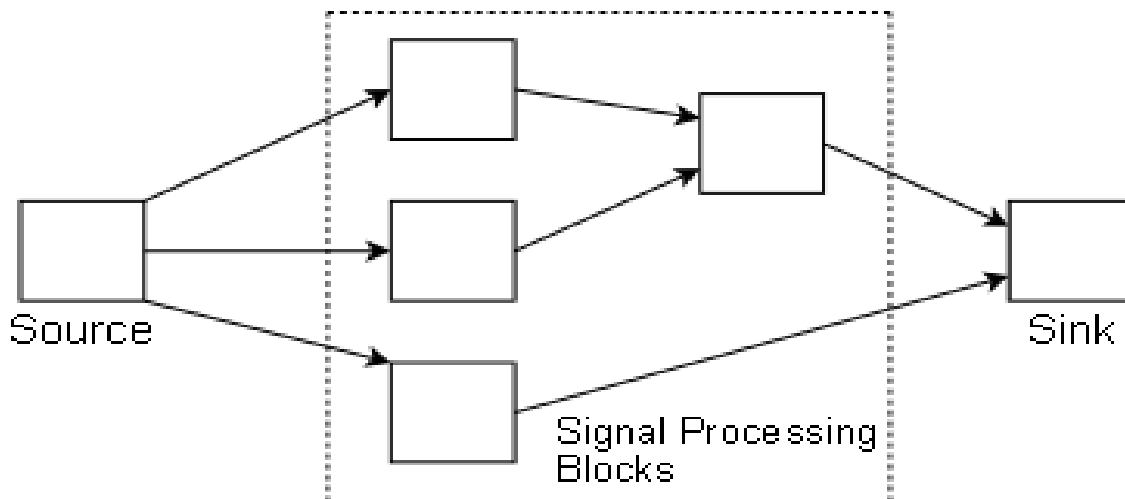


Figure 3.8: GNURadio application structure

Conceptually, blocks process infinite streams of data flowing from their input ports to their output ports. Blocks’ attributes include the number of input and output ports they have as well as the type of data that flows through each. The most frequently used types are short, float and complex. The *Simplified Wrapper and Interface Generator* (SWIG), is what enables the C++ implementation of the various blocks to be used from Python.

Some blocks have only output ports or input ports. These serve as data sources and sinks in the graph. The signal source can have various implementations, but is usually the USRP or a file containing sampled data. The signal stream then flows through any number of processing nodes. The final output of the processing graph terminates in a signal sink, which may be a real time spectrum analyser, a real time oscilloscope, an output file, the USRP or audio hardware. It is estimated that 100 blocks are implemented in GNURadio and new blocks can be written as desired.

This framework allows for simple implementation of powerful signal processing systems.

An elementary application is presented here to present the concepts.

```
#>>> bring in blocks from the main gnu radio package
from gnuradio import gr
#>>> bring in the audio source/sink
from gnuradio import audio

#>>> create the flow graph
fg = gr.flow_graph()

#>>> create the signal sources
#>>> parameters: samp_rate, type, output freq, amplitude, offset
src = gr.sig_source_f(32000, gr.GR_SIN_WAVE, 350, .5, 0)

#>>> create a signal sink
#>>> parameters: samp_rate
sink = audio.sink(32000)

#>>> connect the source to the sink
fg.connect(src, sink)

#>>> run the flow graph
fg.run()
```

### 3.5.2 Common GNURadio Blocks

As mentioned earlier, an estimated 100 signal processing blocks are predefined in the GNU Radio environment. The best way to become acquainted with these is to explore the GNU Radio Documentation. This can be found on line at <http://gnuradio.org/doc/doxygen/index.html>.

For demonstration purposes, two of the frequently used blocks will be mentioned here.

**Block:** `usrp.source_c [s]`

**Usage:**

```
usrp.source_c (s) (int which_board,
                unsigned int decim_rate,
                int nchan = 1,
                int mux = -1,
                int mode = 0 )
```

The suffix *c* (complex), or *s* (short) specifies the data type of the stream from USRP. Most likely the complex source (I/Q quadrature from the digital down converter (DDC)) would be more frequently used. *which\_board* specifies which USRP to open, which is probably 0 if there is only one USRP board. *decim\_rate* tells the digital down converter (DDC) the decimation factor *D*. *nchan* specifies the number of channels, 1, 2 or 4. *mux* sets input MUX configuration, which determines which ADC (or constant zero) is connected to each DDC input ‘-1’ means we preserve the default settings. *mode* sets the FPGA mode, which we seldom touch.

The default value is 0, representing the normal mode. Quite often we only specify the first two arguments, using the default values for the others.

For example:

```
usrp_decim = 250
```

```
src = usrp.source_c (0, usrp_decim)
```

**Block:** `calc_dxc_freq ()`

**Usage:**

```
usrp.calc_dxc_freq(number target_freq,  
                  number baseband_freq,  
                  number fs)
```

This function is a utility to calculate the frequency to be used for setting the digital up or down converter. It returns a 2-tuple (`ddc_freq`, `inverted`) where *ddc\_freq* is the value for the DDC and *inverted* is True if we are operating in an inverted Nyquist zone. *target\_freq* specifies the desired RF frequency in Hz. *baseband\_freq* is the RF frequency that corresponds to DC in the IF and *fs* is the converter sample rate.

### 3.5.3 Hardware

Various hardware options are available for use with GNU Radio. For instance, the sound card can be used as an output sink. Wide band I/O and VXI/cPCI cards can also be used as additional options. However, largely identified as the primary hardware choice as regards GNURadio is the USRP.

## 3.6 Summary

Included in the objectives of the overall PCL project is the development of a radar system at considerably low cost. In pursuit of this, SDR has been identified as a candidate technology. In this chapter a presentation of the definition and paradigm of SDR is made, including their applications and the development tools available.

Furthermore, the considerations in the design of SDR receivers is made, facilitating the characterisation and testing of the SDR toolkit selected for the implementation of our radar receiver.

In the light of this, the USRP and GNURadio are examined, the USRP provides a flexible and powerful FPGA, developed by Altera, as the processing unit, which implements a great deal of the signal processing in the receive and transmit chains. Furthermore, the USRP hosts two Analog Devices AD9862 chips, each providing a two ADCs sampling at a rate of 64 Msamples/second with 12 bits of resolution and two DACs operating at 128 Msamples/second with 14 bits of resolution.

Moreover, the AD9862 chips provide two auxiliary ADCs and three auxiliary DACs which can provide further flexibility in computation and control of external daughterboard components. These daughterboard boards provide front end flexibility allowing for the down-conversion and thus manipulation of the radio spectrum.

GNURadio, is seen to be a powerful toolkit that implements numerous complex signal processing elements and additionally interfaces with the USRP. Thus combining to provide a powerful and widely versatile toolset for the development of a variety of radio devices.

The following chapter tests the USRP and GNURadio in a variety of performance related issues and therefore, allowing for comment on its usefulness for our application.

# Chapter 4

## Receiver Characterisation

### 4.1 Introduction

The most critical component of a wireless system often is its receiver. The purpose of this is to extract the desired signal reliably from the various sources of signals, interference and noise.

The following sections will present the characterisation of the USRP with the TVRx daughterboard and GNURadio as a receiver in the PCL system being investigated.

At this time, various aspects of the overall project are still under investigation and research. As a result, the specific requirements that the receiver system must meet are not available. However, the performance of GNURadio in its control of the USRP with the TVRx daughterboard and some of the fundamental principles of radio receiver and digital radio receiver design are identified, discussed and measured, thereby facilitating this examination.

The results of the characterisation will be presented within the body of each section, in order to facilitate coherency in its reading.

### 4.2 Test System Overview

This section will describe the manner in which the equipment was setup in order to measure the various characteristics described in this chapter.

The test signal is generated by a Hewlett Packard 8656B signal generator, with the output frequency set to 100MHz. The signal generator has the desirable functionality to vary the power of the signal output generated. The signal is fed into the USRP, setup with the TVRx daughterboard, and after digitisation is sent to the PC. In addition to this, a Hewlett Packard 54645D oscilloscope is used to probe the pin outs of the TVRx daughterboard. The individual test conditions will be further described in the relevant subsection.

The test equipment is pictured in Figure 4.1.

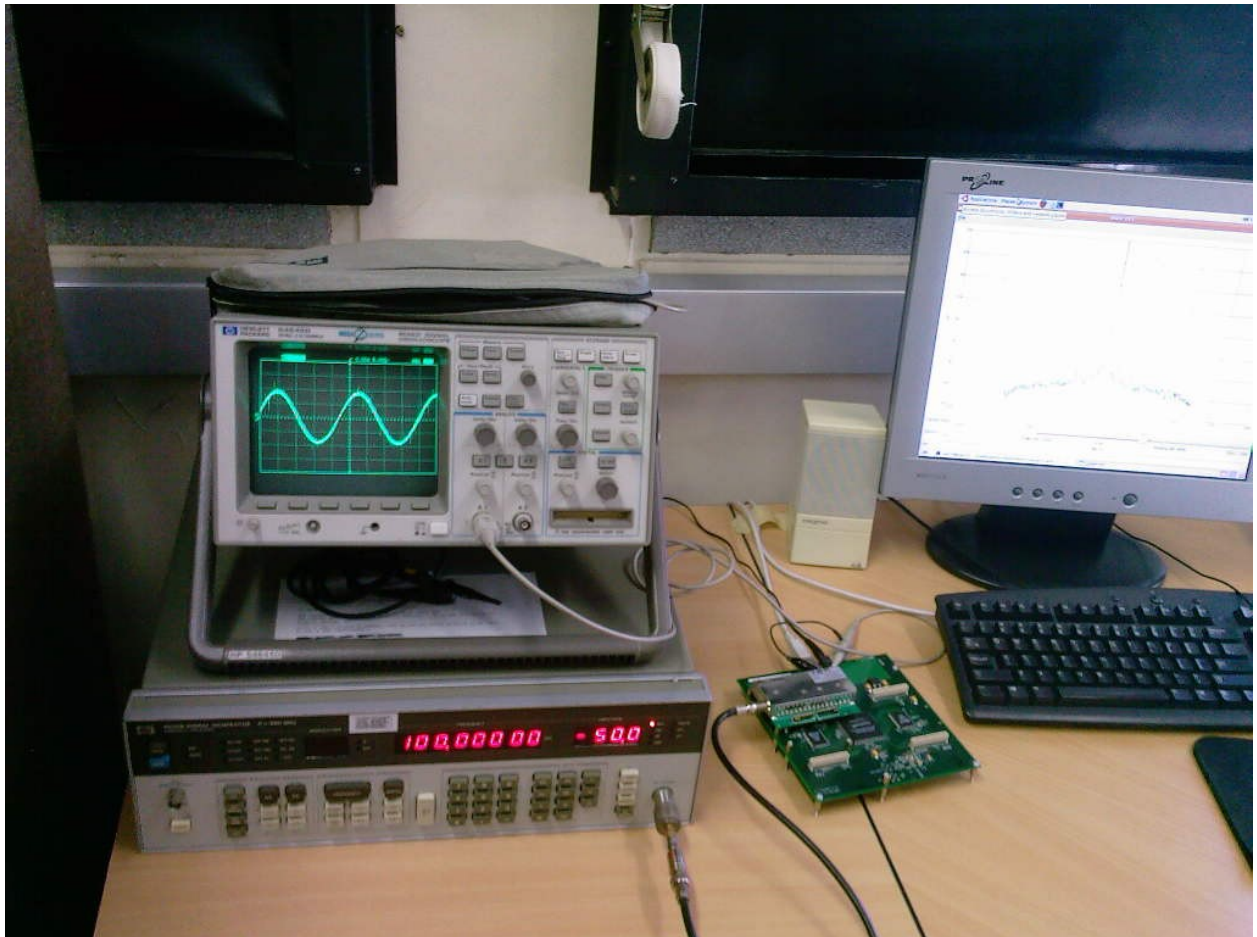


Figure 4.1: Experimental setup used in characterisation tests

### 4.3 Receiver Bandwidth

The TVRx daughterboard is built on the Microtune 4937 D15 RF tuner module. The instantaneous bandwidth by definition is the frequency band over which multiple signals are able to be simultaneously amplified to within a specified gain tolerance [29]. The bandwidth is an important property as it affects the noise and signal and has a direct impact on the level of signal processing gain achievable by the receiver as eluded to by Equation 2.6. This module provides a static 6MHz bandwidth, referenced to the centre frequency that the module is tuned to. With respect to our application, the signals of interest are the Broadcast FM signals and the target returns from the surveillance areas which have a bandwidth of 100kHz. Thus the receiver provides much more than the requisite bandwidth. Furthermore, we can sustain 32MB/second across the USB. All samples sent over the USB interface are in 16 bit signed integers in IQ format, i.e. 16 bit I data followed by 16 bit Q data, resulting in 8M complex samples/second across the USB. This provides a maximum effective total spectral bandwidth of about 8MHz.

The FPGA provides the functionality of altering the decimation rate and thus allowing us to select narrower ranges. For instance, the bandwidth of a FM station is 100kHz, by selecting the decimation factor to be 250, the effective bandwidth across the USB is  $64\text{MHz} / 250 = 256\text{kHz}$ , which is well suited for the 100kHz bandwidth without losing any spectral information.

## 4.4 Gain Range and Control

The TVRx daughterboard has two AGC inputs available to level the signal. A block diagram of this is presented in Figure 4.2. The daughterboard has a RF AGC range of 50dB and an IF AGC range of 33dB. GNURadio achieves this gain variation by varying the voltage on to each of these inputs. As mentioned in the previous chapter the ADC that follows the daughterboard provides an additional level of amplification using its internal PGA, that provides an additional 20dB of gain.

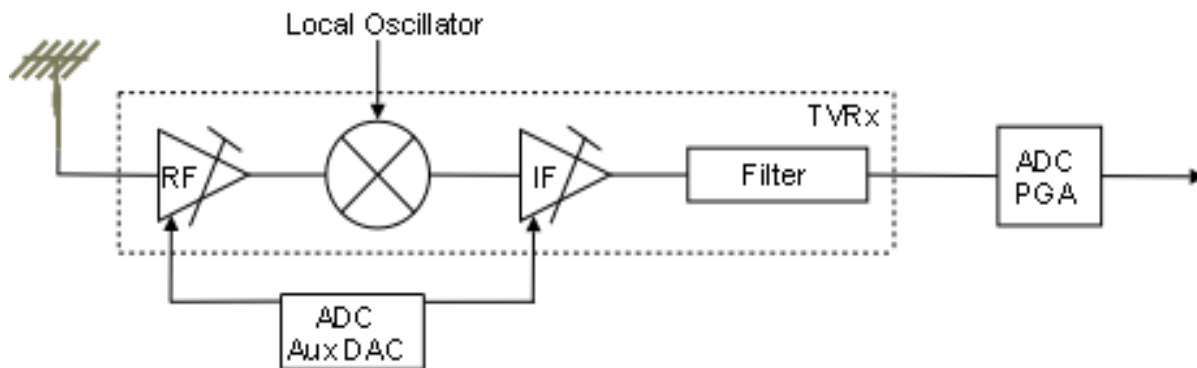


Figure 4.2: Block diagram showing TVRx gain stages

All three stages are set altogether via the `set_gain(gain in dB)` method. However, since multiple signals are to be processed simultaneously, the use of an AGC can result in a reduction of RF sensitivity and will cause weaker signals to be dropped. GNURadio proves its versatility in this instance as the `set_gain` method can be bypassed and each gain stage set manually and independently.

In the following tests conducted on the receiver and in those of later sections, the AGC was disabled and the amplifier stages were set independently. Figure 4.3 and Figure 4.4 show the variation of the voltage applied to the AGC pins of the daughterboards to the gain of the individual stages.

The RF stage exhibits a linear increase in the gain, which accurately describes the behaviour of the amplifier between the 10dB and 40dB range. Above 40dB the amplifier begins to run into saturation [37] and does not continue to show the linear conversion gain. The IF stage additionally exhibits a linear increase in gain. This is an accurate description of the amplifier behaviour in the range from 0dB to 15dB. Thus, GNURadio provides us with an accurate description of the TVRx daughterboard's amplifier behaviour in the region from 10dB to 55dB. The PGA additionally, has a linear gain curve [38] and provides a further 20dB of gain, extending the gain range up to 75dB.

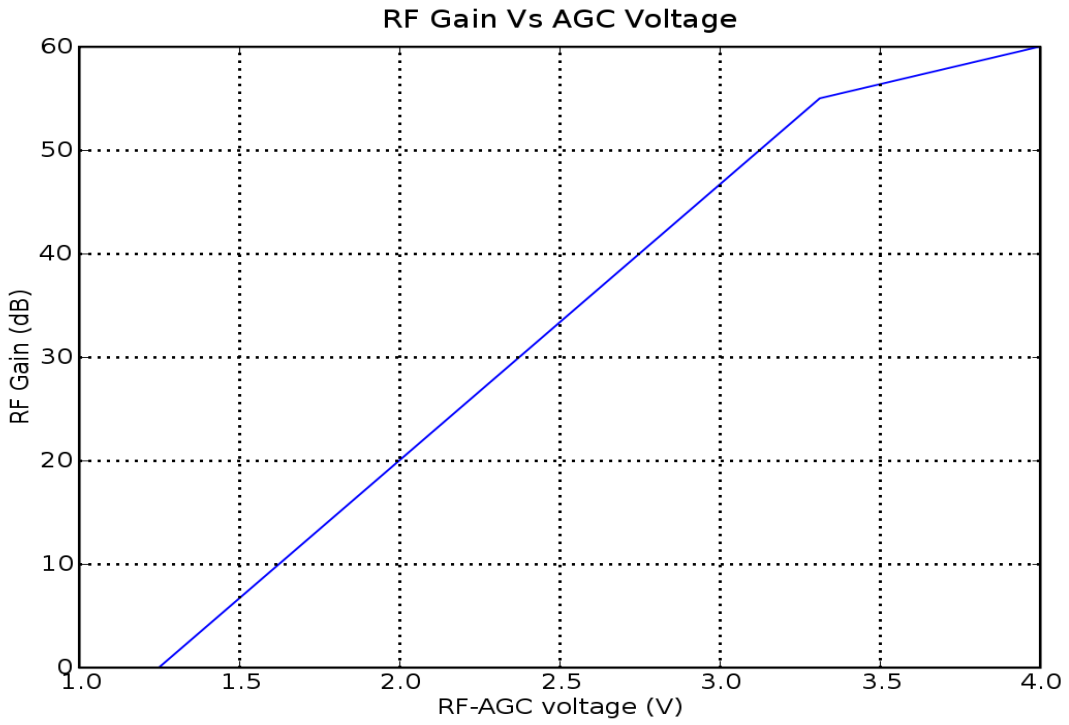


Figure 4.3: Variation of voltage applied to RF AGC against RF Gain

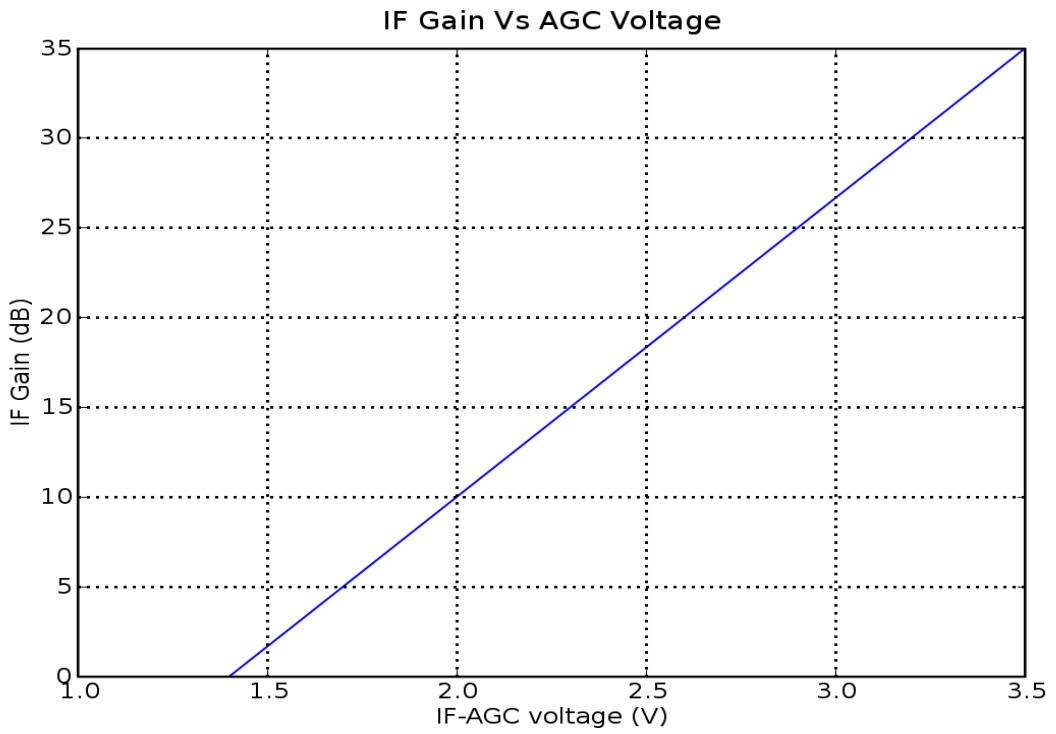
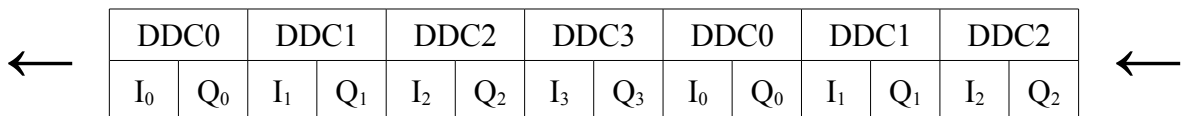


Figure 4.4: Variation of voltage applied to IF AGC against IF Gain

## 4.5 Multiplexer Usage and Data Interleaving

The FPGA multiplexer is like a router. It determines which ADC is connected to each DDC input. There are 4 DDCs and each has two inputs. GNURadio controls the multiplexer using the `usrp.set_mux()` method.

The multiple RX channels, which can be either 1,2, or 4, must all be the same data rate. Therefore, the same decimation ratio must apply to all the channels. This condition additionally applies to the TX channels, however they may be different to the RX rate. When there are multiple channels, GNURadio interleaves the channels. This means that with 4 channels, for instance, the sequence sent over the USB would be:



The USRP can operate in full duplex mode, the transmit and receive sides are completely independent of one another. The only consideration is that the combined data rate over the USB must be 32 MB/sec or less.

The `set_mux` parameter is 32 bits, each nybble of 4 bits controls which ADC is connected to which DDC input. The least significant nybble of the parameter represents DDC0 and the most significant nybble of the parameter represents DDC3.

DDC3		DDC2		DDC1		DDC0	
Q <sub>3</sub>	I <sub>3</sub>	Q <sub>2</sub>	I <sub>2</sub>	Q <sub>1</sub>	I <sub>1</sub>	Q <sub>0</sub>	I <sub>0</sub>

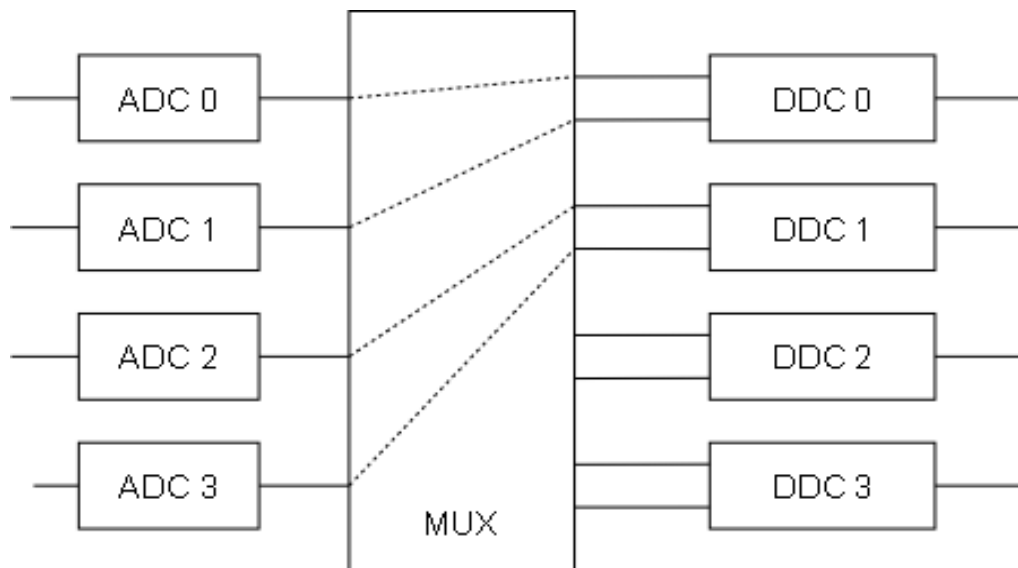


Figure 4.5: Multiplexer setup for two TVRx to DDC0 and DDC1

In Figure 4.5, the multiplexer parameter is set as 0x----3210, we are not concerned about the upper nybble as those bits set DDC3 and 2, represented here by dashes. However, we see that the I and Q values of DDC0 and DDC1 are set up accordingly.

## 4.6 Frequency Range and Control

The TVRx daughterboard that we are using uses a single conversion approach to 43.75MHz with the reception frequency divided into the VHF low, VHF high and UHF bands from 50MHz to 860MHz. The band selection and tuning is done via the I<sup>2</sup>C bus, this coordinated from within GNURadio. The tuning range is the frequency band over which the receiver will operate without degrading the specified performance [29].

The oscillator frequency is driven by a 4MHz crystal reference and determined by the following:

$$f_{osc} = f_{ref} \times 8 \times SF \quad (4.1)$$

where:

$f_{ref}$  is the crystal reference frequency / Reference divider  
 $SF$  is the programmable scaling factor

The reference divider mentioned above can take on one of three values, those being 512, 640 and 1024. This value is set from within GNURadio and the default is set at 640. The value of this reference divider influences the tuning step size, otherwise understood as the granularity of the tuner in setting the local oscillator frequency. The default choice results in a tuning step size of 50.0kHz with a potential minimum of 31.25kHz. This level of resolution is adequate for our application.

GNURadio sets up the appropriate byte values in the I<sup>2</sup>C data by use of the following method.

**Block:** `usrp.tune ()`

**Usage:**

```
usrp.source_x.tune (u,
                    chan,
                    subdev,
                    target_freq)
```

Tuning is a two step process. First we ask the frontend to tune as close to the desired frequency as it can. Then we use the result of that operation and our `target_freq` to determine the value for the digital down converter. The function returns `False` if there is a failure, in the case of success it returns `tune_result`. `U` is the instance of the usrp that we want to tune. `chan` is the DDC channel that we wish to tune. `Subdev` tells the method which daughterboard subdevice to tune and `target_freq` is the centre frequency in Hz.

However, GNURadio does offer the flexibility to control individual parts of the tuning process, e.g. tuning the TVRx frontend and setting the value of the digital down converter independently.

## 4.7 Spurious Artifact

During testing it was found that when a GNURadio application is run, the USRP generates a large spurious output, this applies additionally to instances where the application is stopped and started again. This spurious output does corrupt data that is being stored to memory on the PC for offline post processing. However, when the USRP is used for real time processing it does not present a concern, as the spurious output occurs at the start of the data. Figure 4.6 shows this artifact at the beginning of a data.

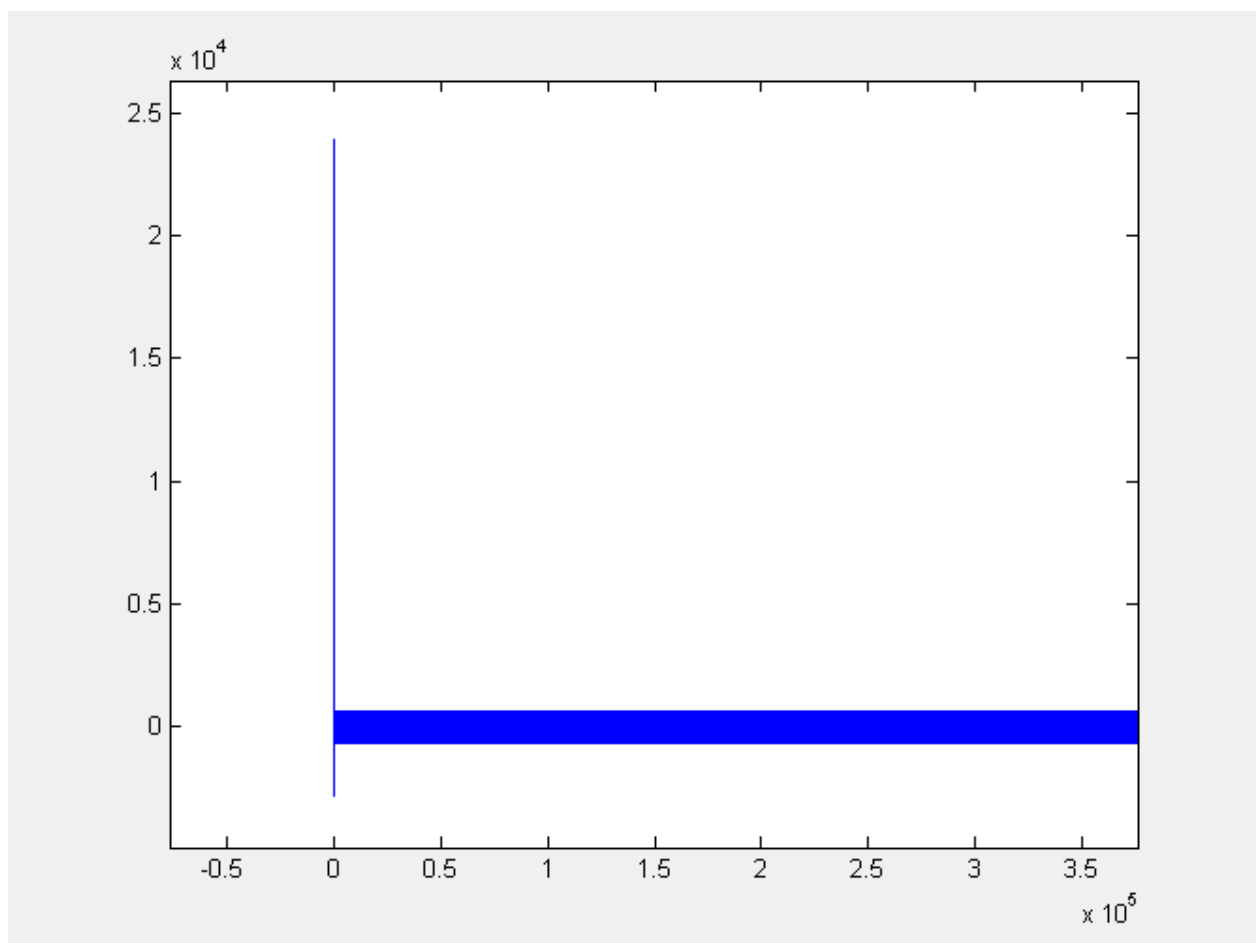


Figure 4.6: Spurious signal generated by USRP on startup

Figure 4.7 shows a zoomed in image of this artifact, illustrating the corruption of the first approximately 80 samples. In order to mitigate the effects of this artifact, this data is simply cut off and the number of remaining samples made note of in the processing that follows.

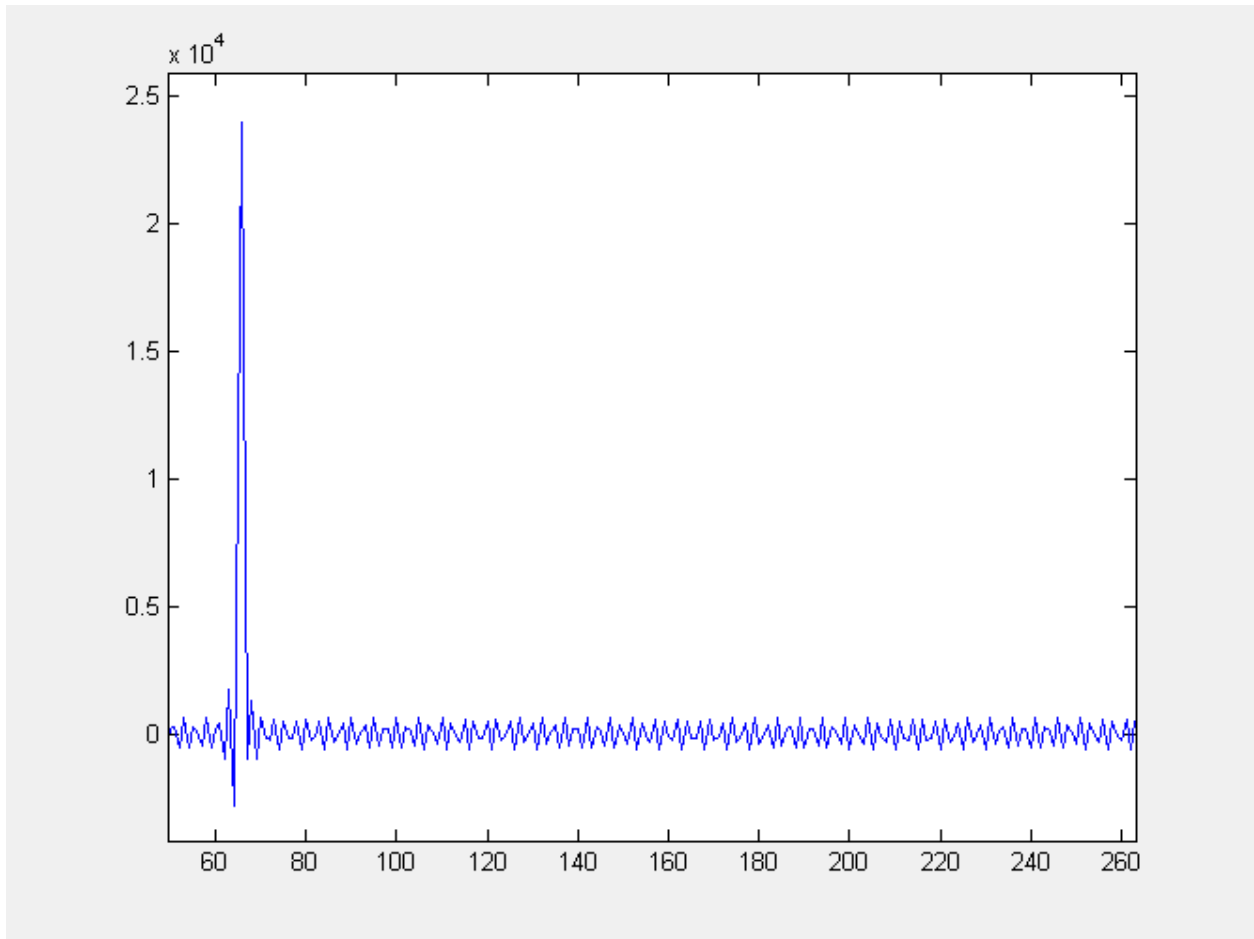


Figure 4.7: Closer look at the spurious signal generated by USRP on startup

## 4.8 Receiver Noise Figure

The noise figure is a measure of how much noise a component or system adds to a signal. The noise figure of a system depends on the losses in the circuit, the nature of the solid state devices, any bias applied and on amplification, to name but a few. When noise and a desired signal are applied to the input of a noiseless system, it is expected then that the noise and signal would be amplified or attenuated by the same factor, thus the SNR through the system would remain unchanged.

A noisy system, however, will introduce noise. Thus the noise power will increase relative to the signal power, thereby reducing the SNR at the output of the system.

The noise figure of a component is, by definition, independent of the noise input into the component and thus is based on a standard input noise source  $N_i$ , at room temperature in a bandwidth  $B$ , thus:

$$N_i = \kappa T_0 B \quad (4.2)$$

Where:

$\kappa$  is the Boltzmann constant

$T_0$  is the room temperature 290K

Assuming a 1Hz bandwidth this value evaluates to the standard,  $4 \times 10^{-21}$  W, which can be further expressed as -204dBW, which is further still expressed as -174dBm. The noise figure in essence is the difference between the noise output of the receiver and the noise output of an ideal, noiseless receiver.

Noise figure is the decibel notation of the noise factor, which is defined as:

$$F = \frac{SNR \text{ at input}}{SNR \text{ at output}} = \frac{S_i / N_i}{S_o / N_o} \quad (4.3)$$

In a typical receiver, the input signal will pass through a number of cascaded components such as filters, amplifiers and mixers, among others. Each stage will inject a degree of noise into the signal, degrading the signal to noise ratio. This makes it important to quantify the overall effect of the noise figure on the system's performance.

Consider the network shown in the figure below, the total noise factor referenced to the input to the system is determined using the Friis equation as:

$$F_{total} = F_1 + \frac{F_2 - 1}{G_1} + \frac{F_3 - 1}{G_1 G_2} + \dots + \frac{F_N - 1}{G_1 G_2 \dots G_{N-1}} \quad (4.4)$$

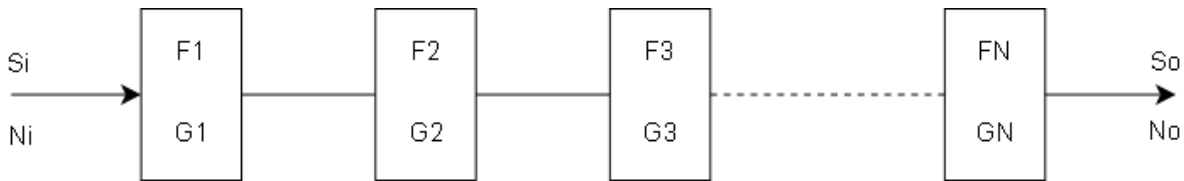


Figure 4.8: Cascaded components

The characteristics of the cascaded system are dominated by the earlier stages. This is as the later stages are reduced by the product of the gains of the preceding stages. Thus the ideal scenario is one in which the first stage or component of a system has a low noise figure and a high gain to ensure the low noise figure for the overall system.

In order to determine the noise figure of the receiver system, a known signal of low magnitude is input. In this instance -50dBm was input. The USRP was setup with a decimation rate of 64, thus providing an effective 1MHz of bandwidth for analysis. A spectrum analyser was setup, with 1024 points of measurement resolution thus providing a reading representing 1kHz per measurement bin. This setup allows for the measurement of the noise floor per bin, by observing how far down the noise is from the input signal. The noise floor is a further 38dB below this level, measured in dBm/Hz. The noise figure is then determined by the difference between this signal and the theoretical level of -174dBm/Hz, derived from Equation 4.2. The noise figure of the TVRx and the USRP is thus determined to be 10dB.

## 4.9 Sensitivity

The sensitivity of a receiver is defined as the lowest power level at which the receiver can detect an RF signal and demodulate data; it is a specification that is associated solely with the receiver system and is independent of the transmitter. As the signal propagates away from the transmitter, the power density of the signal decreases, this makes it more difficult for a receiver to detect the signal as the distance increases. Receivers with desirable sensitivity levels are able to increase the range over which surveillance or reception of meaningful signals is possible.

The more common methods of specifying the sensitivity of a radio receiver include using SNR or *Signal to Noise and Distortion ratio* (SINAD). In the case of the SNR method, the sensitivity is realised by determining the input signal power necessary in order to achieve a specified SNR. The predetermined SNR is a function of the receiver application. For the experiments conducted here the SNR is set to be 10dB.

It is worthwhile to note that, in addition to the basic performance of the receiver, the receiver's bandwidth can affect the SNR specification. It is found that the noise power decreases as the system bandwidth decreases. This implies that systems with smaller bandwidths collect less noise power [23].

The SINAD measurement takes into account the degradation of the signal by unwanted contributions including noise and distortion. More specifically, SINAD is defined as the ratio of the total signal power level, that being the signal, the noise and the distortion to the unwanted signal power, that being the noise and distortion.

$$SINAD = 10\log\left(\frac{SND}{ND}\right) \quad (4.5)$$

where:

$SND$  is the combined signal, noise and distortion power level

$ND$  is the noise and distortion power level

Similarly the sensitivity is assessed by determining the input level required in order to achieve a given figure of SINAD.

In Figure 4.9, it is shown how the sensitivity of the TVRx and USRP varies. As the level of gain is increased, it is shown that a minimum signal of -105dBm is needed in order to produce the requisite 10dB of SNR.

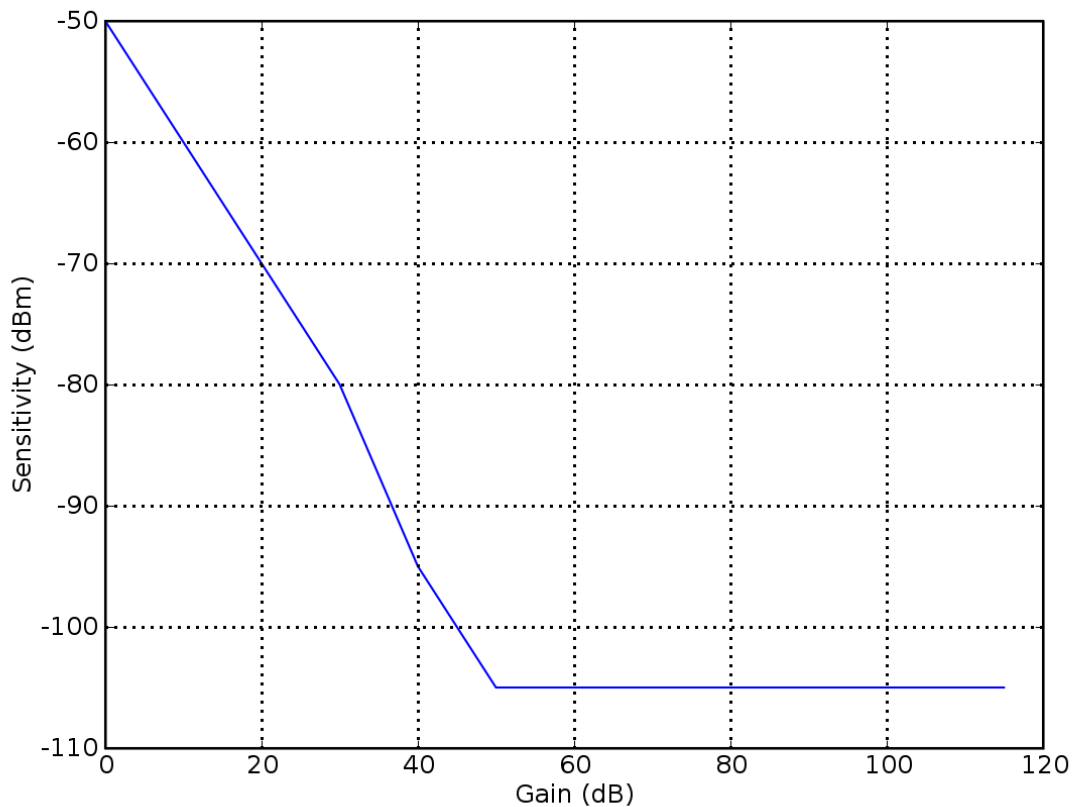


Figure 4.9: Variation of receiver sensitivity

## 4.10 Dynamic Range, Minimum Detectable Signal and Gain Compression

The standard operation of a receiver system is typically in the region where the output power is linearly proportional to the input power [3]. The constant of proportionality in this region is known as the conversion gain or conversion loss. It is this region of proportionality that is referred to as the dynamic range of a receiver. If the input power goes below the minimum acceptable signal, the *minimum detectable signal* (MDS), the noise effects dominate the receiver and results in nonlinear behaviour. This is due to the effects of the various sources of noise into the receiver including the components themselves.

If the input power goes above the maximum allowable power of this region the receiver will display nonlinear characteristics as well. This behaviour may be as a result of damage to the receiver components at high power levels or due to gain compression or the generation of spurious frequency components, due to device nonlinearities. These effects are undesirable as they may lead to increased losses, signal distortion and depending on the application possible interference with additional radio channels or services.

Thus the definition of dynamic range can be summarised as:

*Maximum allowable signal power (dB) - Minimum detectable signal power (dB)*

In the first instance, the maximum allowable signal has been shown to be as a result of gain compression or saturation. Physically this effect is due to the limitation on the instantaneous power output imposed by the power supply used to bias the device [23]. In order to quantify the range over which the device is considered to be operating in the linear region, the 1dB compression point is defined. This is, the power level for which the output power of the device has deviated by 1dB from the ideal characteristic, for receiver systems this is usually specified in terms of the input power.

Although 1dB compression points are most commonly used, 3dB and 10dB compression points are also used in some system specifications. The 1dB compression point is an important measure which can be used in the derivation of a receiver system's gain, bandwidth, noise figure and dynamic range [3]. In this instance, dynamic range is defined as:  $DR = (P_{in, 1dB}) - MDS$ .

This is shown in Figure 4.10.

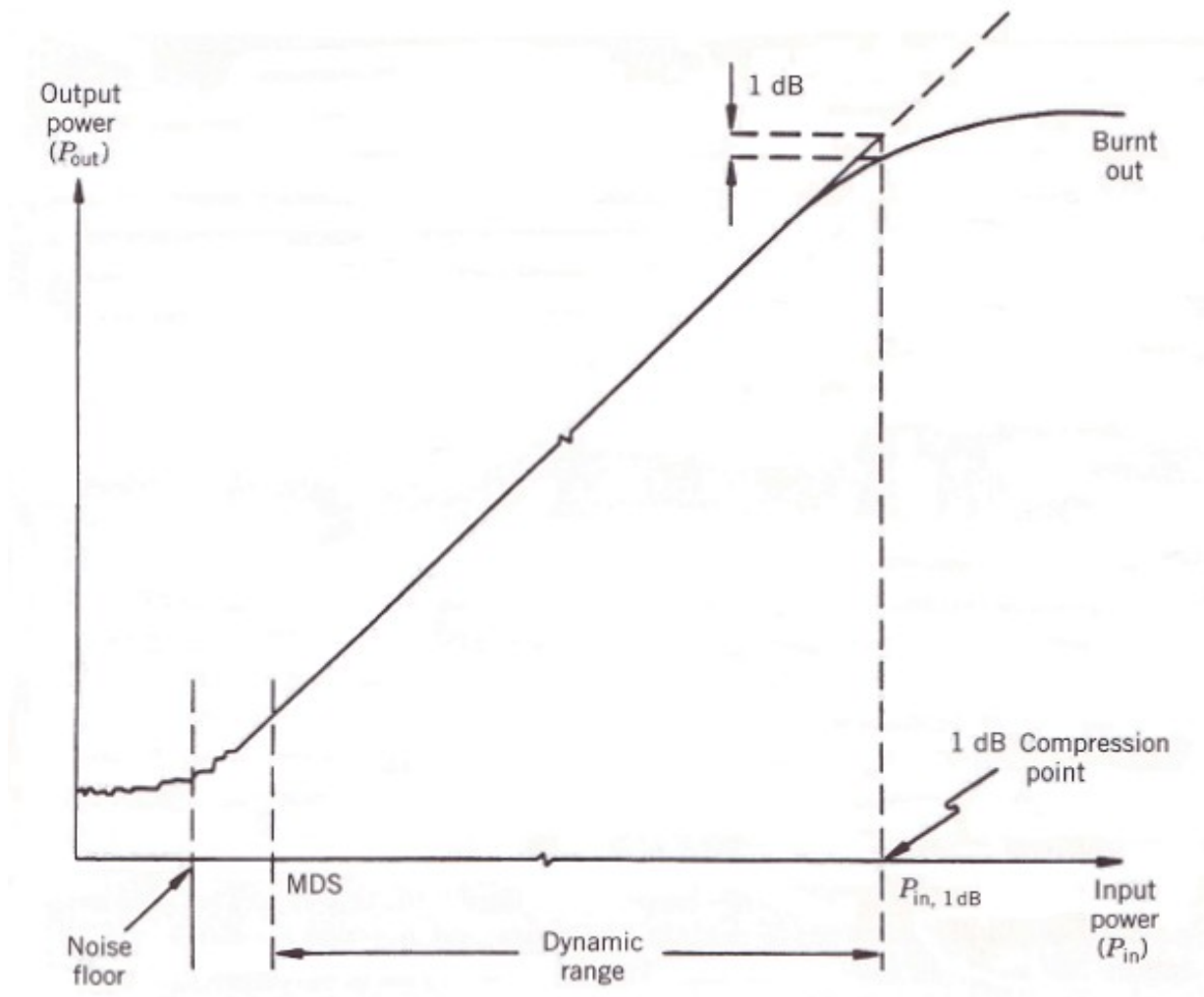


Figure 4.10: MDS, 1 dB compression point and dynamic range [3]

The maximum allowable signal has been shown furthermore to be as a result of the generation of spurious frequency components. This leads to an alternative definition of dynamic range, the *spurious free dynamic range* (SFDR). When a single frequency or *tone* is considered, generally

the output will consist of harmonics of the frequency in the form  $n\omega_0$ , where  $n = 0, 1, 2, \dots$ . Usually these harmonics do not affect the desired signal frequency.

This, however, is not the case when the signal is comprised of two or more closely spaced frequencies  $\omega_1$  and  $\omega_2$ . In particular, the third order intermodulation products,  $2\omega_1 - \omega_2$  and  $2\omega_2 - \omega_1$ , are of interest. These terms are located near to the input frequencies and generally they are of relatively large magnitude, making them difficult to filter from the desired output and resulting in distortion of the output signal.

Thus the *third order intercept point* (IP3 or TOI) is defined, as a measure of the intermodulation suppression. A high intercept point is indicative of a high suppression of undesired intermodulation products and is the fictitious point where the desired signal power and the third order signal powers are equal. In general the IP3 point occurs at about a 12dB - 15dB higher power level than the 1dB compression point. The IP3 point is an important measure of a systems linearity and is additionally specified in terms of the input power to the receiver.

In this instance, dynamic range is defined as:  $DR_{sf} = \frac{2}{3} (IP3 - MDS)$ .

This is shown in Figure 4.11.

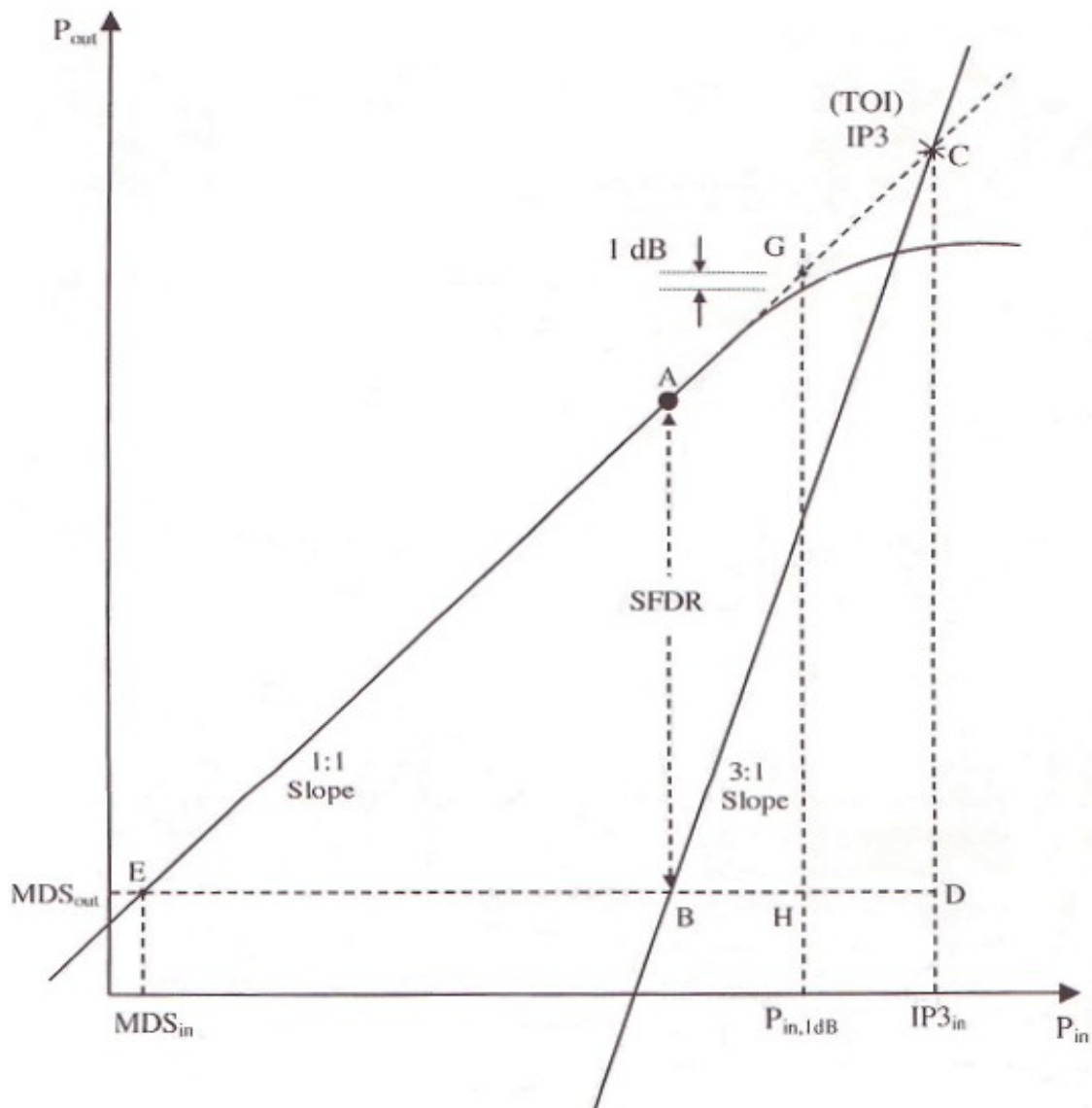


Figure 4.11: Spurious Free Dynamic Range [3]

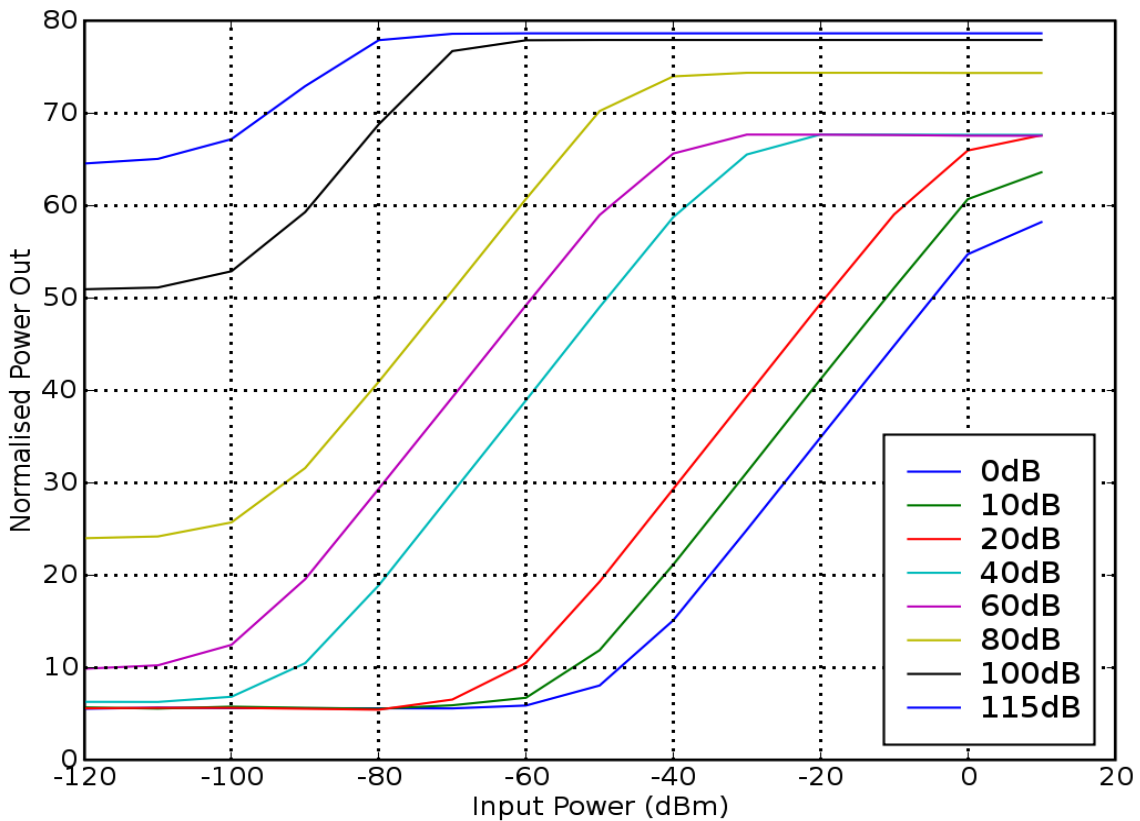


Figure 4.12: Input power against output power, showing receiver dynamic range

Figure 4.12 shows the variation of the output power with the power input to the receiver; from this we see as gain is increased from 0dB the MDS is determined at increasingly lower power levels. This is indicative of the increasing receiver sensitivity. Furthermore, as the gain setting increases we see three distinctive bands as each of the amplifier stages of the TVRx begin to run into saturation, thus the 1dB compression point begins to travel lower. This effectively indicates the reduction of the receiver's dynamic range at these high gain levels. The best achievable dynamic range of the receiver is noted as 62dB. This is in the region, mentioned in section 4.4, where GNURadio most accurately modelled the TVRx amplifier stages.

Figure 4.13 relates the measured dynamic range of 62dB to the theoretical SNR of the 12 bit ADC, which is calculated to be approximately 72dB using Equation 3.1. In practice however, the dynamic range available from the ADC is reduced as a result of thermal noise, reference noise, clock jitter, quantisation noise, etc. Figure 4.13 shows a 6dB loss in the ADC dynamic range as a result of noise, thus providing an effective 66dB of dynamic range. The minimum detectable signal from the TVRx, using the gain setting determined from Figure 4.12, was found to be 3dB above the ADC noise floor. As a result a further 3dB is lost from the ADC dynamic range as weaker signals from the TVRx will be noisy and not useful. Furthermore, the 1dB compression power output from the TVRx is found to be 1dB within the range that the ADC can extend to. Although this 1dB is available to the TVRx, stronger signals into the TVRx will begin to drive the amplifiers into saturation. Therefore, although 66dB of dynamic range is available at the ADC, the TVRx is able to provide 62dB of dynamic range.

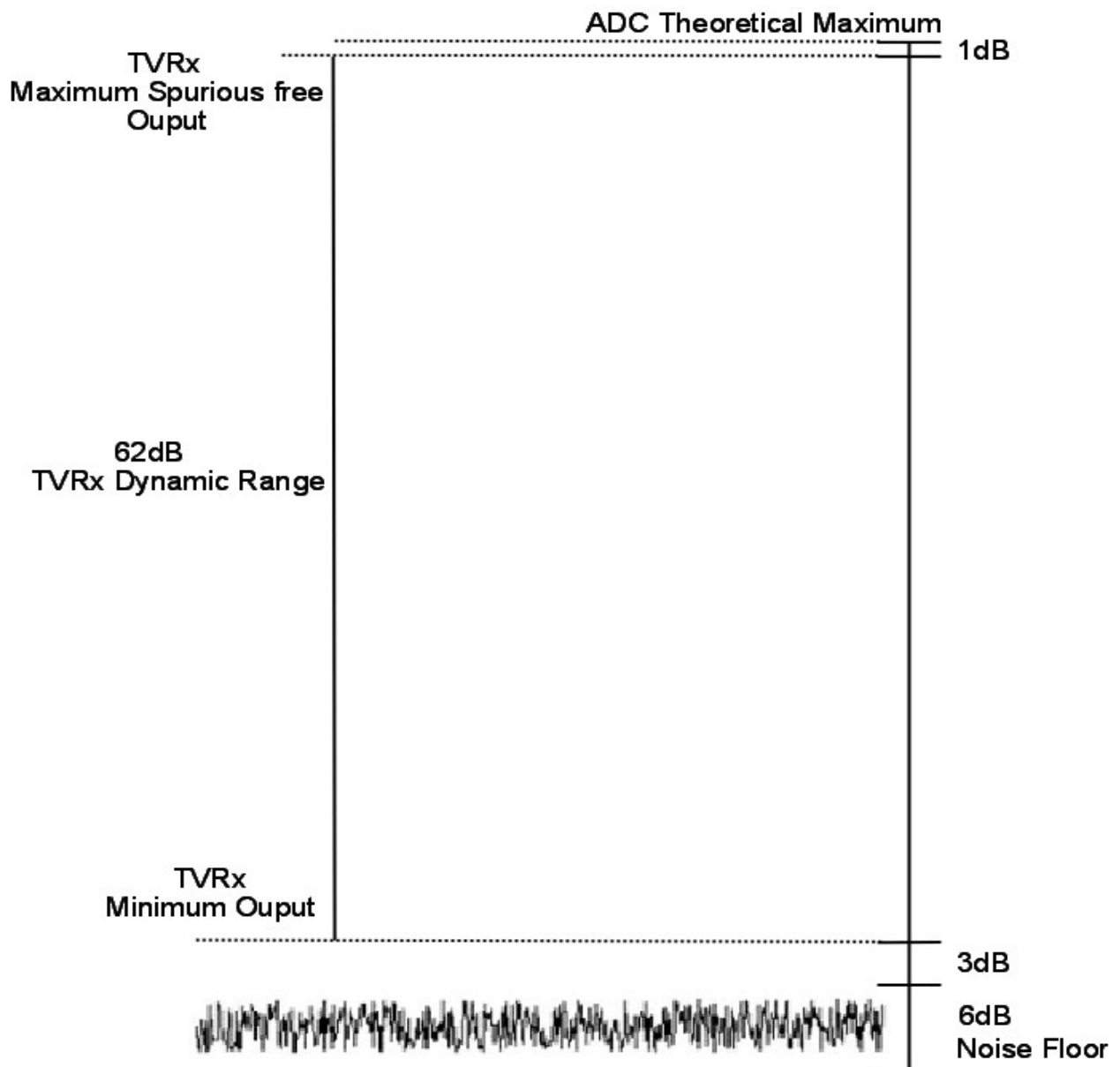


Figure 4.13: TVRx and ADC dynamic range comparison

## 4.11 Summary

A number of the TVRx and USRP receiver system parameters as well as the GNURadio interface to the controllable aspects are examined. The receiver's frontend provides a static bandwidth of 6MHz and a tunable range between 50MHz and 800MHz, with a tuning step size as low as 31.25kHz. This is sufficient for the manipulation of FM Broadcast signals as the radar waveform and provides further functionality and versatility to incorporate additional areas of the frequency spectrum if desired, i.e. the television video and sound carriers.

The multiplexer implemented in the FPGA and the ability to directly control its operation through GNURadio further extends the receiver's flexibility in its digital manipulation of signals through it. The noise characterisation of the receiver reveals a NF of 10dB, a sensitivity of -105dB and a dynamic range of 62dB.

Furthermore, it is observed that when the GNURadio application is started, when the USRP is setup as a source and includes the occasion when the application is stopped and restarted, a spurious spike occurs at the beginning of the data set. This phenomena is unexplained but noted by the USRP developers, The effects of which are mitigated by simply cutting out that part of the data set.

The following chapter will examine the suitability of FM broadcast signals as a candidate for the waveform or part of a group of waveforms used in the PCL radar. This is achieved by examination of the ambiguity plot and the variation of the instantaneous signal bandwidth.

# Chapter 5

## Ambiguity Plot Analysis

### 5.1 Introduction

In considering the use of broadcast FM signals for our PCL system, it is necessary to fully understand the nature of the signal parameters and the resulting effect and limitation on the system's performance. Range and doppler resolution in addition to range and doppler ambiguity are such parameters and they govern the ability to distinguish between two or more targets by virtue of their spatial or frequency differences and the ambiguity function has long been used to evaluate them [29] [24] [22].

The nature of the transmitted waveform determines these properties, for example, FM broadcasting uses the frequency range 88 – 108MHz [21] and the specified bandwidth is approximately 150kHz which gives a range resolution of 1–2km. This is further exemplified in the consideration of the nature of analogue television whereby the 64 $\mu$ s line repetition rate generates strong ambiguities [12] and consequently imposes a severe restriction and complication on its performance and applications.

As can be imagined, the programme content and thus the instantaneous modulation of a particular broadcast FM signal varies with time. Therefore, the ambiguity behaviour will vary as a function of the time and it is necessary to determine this behaviour.

### 5.2 System Overview

The receiving system used to capture and digitise the FM broadcast signals is described here. The system was situated on level 6 of the Menzies building at the University of Cape Town and detects and digitises broadcast signals originating from the Constantiaburg transmitter. It uses an antenna feeding the USRP, with the TVRx daughterboard plugged in and is thus in line with the project's low budget objectives. The daughterboard provides the down-conversion of the FM signal to the IF of 43.75MHz and is subsequently digitised on the USRP. The digitised signal is then further down converted to baseband and then decimated, using the standard USRP FPGA

implementation. The data stream is then transported via USB and stored in the memory of a standard PC.

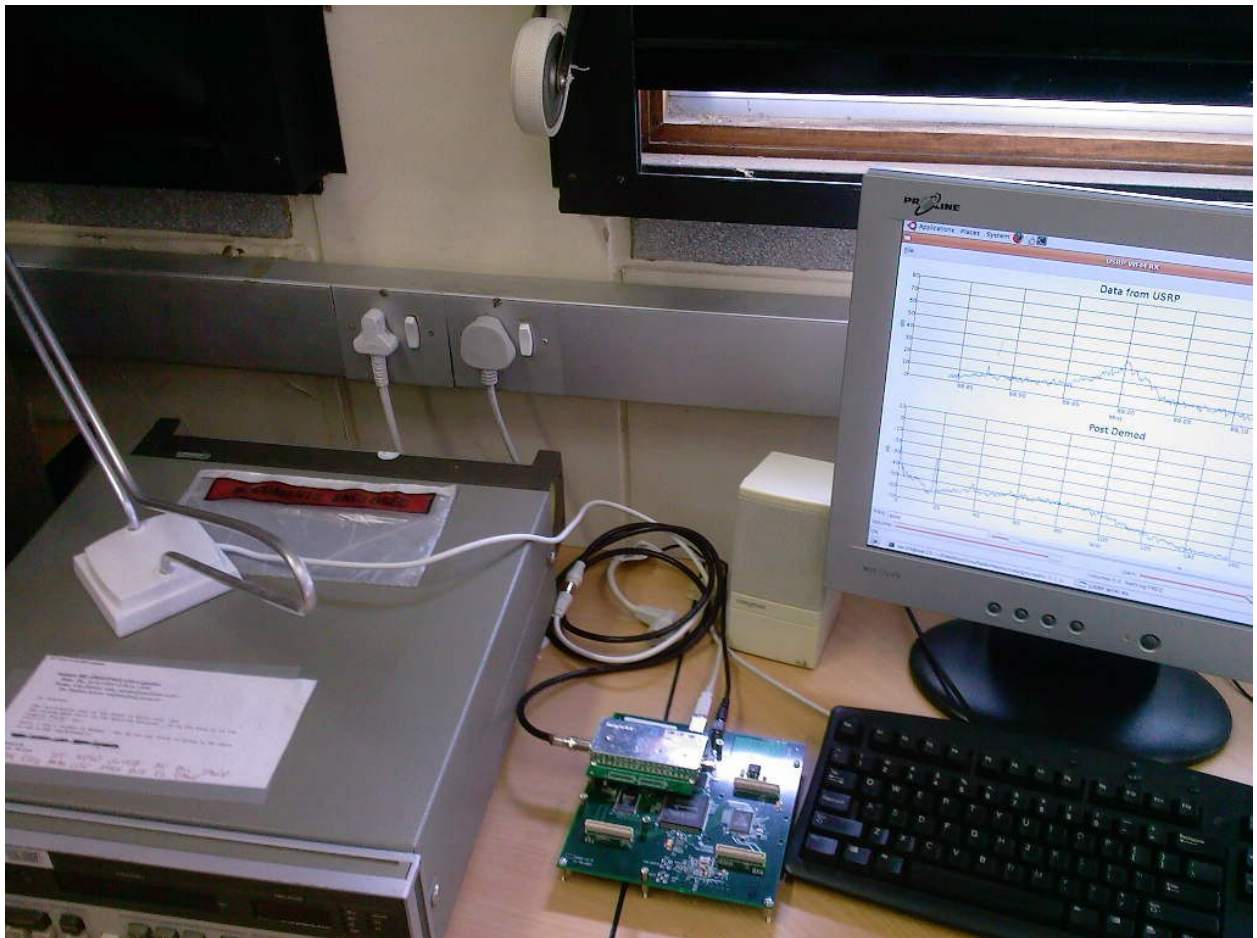


Figure 5.1: Experiment setup to capture signals for ambiguity function analysis

This choice of setup allows for the system to be flexible, as the TVRx module can be tuned to operate over the frequency range of interest and the captured data can be processed off-line, as desired.

We then compute the ambiguity function and the results of this computation are presented in a later section. Figure 5.1 above shows the experimental equipment and Figure 5.2 below represents this schematically.

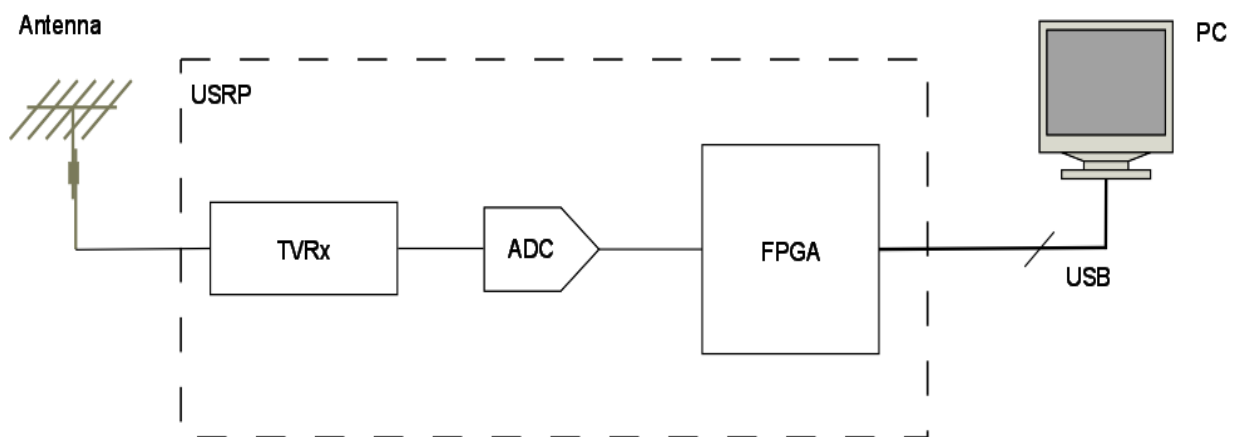


Figure 5.2: Block Diagram of experimental setup

## 5.3 Algorithm Concept

The purpose of this investigation is to determine the best achievable resolutions offered by the FM broadcast signals and the variation of these signal properties with respect to time. It is important to understand this variation due to its effect on the overall range and doppler resolutions. For this process, knowledge of the relative positions of the transmitter, receiver and target are not required and thus the monostatic geometry is assumed in the following setup. This work is based upon the literature presented by Baker et al and by Howland et al and duplicates their research.

As previously discussed, the nature of the transmitted waveform determines these properties and is evaluated by computation of the ambiguity function, given by Equation 2.21.

The output of a matched filter is represented by the ambiguity function and thus, computation of the ambiguity function results in a three dimensional plot for which one axis is time delay, the second axis is Doppler frequency and the third is the normalised output power, computed by matched filtering the directly received transmitter signal. This processing is exemplified in the figure below.

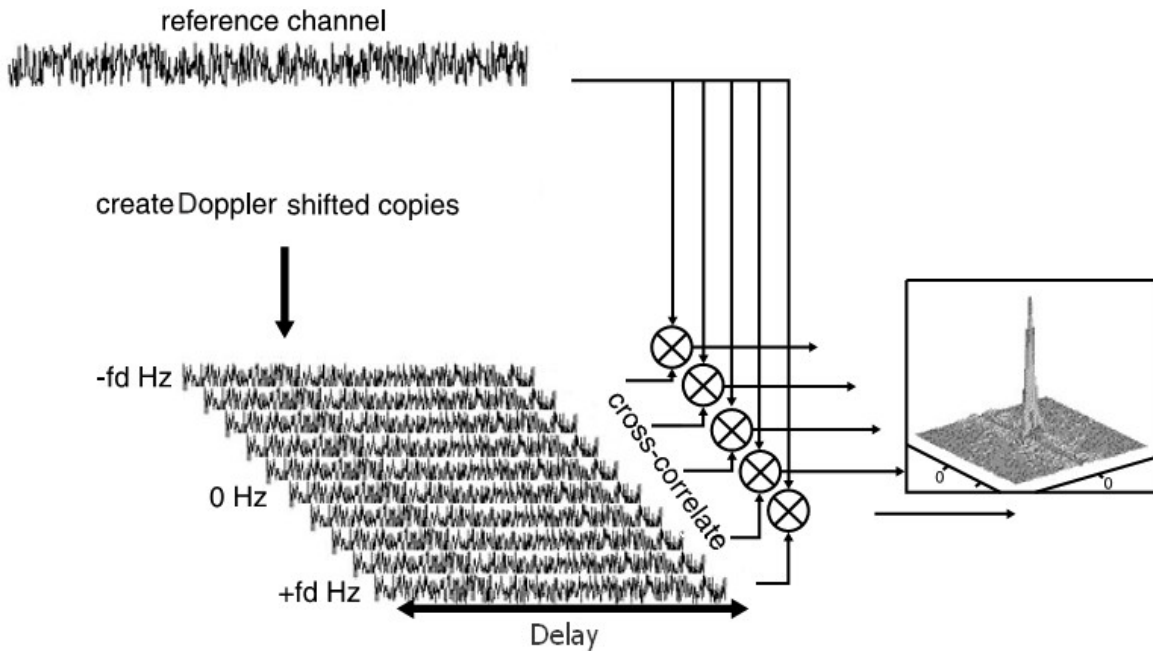


Figure 5.3: Signal processing algorithm[16]

In the context of a PCL system, this signal is known to be the reference signal and is the waveform that is correlated with the indirect target scattering in order to produce the output that is applied to the CFAR detectors, to obtain range and doppler information of each target.

This processing is written in discrete time notation as:

$$|\psi(R_R, f_d)|^2 = \left| \sum_{n=0}^{N-1} s(n) s^*(n - R_R) \exp[j2\pi f_d n/N] \right|^2 \quad (4.6)$$

A 0.1 second data sample of each FM Broadcast frequency of interest is digitised, with the USRP decimation rate set to the maximum value (256) this reduces the processing load and lowers the algorithm computation times. The effective sample rate is thus set to be 250kHz, which is well within the Nyquist criterion. The algorithm operating on each sample of data generates doppler shifted copies of the reference signal, each matched to a different target velocity.

The implementation of the processing begins by rotating and then conjugating the samples of the reference signal  $s(n)$ , producing the values representing the time delay,  $s^*(n-R_R)$ . These values are multiplied with the original reference signal and produce the result  $s(n)s^*(n-R_R)$ . The Fourier transform of this result is determined and repeated for each range of interest.

The USRP and GNURadio were setup to digitise twenty successive 0.1 second samples, thereby providing 2 seconds of contiguous data for the analysis of the variation of range resolution with respect to time, for the transmission types of interest. The findings of this analysis follow.

## 5.4 Results

The ambiguity plots derived from the system above will be analysed in this section, illustrating the variability of the responses. Only the first set of plots and the associated table illustrating the variation of the signal bandwidth will be shown in this section.

The ambiguity plots and the associated zero doppler and delay cuts as well as the tables of the remaining signals will be presented in appendix A, however a discussion of the results will be included in this section.

The ambiguity plots shown are those of the six FM radio stations available from the Constantiaburg transmitter, namely these are (a) RAD5, the content on this channel is comprised mainly of rock, pop, RnB, hip hop and dance. This is dependant on the time of the day and week. Every hour, however, a five minute news bulletin is broadcast. (b) Radio 2000, the majority of this content is a mixture of rock, jazz and talk. (c) Umhlobo, depending on the time of day broadcasts talk shows in the Xhosa medium, RnB and reggae. (d) Classic FM, which broadcasts an array of contemporary and classic works. (e) RGHP, offers a selection of rock and country music. (f) RSGR, the dominant medium of the content that is broadcast is Afrikaans. Talk shows, pop, rock and country are all broadcast. (g) SAFM, which broadcasts news and talk programmes of various subjects and topic.

Figure 5.4 below shows the ambiguity function for a RAD5 transmission. The signal content was comprised of rock. The ambiguity function plot shows a narrow defined peak and demonstrates fast fluctuating detail in the sidelobe regions. This indicates a wide bandwidth and due to the randomness in the signal modulation, exhibits noise-like characteristics and behaviour. which is consistent with what might be expected for rock music as compared to speech, which will be shown later. The zero range and doppler sections, in Figure 5.4a and Figure 5.4b below, show sidelobes to be usefully low with good performance in the range domain, which is reflective of the high rate modulation in the rock waveform. Sidelobe levels are good with about 27dB in the frequency domain and around 33dB for range.

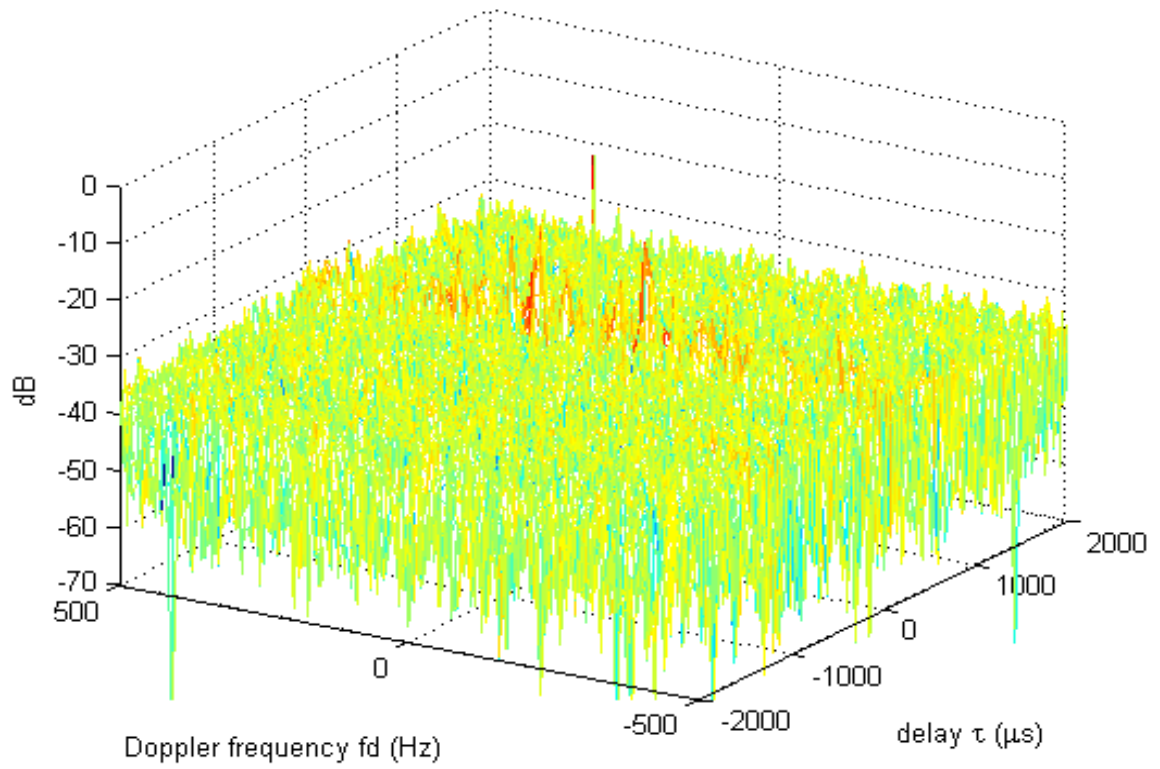


Figure 5.4: Ambiguity plot of Rad5 transmission

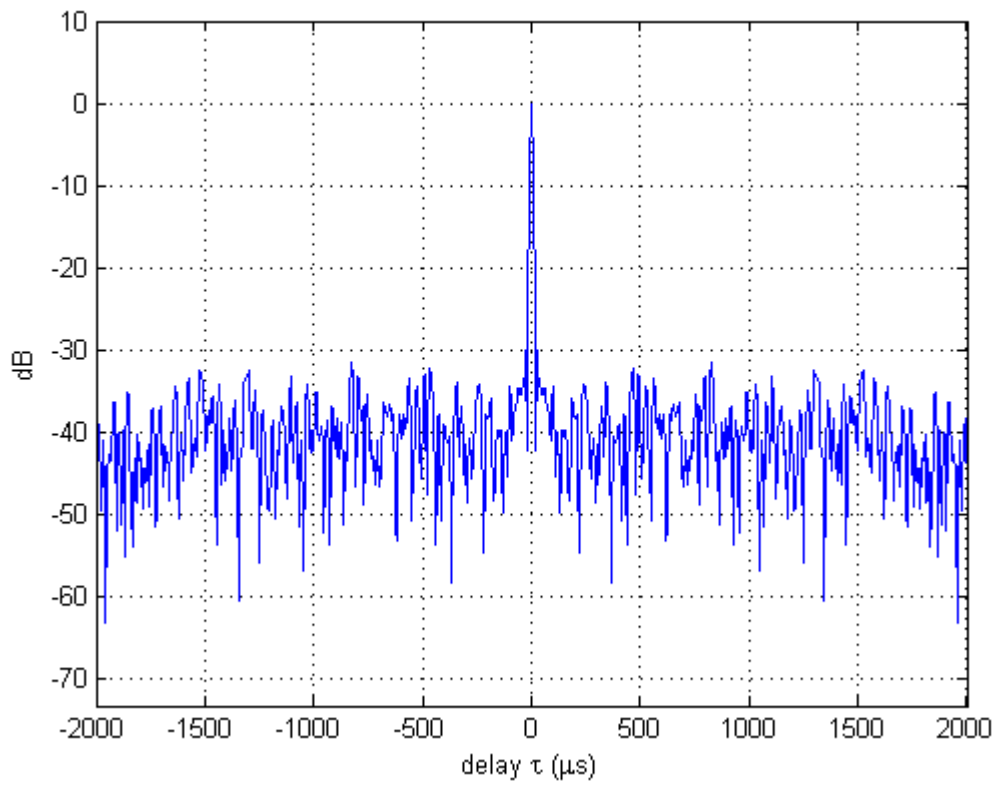


Figure 5.4a: Zero doppler cut through ambiguity plot

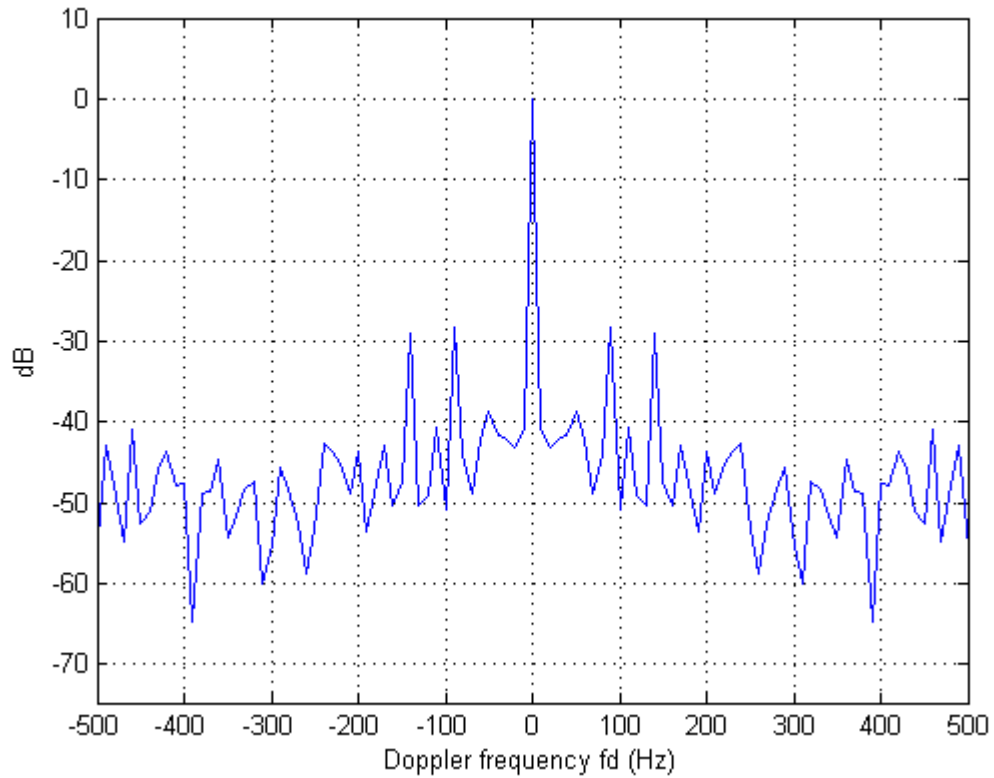


Figure 5.4b: Zero delay cut through ambiguity plot

Upon analysis of the time dependant performance of this transmission, over a 2 second period, the behaviour is shown to be relatively consistent. This is illustrated in Table 5.1 below, which shows the bandwidth in kHz for twenty waveform samples.

Table 5.1: Bandwidth Variation of RAD5 waveform

Elapsed Time (s)	Bandwidth (kHz)
0.1	30
0.2	50
0.3	42
0.4	55
0.5	45
0.6	52
0.7	40
0.8	43
0.9	10
1.0	32
1.1	50
1.2	47
1.3	40

1.4	40
1.5	44
1.6	50
1.7	47
1.8	43
1.9	40
2.0	42
Average Bandwidth (kHz)	44.38

The bandwidth is seen to vary in between 30kHz and 55 kHz, however, an anomaly of 10kHz is observed. This can be attributed to a break or pause in the modulating signal. The signal bandwidth averages 44.38kHz, making use of approximately 30% of the available bandwidth. Consequently, as the bandwidth is shown to be a function of time, the performance of the radar system will also be a function of time.

Figure A.1 shows the ambiguity function for a Radio 2000 transmission.

The ambiguity function plot again shows a defined peak, indicating a waveform with noise like properties. In this instance, distinct peaks in the sidelobe regions are observed, and thus potential ambiguity. However, the zero range and doppler sections provide further insight and show the sidelobe levels are good with about 30dB in the frequency domain and around 30dB for range and useful resolution in range and thus eliminating concerns over ambiguity.

Table A.1 examines the time dependent bandwidth of the Radio 2000 transmission. Generally the values of bandwidth are a factor of two lower than that of the RAD5 transmission, this can be attributed to the nature of the modulating content. The variation swings between 0.5kHz to 50kHz, which is much greater than that shown above and much more significant in its influence of the radar's performance. Additionally, the modulation bandwidth measured is 13% of that available.

Figure A.2 , derived from a Classic FM transmission, shows a well defined ambiguity function peak, however, wider than those we have seen thus far, this can be attributed to the narrower bandwidth associated with this waveform modulation.

The zero range and doppler sections shown in Figures A.2a and A.2b demonstrate the range and doppler resolutions more clearly. The range resolution shows a slight degradation in performance, as is expected, due to the narrower bandwidth offered. Sidelobes are seen close to the main peak but with reasonable levels at about 26dB in the range domain and around 40dB in the frequency domain. The peaks seen in the frequency domain away from the peak is measured at 33dB and thus does not impede the doppler performance.

Table A.2 exhibits a variation in bandwidth from 0.6kHz to 32.5 kHz of the Classic FM transmission. The signal bandwidth averages 18.81kHz, making use of approximately 13% of the available bandwidth.

Figure A.3 shows the ambiguity function for a Umhlobo FM transmission.

The ambiguity function plot again shows a narrow defined peak, offering attractive range resolution and some detail in the sidelobe regions. In this analysis the signal content was comprised of kwaito music. This is loosely described as a South African variant of rock. Examining the zero range and doppler sections exhibit fast fluctuating detail associated with signals modulated with pop music. Indicating a more noise like waveform structure and a wider bandwidth than that associated with rock, jazz and classic music. Doppler sidelobe levels are

about 39dB and range sidelobe levels are additionally attractive with around 28dB, the range resolution offered by the signal is useful.

Table A.3 examines the time dependent bandwidth of the Umhlobo FM transmission. Generally the values of the bandwidth offered are greater and the variation measured is less. The modulation bandwidth measured is on average 30% of that available.

Figure A.4 shows the ambiguity function for a RGHP transmission.

The ambiguity function plot again shows a defined peak, although narrower, relative to the other plots examined. This is indicative of the greater bandwidth offered by the modulating music waveform, in this instance RnB music. In the regions away from the main peak, we see a very clean structure with attractive sidelobe behaviour. This behaviour is more reflective of a random noise-like behaviour, which approaches the idealised “thumbtack” surface. An examination of the zero range and doppler sections displays fast fluctuating detail and is associated with signals modulating music. Indicating a more random and noise like waveform structure and a wider bandwidth than those examined thus far. Doppler sidelobe levels are about 32dB, which shows some measure of degradation relative to the previous signals, although not significant for our application. Range sidelobe levels however are good with around 28dB, with a very good range resolution offered.

Table A.4 examines the RGHP transmission. Generally the values of bandwidth are much improved over the alternative modulating types, averaging 63.6kHz, which translates to 42% of that available.

The signal from RSGR, in Figure A.5, was comprised of Afrikaans music. The peak of the ambiguity function is well defined but wider than those we have seen thus far for the alternative modulation types. The detail in the regions away from the main peak does not fluctuate as fast as the alternative signals examined thus far, this too is a function of the modulation present in this component of the waveform. This behaviour is not reflective of pure noise-like behaviour, however, is consistent with the matched filter response that might be expected with a narrower bandwidth. The zero range and doppler sections shown below in Figures A.5a and A.5b demonstrate the range and doppler resolutions more clearly. The range resolution shows a degradation in performance, consistent with the decrease in the bandwidth associated with the signal. Sidelobe levels however are good with about 36dB in the frequency domain and around 30dB for range.

Table A.5 below demonstrates the behaviour of the RSGR transmission. Generally the values of bandwidth are less than that of the rock, pop, and classic music modulating signals. The bandwidth is on average 11% of that available.

The signal from SAFM in Figure A.6 was comprised of speech in a news broadcast. The peak of the ambiguity function is extremely wide. This too is a function of the modulation present in this component of the waveform and is consistent with the correlation that might be expected of a pause or break in speech. The zero range and doppler sections shown in Figures A.6a and A.6b demonstrate the range and doppler resolutions and sidelobe levels with about 40dB in the frequency domain and performing extremely poorly in range. This result is indicative of ambiguous performance as the bandwidth offered is very low, thus the potential resolution of the radar would be not at all useful in this instant.

In Table A.6, the bandwidth is seen to vary from 1.4kHz to 47.5kHz. This average bandwidth used is 13% of that available. This is consistent with the analysis expected of a speech (news broadcast) transmission.

All the bandwidths presented here are calculated from the -3dB width of the zero doppler section, through the ambiguity plot. It is evident that there is a great deal of variation in the performance of the available waveforms to be exploited. This variation is dependent on the type of transmission, its content and the time of transmission. This can be understood, for example, if there is a long pause on a channel or with speech, the signal spectral content is reduced, thus range resolution information will be degraded or lost.

This is illustrated in Figure 5.5a and Figure 5.5b, which compares the range resolution against time for the different transmissions.

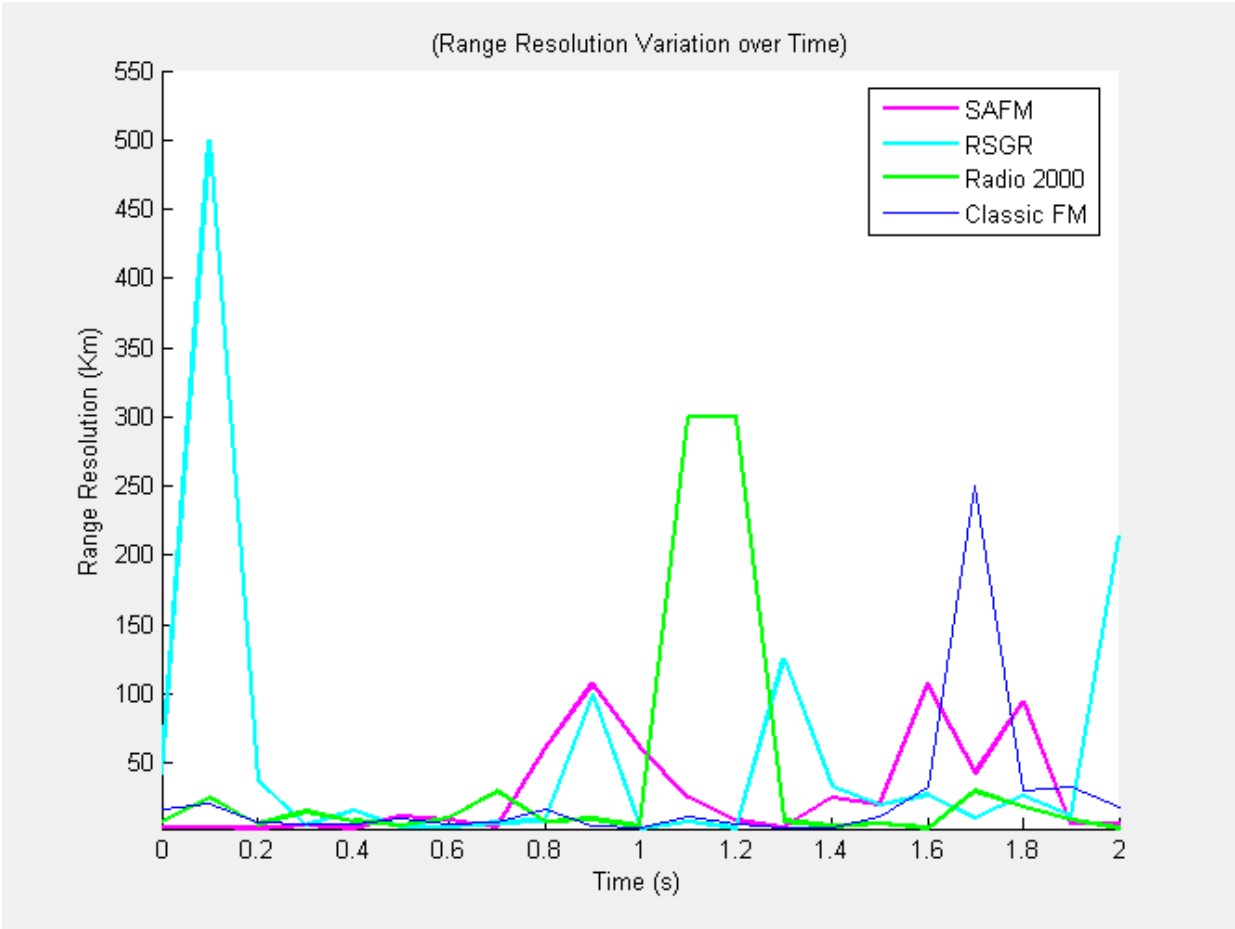


Figure 5.5a: Variation of signal range resolution with time

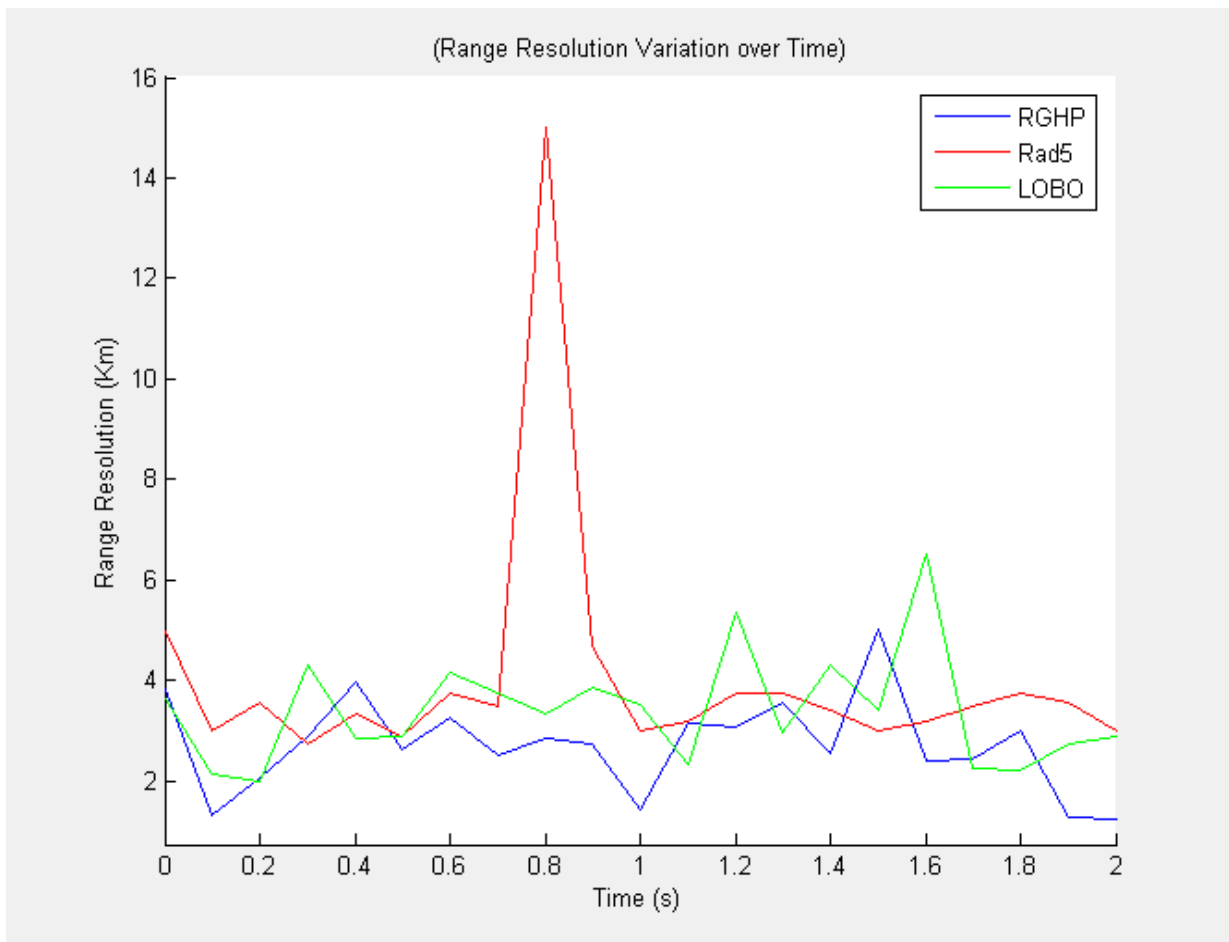


Figure 5.5b: Variation of signal range resolution with time

Here we see that RSGR and SAFM (talk show) show a high degree of temporal variability in range resolution compared to the music channels as is expected, with the resolution degrading in the order of hundreds of kilometres. The classical music does not show as much variation, thus demonstrating an increased performance. However, the pop and dance channels exhibit the least variation, with resolution varying between 1km and 15km.

Thus the signal performance has quite a considerable variation and the effect on overall system performance will require careful consideration.

## 5.5 Summary

From the results it is evident that the measured FM Broadcast signals due to the randomness in their modulation, exhibit noise like characteristics and behaviour. This is observed as the ambiguity function plots can be approximated by the ideal thumbtack ambiguity function, therefore providing the radar with excellent range and doppler information. However, it is additionally clear that the ambiguity function depends largely on the modulating format.

Thus there is a variation in performance between the pop music and dance music channels and the rock and classical music channels which exhibit a slightly degraded performance. Speech content shows the poorest performance though, as the performance does vary significantly with time, especially during pauses in words due to the low spectral content. This variation in performance does have a significant impact on the radar's potential detection ability and will be one that does vary with time, as seen from Equation 2.6 and Table A.6, this variation translates to a change in processing gain of 15dB.

Table 5.2 below summarises the ambiguity function performance of the measured signals.

Table 5.2: Summary of waveform ambiguity function performances

Signal	Range Resolution (km)	Effective Bandwidth (kHz)	Peak range Sidelobe level (dB)	Peak doppler Sidelobe level (dB)
RAD5	3.38	44.3	- 30	- 27
Radio 2000	7.94	18.9	- 18	- 34
Classic FM	7.98	18.8	- 30	- 33
Umhlobe	3.33	45.0	- 31	- 25
RGHP	2.36	63.6	- 30	- 37
RSGR	9.32	16.1	- 18	- 36
SAFM	7.54	19.9	- 20	- 40
Average	5.98	32.37	-25.29	-33.14

# Chapter 6

## Oscillator Stability

### 6.1 Introduction

A significant limiting factor in the performance of radar applications is the ability of the radar's frequency reference to maintain timing accuracy.

Reviewing the theory of previous chapters, it is understood that in radar, the range of the target is related to time.

$$R = \frac{c \cdot \tau_d}{2}$$

Where:

$R$  is the range of the target, from the radar receiver.

$\tau_d$  is the round trip time delay of the signal, between the transmitter and receiver.

Thus, a radar's range accuracy is directly proportional to the error in the timing signal [24], as an error in  $\tau_d$  is directly proportional to an error in  $R$ .

In a doppler radar, the signal received by the radar from a moving target differs in frequency from the transmitted frequency and thus differs in phase too, by an amount that is proportional to the radial component of the velocity relative to the radar.

This shift is given by:

$$f_d = \frac{2v_r}{\lambda}$$

As a result, the velocity of the target and the radar frequency are primary determinants of the phase noise requirements [27]. A fast moving target will cause a large doppler frequency, and thus will require a low phase noise at frequencies far from the carrier. In quartz crystals most of the noise power lies close to the carrier [3] [23], consequently, low phase noise close to the carrier, required for a slow moving target, is not easily achieved [24].

Moreover, coherence, in radar applications is defined as whether the phase relationship (at the carrier frequency) between successive pulses are known and stable [24]. If a radar is coherent, then  $M$  successive pulses, from a non-fluctuating target, can be added. This summing will improve the radar's SNR by a factor of  $M$ . However, if the receiver is not coherent, these pulses will not add in phase and summing will not improve the SNR. Refer to chapter 2.6.4 for a more thorough treatment of this point.

Furthermore, as the radar's probability of detection is directly related to the SNR, degradation of the radar's coherence will decrease the SNR. As a result, in coherent radar and thus PCL, the target detection capability decreases with an increase in phase noise of the frequency reference.

In a bistatic or multistatic radar configuration, the complexity of synchronisation and coherence is further increased. The local oscillators in all the receivers, need to be synchronised not only in frequency but the phase offsets between them needs to be known as well [27]. The degree to which these phase offsets stay constant during target detection will influence the level of coherence. In a passive bistatic radar system the echo signal is correlated with a bank of doppler shifted replicas of the transmitted signal, over a predetermined sample period, in order to achieve the necessary signal processing gain and for target detection. Thus the phase coherence is only required during this sample period. The degree of coherence can be thought of as how stable the local oscillator clock, in the TVRx, remains.

Assuming a target velocity of 150m/s, a broadcast FM transmission frequency of 100MHz and using Equation 2.17, a target will produce a doppler shift of 100Hz. In order to qualify the results of this chapter a 5% error in the calculated doppler shift is set as the maximum acceptable limit of frequency shift. Thus a frequency drift of no greater than 5Hz is set as the requirement of the system.

## 6.2 Quartz Crystal Oscillators

The local oscillator in the TVRx daughterboard of the USRP is derived from a 4MHz quartz crystal oscillator. For this reason discussion will focus on the properties of crystal oscillators and the associated performance parameters of interest. These parameters of interest include accuracy, reproducibility and stability, although, oscillator stability will dominate the discussion.

Accuracy, in the case of frequency, is a measure of how well the frequency source relates to the definition of one second. Reproducibility, is a measure of how well a number of sources agree in frequency as they are adjusted, this is more relevant as a factory acceptance test. Stability is a measure of how well a frequency source is able to generate a given frequency over some measure of time, once it has been set. Thus the difference between the frequency at one moment in time and another moment is called stability [19] and is usually given for a number of time periods, ranging between seconds and years.

Crystal oscillators are widely used as frequency sources and find application in a wide variety of areas from wristwatches to complex and elaborate instruments found in laboratories. These oscillators provide good performance at a reasonable price and dominate the field of frequency sources [19].

The quartz crystal in the oscillator resonates mechanically and the associated oscillations of the resonator have to be sensed. This is done by taking advantage of the piezoelectric effect. The piezoelectric effect is observed when a physical compression of the crystal generates a voltage across the crystal. Conversely, the application of an external voltage across the crystal causes the crystal to either expand or contract depending on the polarity of the voltage.

Limitations in stability stem mainly from oscillator drift and ageing effects. Further discussion regarding this will follow in section 6.2.1.

## 6.2.1 Ageing and Temperature of Crystals

The most influential factors affecting oscillator performance are ageing and temperature. There is a temperature dependence of the quartz crystal that affects its resonance frequency, and there is also instability of the resonance frequency due to ageing [19]. Drift is due to ageing plus changes in the environment and other factors external to the oscillator, thus oscillator drift is defined as the systematic change in frequency with time of an oscillator. Ageing, on the other hand, is defined as the systematic change in frequency due to physical changes in the oscillator [27]. This ageing rate decreases with time.

Ageing is a characteristic common to crystal oscillators and can be approximated as a linear change in resonance frequency with time. In general, the drift is negative, meaning that the resonance frequency decreases. This decrease is indicative of an increase in the size of the crystal. Possible causes of this phenomenon are contamination on the surface of the crystal, variations in the electrodes or the metallic plating, the movement of loose surface material from grinding and etching or changes in the internal crystal structure.

Furthermore, the continuous expansion and contraction of the crystal, due to the piezoelectric effect, may be the cause of or at least exacerbating these effects. Improvements in crystal holder design combined with clean vacuum enclosures, have led to a reduction in oscillator ageing [19].

The temperature effects on crystal performance are as a result of slight changes in the elastic properties of the crystal. Special crystal cutting techniques and variations known as crystallographic orientations minimize this effect of temperature over a range of temperatures. Temperature coefficients of less than one part in 100 million per degree of temperature are possible.

Crystal oscillators must be carefully designed if very high frequency stabilities are desired. If large environmental temperature fluctuations are to be tolerated, the crystals themselves are enclosed in electronically regulated ovens which maintain a constant temperature. These oscillators are known as *Oven Controlled Crystal Oscillators* (OCXO).

## 6.3 Characterisation of stability

The techniques associated with the specification of stability are presented in the following sections and in order to appreciate this, a presentation of the relationship between frequency and phase will, additionally, be made.

It is assumed that the average output frequency of a precision oscillator is determined by a narrow band circuit (crystal oscillator), so that the signal can be approximated as a sine wave [19] and thus the signal output is generalised by the following formula.

$$V(t) = [V_0 + \epsilon(t)]\sin[2\pi\nu_0 t + \phi(t)] \quad (6.1)$$

where:

- $V_0$  is the nominal peak voltage amplitude
- $\epsilon(t)$  is the deviation of the amplitude from the nominal
- $\nu_0$  is the nominal fundamental frequency
- $\phi(t)$  is the deviation of the phase from the nominal

This can be furthermore generalised and rewritten as the  $\epsilon(t)$  in precision oscillators is generally ignored.

$$\begin{aligned} V(t) &= V_0 \sin[2\pi\nu_0 t + \phi(t)] \\ &= V_0 \sin\Phi(t) \end{aligned} \tag{6.2}$$

where:

- $\Phi(t)$  is the total oscillator phase

Here we note that due to a change in amplitude,  $\Delta v$ , over an associated change in time,  $\Delta t$ , we are able to determine the average frequency over this period. Furthermore, in the limit as  $\Delta t$  approaches zero an instantaneous frequency can be measured. This is however, in practice, not possible as it requires an infinite bandwidth. As a result we are only able to measure the frequency that has been averaged over a time period  $\Delta t$ .

Furthermore, the frequency of a signal is additionally related to the rate of change of its phase. The instantaneous angular frequency is defined as the time derivative of the total oscillator phase. Thus,

$$\begin{aligned} \omega(t) &= \frac{d}{dt}[2\pi\nu_0 t + \phi(t)] \\ &= 2\pi\nu_0 + \frac{d\phi}{dt} \end{aligned} \tag{6.3}$$

The instantaneous frequency is then written as:

$$V(t) = \nu_0 + \frac{1}{2\pi} \frac{d\phi}{dt} \tag{6.4}$$

For precision oscillators, the second term on the right hand side is quite small and useful to define the fractional frequency.

$$\begin{aligned}
 y(t) &= \frac{\nu(t) - \nu_0}{\nu_0} & (6.5) \\
 &= \frac{1}{2\pi\nu_0} \frac{d\phi}{dt} \\
 &= \frac{dx}{dt}
 \end{aligned}$$

where:

$$x(t) = \frac{\phi(t)}{2\pi\nu_0} \quad (6.6)$$

$x(t)$  is an expression of the phase in units of time and is thus representative of the total cumulative time deviation of the reference clock due to instability.

This quantity can be additionally determined by integrating the fractional deviation  $y(t)$ , with respect to time.

However, the bandwidth limitations that apply to the measurement of instantaneous frequency are additionally applicable to instantaneous phase measurement. Therefore, the average fractional frequency is defined as:

$$\bar{y}(t) = \frac{x(t + \tau) - x(t)}{\tau} \quad (6.7)$$

$x(t)$  and  $x(t + \tau)$  are the respective time deviations measured.  $\tau$  is known as the sampling or averaging time. This is illustrated in the Figure 6.1.

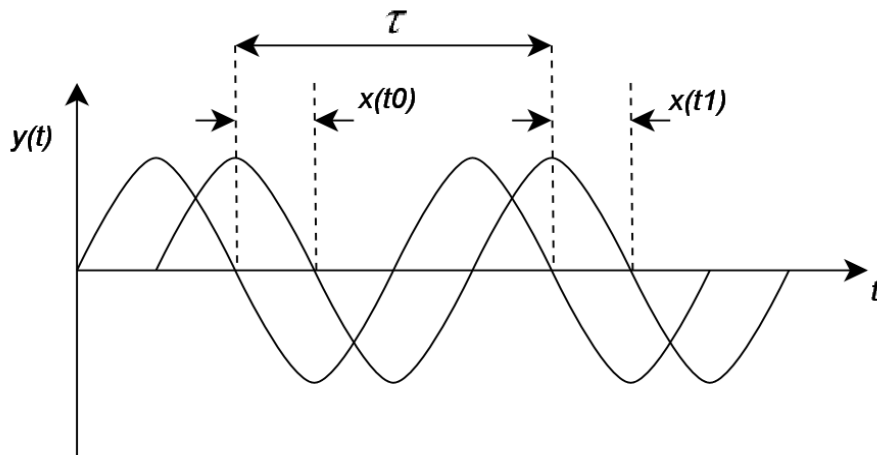


Figure 6.1: Determining the fractional frequency

In Figure 6.2,  $v(t)$  represents a stable reference oscillator and  $w(t)$  represents an oscillator with instabilities. If viewed over a timescale smaller than  $t_1$ ,  $w(t)$  is unstable relative to  $v(t)$ . However, above this time the oscillators are in phase and as a result, the instability of  $w(t)$  would have gone undetected if time measurements greater than  $t_1$  were made. Furthermore, over the period  $t_1$  to  $t_2$ , although no instabilities are apparent, when analysed over a smaller time period, instabilities are noted.

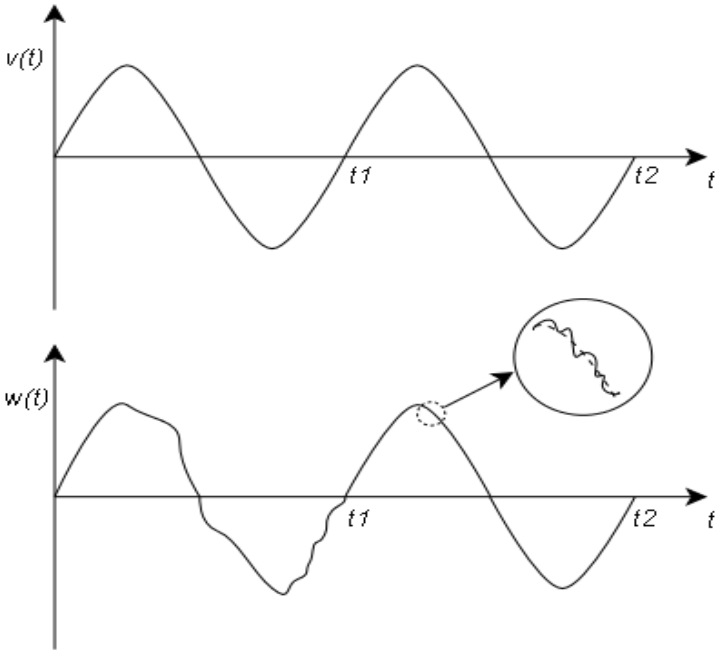


Figure 6.2: Dependence of stability measurement on time window

### 6.3.1 Measurement of Stability

A variety of methods and their variations exist in order to measure the stability of frequency sources. The methods most prominent in the literature will be reviewed in this section.

Frequency stability can be measured by taking a reasonably large number of successive readings of the frequency of the device to be evaluated. Each reading, measured in hertz is obtained by averaging the output frequency for some specified time period. Furthermore, variations in the readings of measured frequency might be expected to average out if observed for long enough. This however, is not always the case [19].

The results are then expressed, often, as a relative or fractional value, given by the following formula.

$$F = \left[ \frac{f_{(actual)} - f_{(nameplate)}}{f_{(nameplate)}} \right] \quad (6.8)$$

The nameplate frequency refers to the expected oscillator operating frequency. If an oscillator operated exactly at its nameplate frequency, it would be considered a perfect frequency source. However, in practice there is some frequency error and thus a difference  $\Delta f$  between the actual and nameplate frequencies. The value of the fractional frequency will become negative if the measured value is below that of the nominal frequency.

The process of dividing the  $\Delta f$  by the nameplate frequency, normalises the error and allows frequency stability to be directly manipulated as it is independent of the actual operating frequency of the oscillator being discussed. For example this makes it possible to compare the stability of a 10MHz oscillator to a 10kHz oscillator without any additional information.

As a further example, a 1MHz oscillator that is higher in its frequency by 1Hz will have a fractional frequency equal to  $10^{-6}$  or 1 *Part Per Million* (PPM). The same 1Hz error for a 10MHz oscillator is a smaller part of the nominal frequency and gives us a smaller relative frequency equal to  $10^{-7}$  or 0.1PPM. Thus, this division of  $\Delta f$  by the nominal (nameplate) frequency, removes the concern of whether the nameplate frequency is 1 MHz or 10MHz and is extended to any other frequency of interest.

In addition to this, this notation allows the measurement of the oscillator output directly or the use of a divided version of the oscillator. For example, an oscillator with a 1MHz output can have its output divided to 1Hz without changing the result of its stability. This attribute provides the ability to deal with sources of any frequency by using dividers to make the measurement problems more manageable, as it is much easier to deal with lower frequencies, and the final results are the same.

In describing the second measure of frequency stability, it is useful to mention the relationship between the time and frequency domains of a signal.

This is understood by use of the continuous Fourier transform pair, defined as:

$$X(f) = \int_{-\infty}^{\infty} x(t) \exp[-j2\pi f t] dt \quad (6.9)$$

and

$$x(t) = \frac{1}{2\pi} \int_{-\infty}^{\infty} X(f) \exp[j2\pi f t] df \quad (6.10)$$

The frequency domain representation of the signal  $x(t)$ , the total cumulative time deviation, is also known as its power spectrum and provides an indication of the distribution of the signal's power with frequency. The power density spectrum,  $S_x(f)$ , can then be obtained by normalising the power spectrum, such that the total area under the curve is equated to unity [30].

Furthermore, the power spectrum contains frequency components for both phase and amplitude fluctuations and when dealing with precision oscillators, the mean squared value of the amplitude fluctuations are small enough to be neglected. The spectral density, can be then further scaled to represent the phase power density spectrum,  $S_\phi(f)$ . Finally,  $S_y(f)$  represents the spectral density of the instantaneous fractional frequency fluctuations  $y(t)$ .

These spectral densities are related in the following manner:

$$S_y(f) = \frac{f^2}{v_0^2} S_\phi(f) \quad (6.11)$$

$$S_x(f) = \frac{1}{(2\pi v_0)^2} S_\phi(f)$$

$$S_\phi(f) = (2\pi f)^2 S_y(f)$$

The third measure of frequency stability is to use the sample variance,  $\sigma_y^2(\tau)$ , of the fractional frequency fluctuations. This variance determines the extent of the variation of the oscillator's average frequency between two adjacent measurement intervals. If the time or frequency fluctuations between a pair of oscillators is measured, a process whereby  $N$  values of the fractional frequency  $\bar{y}_i$  are measured over a time  $\tau$  and measurements are repeated after an interval of time  $T$ . There is a dead time between each frequency measurement, if the measurement repetition interval is greater than the averaging time and is given by  $T - \tau$ , this is illustrated in Figure 6.3.

The  $N$  sample variance can be then computed,

$$\langle \sigma_y^2(N, T, \tau) \rangle = \left\langle \frac{1}{N-1} \sum_{n=1}^N (\bar{y}_n - \frac{1}{N} \sum_{k=1}^N \bar{y}_k)^2 \right\rangle \quad (6.12)$$

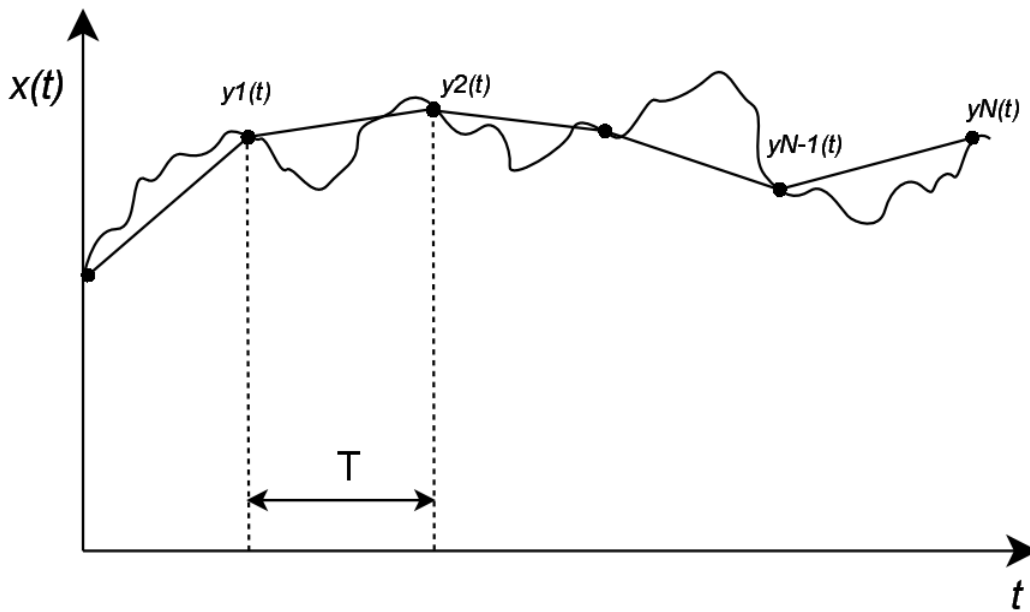


Figure 6.3: measurement process [30]

The angle brackets in Equation 6.12 denote the infinite time average. Frequently, however, this result does not converge as  $N \rightarrow \infty$ . This is as a result of noise processes in the oscillator that diverge at low Fourier frequencies. Thus the precision of the estimation of the variance, does not simply improve as the sample size is increased. For this reason, the Allan variance is preferred as a measure of stability and is shown to converge rapidly as the sample size is increased [30]. A low Allan variance is a characteristic of a clock with good stability of the measured period.

The Allan variance is described as [30]:

$$\sigma_y^2(\tau) = \left\langle \frac{1}{2} (\bar{y}(t + \tau) - \bar{y}(t))^2 \right\rangle \quad (6.13)$$

This equation can be stated equivalently in terms of phase data as [30]:

$$\sigma_y^2(\tau) = \left\langle \frac{1}{2\tau^2} (x(t+2\tau) - 2x(t+\tau) + x(t))^2 \right\rangle \quad (6.14)$$

where:

$x(t)$  is the measured phase difference. This can still furthermore, be manipulated in order to operate on a discrete time data set as [30]:

$$\sigma_y^2(\tau) \simeq \frac{1}{2(N-2)\tau^2} \sum_{i=1}^{N-2} (x_{i+2} - 2x_{i+1} + x_i)^2 \quad (6.15)$$

## 6.4 System Overview

This section will describe the experimental test setup. The test signal is generated by a Hewlett Packard 8656B signal generator, with the output frequency set to 100MHz. This signal is split and sent to the USRP with two TVRx daughterboard modules plugged in and running simultaneously. This is representative of the setup that will be expected of the PCL receiver with independent TVRx modules for the reference channel and the channel monitoring target returns.

The independent signals are then digitised by the USRP, synchronisation of the ADCs is ensured as they are clocked by the same master clock running the USRP. The digitised signals are then written to file on a PC for offline processing of the data. The functional block diagram of the system is shown in Figure 6.4 and a photograph of the test equipment is shown in Figure 6.5.

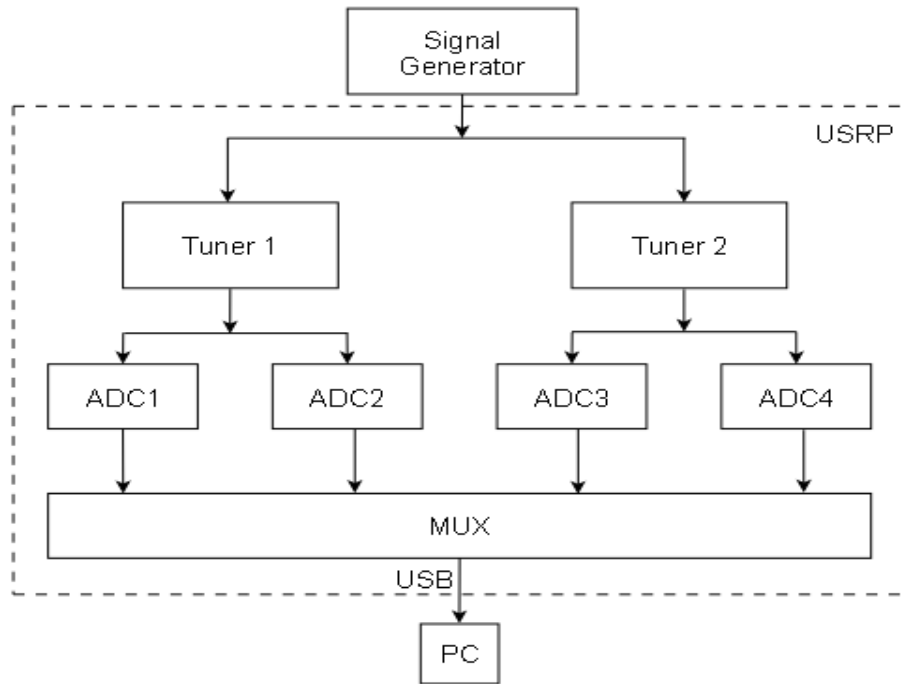


Figure 6.4: Block diagram of experimental setup

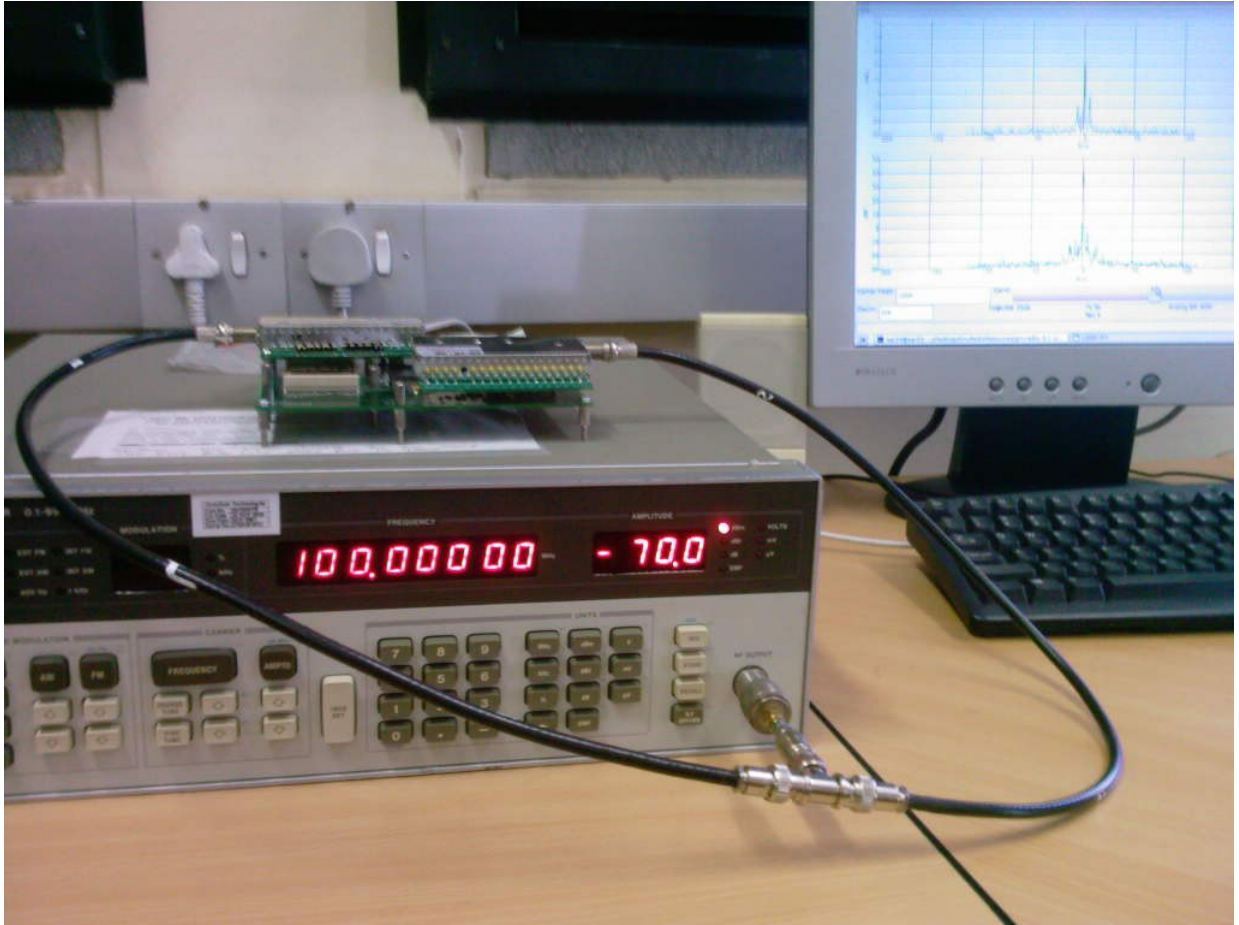


Figure 6.5: Experiment setup for stability tests

GNURadio was configured such that the signals from tuner 1 and tuner 2 are written to separate files on the PC, allowing for greater flexibility in post processing. The experiment was conducted with three variations of the decimation rate, that being 256, 128, and 64. This translates to data rates varying between 250ksps and 1Msps.

Furthermore, the system was setup in order to determine the oscillator stability over a 30 minute period. This was achieved by taking successive readings of the frequency output by each tuner over the 30 minute period. Each reading, was obtained by averaging the output frequency for a 1 second time gate, every minute over the 30 minute test time.

The resolution of the measured frequency is given by:

$$\Delta f = \frac{1}{T} \quad (6.16)$$

Where  $T$  is the time gate over which the frequency is averaged.

Furthermore, the phase variation between the signals at the measured intervals was determined and used in order to verify and confirm the frequency variation that had been determined. A set of fractional frequencies describing the behaviour of the stability of the oscillator were then obtained. These results are used in order to generate the Allan deviation of the oscillators.

## 6.5 Results

The following section will present the results of the tests conducted, using the experimental setup outlined in the above section.

In Figure 6.6, the fractional frequency is observed over the 30 minute time frame. As expected the crystal ageing effect is gradually reduced over the period, showing a variation from 2.3 to 0.8 parts per 10 million. The large separation initially can be attributed to the innate crystal oscillator behaviour described as the warm up effect, which is caused by the rise in temperature of the oscillator from the time the oscillator and instrument is turned on until the time a stable operating temperature is reached. The temperature rise is brought about directly by power dissipation in the oscillator or indirectly by the generation of heat in the circuitry of the instrument. Additionally, the Allan variance of these fractional frequency deviations is shown in Figure 6.7.

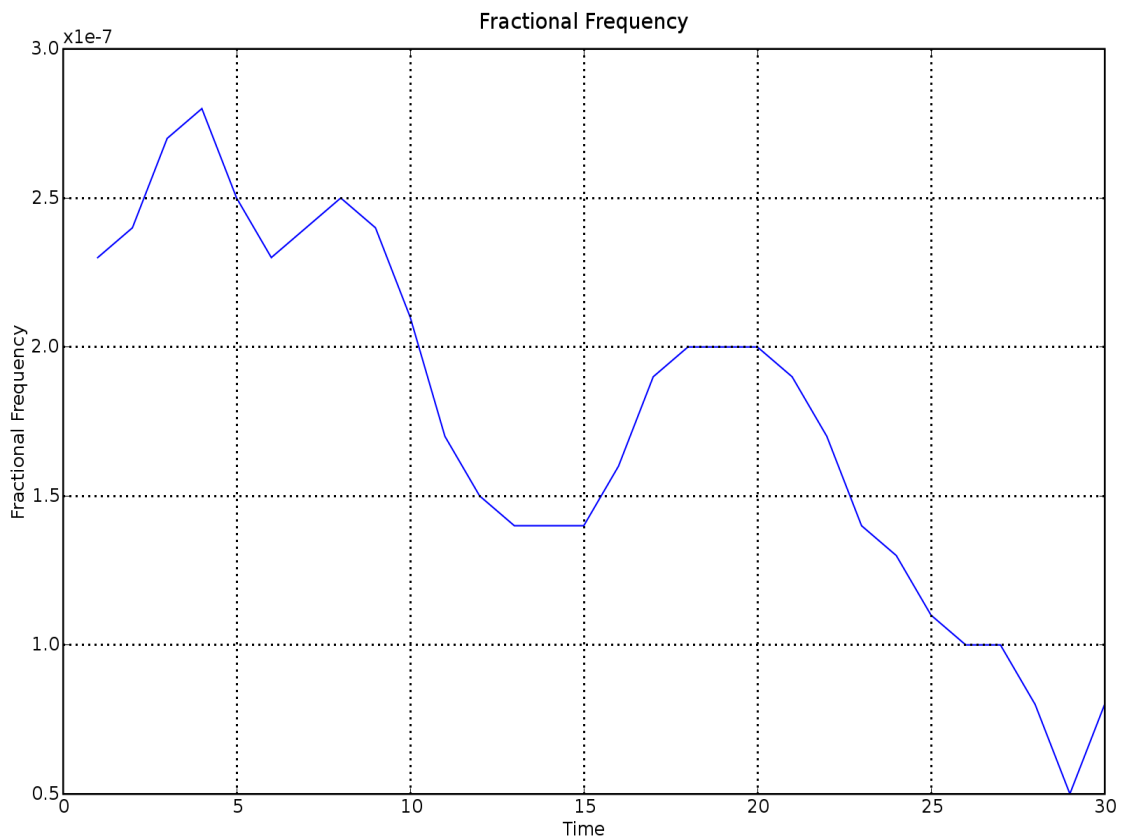


Figure 6.6: Fractional frequency variation of the daughterboards

The Allan variance determines the extent of the variation of the oscillator's average frequency between two adjacent measurement intervals. Thus, although we observe an overall decline in the fractional frequency to 0.8 parts per 10 million, the magnitude of the variation between successive measurements is less severe. The oscillation of the variation indicates movement of the oscillator frequencies towards and away from each other. The largest measure of the instantaneous drift is 4Hz. This oscillation can be attributed to physical attributes of the crystal, losses in the oscillator circuitry, vibration or temperature effects.

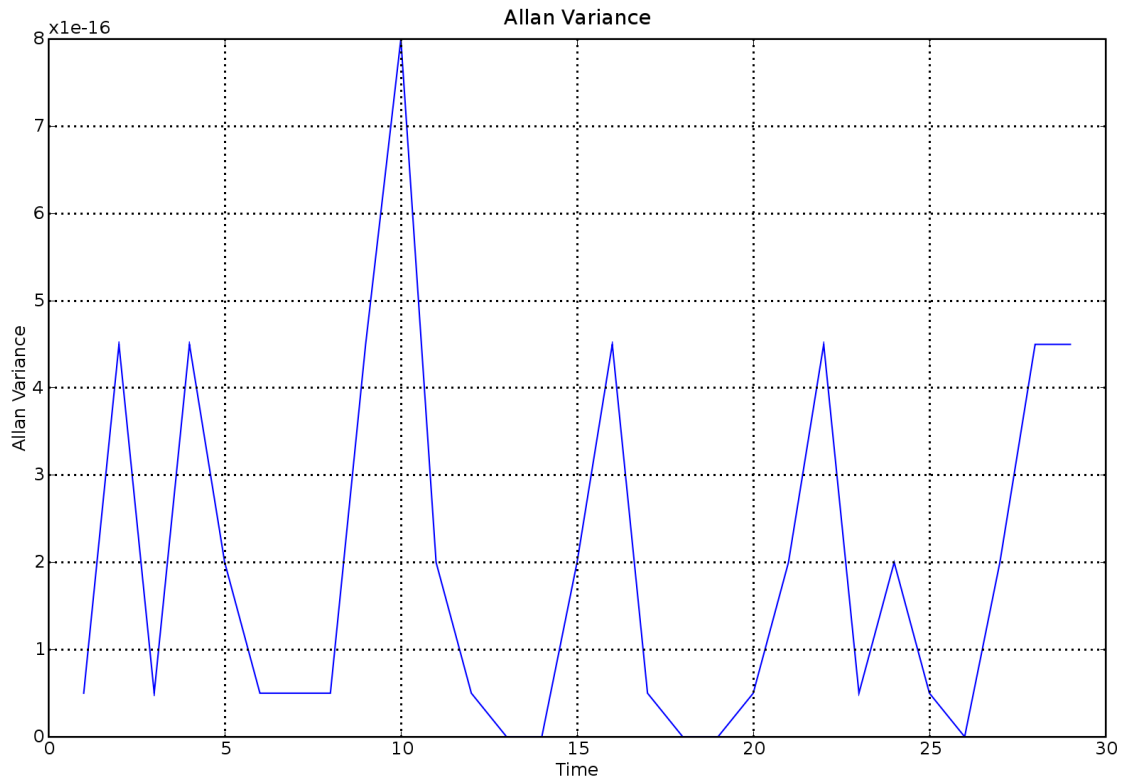


Figure 6.7: Allan Variance of the fractional frequencies

## 6.6 Summary

In this chapter it is shown that a critical limiting factor in the performance of radar applications is the ability of the radar's frequency reference to maintain timing accuracy.

The local oscillator in the TVRx daughterboard of the USRP is a 4MHz quartz crystal oscillator. It is for this reason that the properties of crystal oscillators and the associated performance parameters of interest were investigated. These parameters include accuracy, reproducibility and stability. It was found that crystal oscillators provide good performance at a reasonable price and dominate the field of frequency sources [19].

Furthermore, the techniques associated with the specification of stability were presented, including measurement of the frequency deviation and the Allan variance. These tests concluded that the crystal ageing effect is reduced over the measurement period of thirty minutes, showing a fractional frequency variation from 2.3 to 0.8 parts per 10 million and a frequency drift no greater than 4Hz. This falls within the maximum allowance of 5Hz, calculated in section 6.1.

# Chapter 7

## Conclusions and Recommendations

This dissertation provides a comprehensive discussion around bistatic radar with specific reference to PCL. Various uses of these radar systems, such as military and civilian applications have been presented, as well as the advantages and disadvantages of the system have been discussed in detail, and make this type of system desirable for our applications. However, at the time of writing this dissertation various aspects of the overall project were still under investigation and as such explicit system requirements were not available, thus, an exhibition highlighting existing literature and work as well as an examination of the various performance metrics is made.

In particular the ambiguity function is examined and the performance of commercial FM radio broadcasts as the radar waveform is determined and summarised by Table 5.2, reproduced here.

Table 5.2: Summary of waveform ambiguity function

Signal	Range Resolution (km)	Effective Bandwidth (kHz)	Peak range Sidelobe level (dB)	Peak doppler Sidelobe level (dB)
RAD5	3.38	44.3	- 30	- 27
Radio 2000	7.94	18.9	- 18	- 34
Classic FM	7.98	18.8	- 30	- 33
Umhlobe	3.33	45.0	- 31	- 25
RGHP	2.36	63.6	- 30	- 37
RSGR	9.32	16.1	- 18	- 36
SAFM	7.54	19.9	- 20	- 40
Average	5.98	32.37	-25.29	-33.14

The analysis of the FM broadcast signal ambiguity plots reveal the attractive performance of the signals as they in general tend toward the idealised thumbtack. However, this is greatly dependant upon the instantaneous modulating content, revealing highly degraded performance in the case of a signal with low spectral content such as speech with many pauses and breaks.

Furthermore, the SDR paradigm and technology is examined, with discussion around the design considerations. The USRP, the TVRx daughterboard and GNURadio are examined further as a potential receiver and development environment, in this light.

GNURadio, is found to be a powerful toolkit that implements numerous complex signal processing elements and additionally interfaces with the USRP that provides flexible and powerful computing capabilities. Thus combining to provide a powerful and widely versatile toolset for the development of a variety of radio devices.

The system meets the low cost ambitions costing just over US\$500.00 for the USRP motherboard and a single daughterboard. The receiver's frontend provides a static bandwidth of 6MHz and a tunable range between 50MHz and 800MHz. The noise characterisation of the receiver reveals a NF of 10dB, a sensitivity of -105dB and a dynamic range of 62dB.

Finally, the investigation into the stability of the daughterboard frontend oscillators due to ageing effects is shown to be steady through examination of the fractional frequency variation as well as the Allan variance, showing a fractional frequency variation from 2.3 to 0.8 parts per 10 million and a frequency drift no greater than 4Hz. This falls within the maximum allowance of 5Hz, calculated in section 6.1.

In order to further increase the performance of the system, investigation into the use of multiple waveforms is recommended. The bandwidth of the TVRx lends itself to this. Furthermore, the effect of multiple USRP receivers and the effect of location and thus multiple simultaneous locations can be investigated providing a richer information source for the relevant signal processing.

Special attention should be paid to timing and synchronisation effects and the examination of the “cross ambiguity function” modelling the bistatic geometry. In addition to this, the versatility of GNURadio can be further explored, using the inbuilt signal processing blocks to improve the end to end performance of the PCL system. i.e. The support and performance of adaptive filtering and various pre-correlation signal conditioning techniques may be explored.

# Bibliography

- [1] Asad A. Abidi, *Direct-Conversion Radio Transceivers for Digital Communications*, IEEE journal of solid-state circuits, Vol 30, no 12, December 1995
- [2] Blyakman A.B, Ryndyk A.G, Sidorov S.B, *Forward Scattering Radar Moving Object Coordinate System*, Radar, Sonar and Navigation, IEE Proceedings, Volume 152, Issue 3, 3 June 2005 Page(s): 107 - 115
- [3] Chang K, *RF and Microwave Wireless Systems*, Wiley Inter-Science, 2000
- [4] Del Mistro M, *A Study of Bistatic Radar and the Development of an Independent Bistatic Receiver*, University of Cape Town, 1992
- [5] Eric Blossom, *GNURadio: Tools for Exploring the Radio Frequency Spectrum*, <http://www.linuxjournal.com/article/7319>, 2008
- [6] Ettus Research LLC, *TX and RX Daughterboards for the USRP Software Radio System*,
- [7] Fette B.A., *RF and Wireless Technologies*,
- [8] Griffiths H D, Garnett A. J., *Bistatic radar using satellite-borne illuminators of opportunity*, Radar 92. International Conference, Volume , Issue , 12-13 Oct 1992 Page(s):276 - 279
- [9] Griffiths H.D., *Bistatic and Multistatic Radar*, University College London
- [10] Griffiths H.D., Baker C.J., *Passive Coherent Location Radar Systems. Part 1: Performance Prediction*, Radar, Sonar and Navigation, IEE Proceedings, Volume 152, Issue 3, 3 June 2005 Page(s): 153 - 159
- [11] Griffiths H.D., Baker C.J, *Measurement and Analysis of Ambiguity Functions of Passive Radar Transmissions*, Radar Conference, 2005 IEEE International, Volume , Issue , 9-12 May 2005 Page(s): 321 - 325
- [12] Griffiths H.D., Long B.A., *Television bases Bistatic Radar*, IEE. Proceedings, Vol. 133, Part F, No.7, December 1986 Page(s) 649-657
- [13] Guner A., Temple M.A., Claypoole R.L. , *Direct path filtering of DAB waveform from PCL receiver target channel*, Electronics Letters, Volume 39, Issue 1, 9 Jan. 2003 Page(s): 118 - 119
- [14] Hanle E, Ing Dr, Gunpath H.R., *Survey of Bistatic and Multistatic Radar*, IEE Proceedings, 133(PtF No7):587– 595,Dec 1986.
- [15] Howland P.E. *Television Based Bistatic Radar*, University of Birmingham,1997
- [16] Howland P.E., Maksimiuk D., Reitsma G., *FM based Bistatic Radar*, Radar, Sonar and Navigation, IEE Proceedings, Volume 152, Issue 3, 3 June 2005 Page(s): 107 - 115
- [17] Jackson M.C, *The Geometry of bistatic radar systems*, Communications, Radar and Signal Processing, IEE Proceedings, Volume 133, Issue 7, December 1986 Page(s): 604 - 612
- [18] Jiabing Z., Liang T., Yi H., *Study on Moving Target Detection to Passive Radar based on FM broadcast transmitter*, Journal of Systems Engineering and Electronics, Volume 18, Issue 3, 2007, Pages 462-468
- [19] Kamas G., Lombardi M.A., *Time and Frequency Users Manual*, NIST Special publication 559, U.S. Government Printing Office, Washington DC,1990
- [20] Mitola J., *Software Radio Architecture Evolution: Foundations, Technology Tradeoffs, and Architecture Implications*, IEICE Trans. Commun.E83-B1165–73
- [21] Mr Creese, *Sentech Transmitter specification*,
- [22] Nathanson F.E., *Radar Design Principles*, McGraw-Hill, 1969
- [23] Pozar D.M., *Microwave and RF Design of Wireless Systems*, Wiley, 2001
- [24] Quegan S, Kingsley S, *Understanding Radar Systems*, McGraw-Hill, 1992
- [25] Reed J. H., *Software Radio: A Modern Approach to Radio Engineering*, Prentice Hall, 2002
- [26] Sahr J.D., Lind F.D., *The Manastash Ridge Radar: a passive bistatic radar for upper atmospheric radio science*, Radio Science, Volume 32, 1997 Page(s) 2345 - 2358

- [27] Sandenbergh J.S, *A GPS synchronised, Quart Crystal Frequency Standard*, University of Cape Town, 2005
- [28] schoenenberger, *Principles of Independent Receivers for use with Cooperative Radar Transmitters*, The Radio and Electronic Engineer, vol. 52, No. 2, February 1982 Page(s) 93-101
- [29] Skolnik M, *Introduction to Radar Systems*, McGraw-Hill, 1962
- [30] Stein S.R., *Frequency and Time, Their measurement and characterisation*, Precision Frequency Control, Volume 2, E.A Gerber and A. Ballato, Eds., Academic Press, New York, 1985 Page(s) 191 - 232
- [31] The Software Defined Radio Forum, <http://www.sdrforum.org>, 2008,
- [32] Watermeyer K, *Design of a hardware platform for narrow-band Software Defined Radio applications*, University of Cape Town, 2007
- [33] Wikipedia The Free Encyclopedia, Passive Radar, [http://en.wikipedia.org/wiki/Passive\\_radar](http://en.wikipedia.org/wiki/Passive_radar), 2008
- [34] Willis N.J., *Bistatic Radar*, Artech House, 1991
- [35] Willis N.J., *Bistatic radars and their third resurgence: passive coherent location*, IEEE Radar Conference, Long Beach, USA, 2002
- [36] Woodward P.M., *Probability and Information Theory, with applications to Radar*, Norwood, MA: Artech House, 1980
- [37] Microtune, *4937 D15 RF Tuner Module, 3x889 (3x7702), Advance Data Sheet*, 2001
- [38] Analog Devices, *AD9860/AD9862 Datasheet*,
- [39] GNURadio website, <http://www.gnu.org/software/gnuradio>, 2008
- [40] Chang C.W.W, *System Level Investigations of Television Based Bistatic Radar*, University of Cape Town, 2005

# Appendix A

## Ambiguity Analysis Results

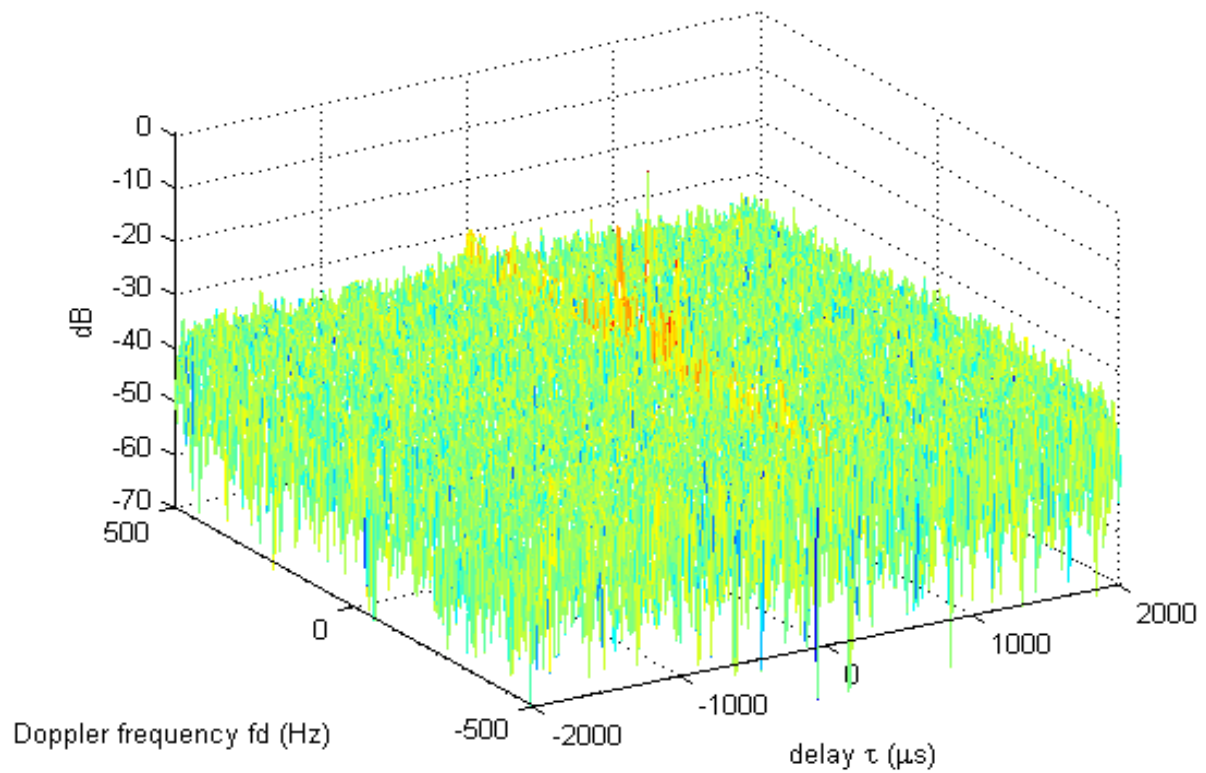


Figure A.1: Ambiguity plot of Radio 2000 transmission

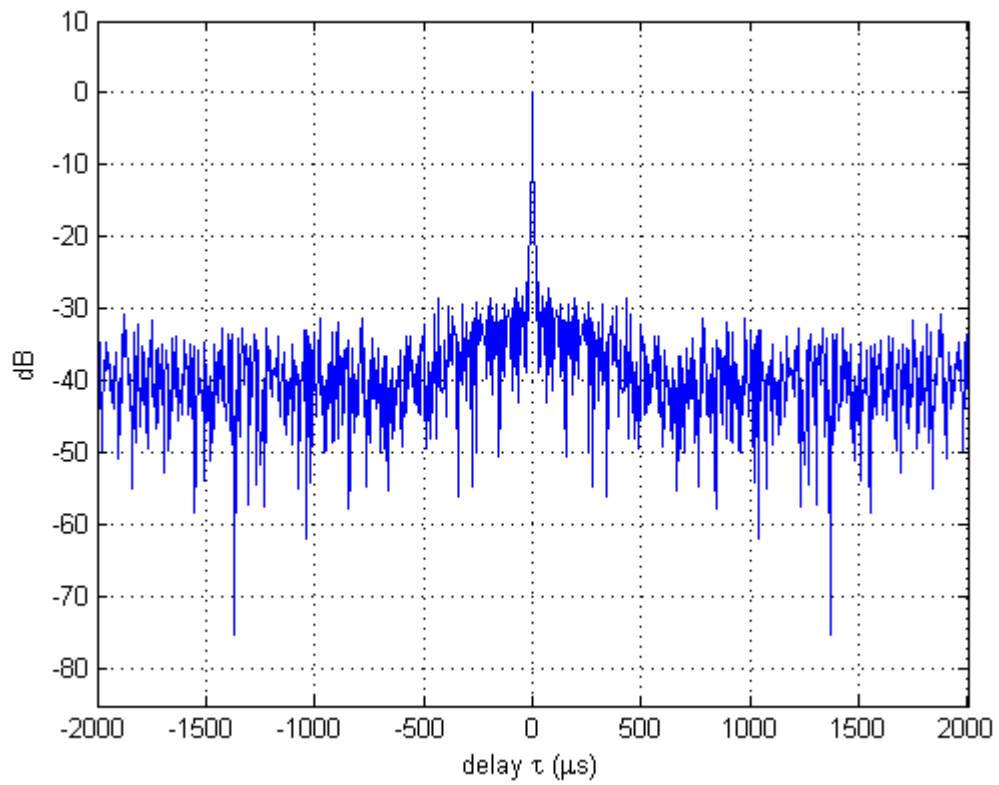


Figure A.1 a: Zero doppler cut through ambiguity plot

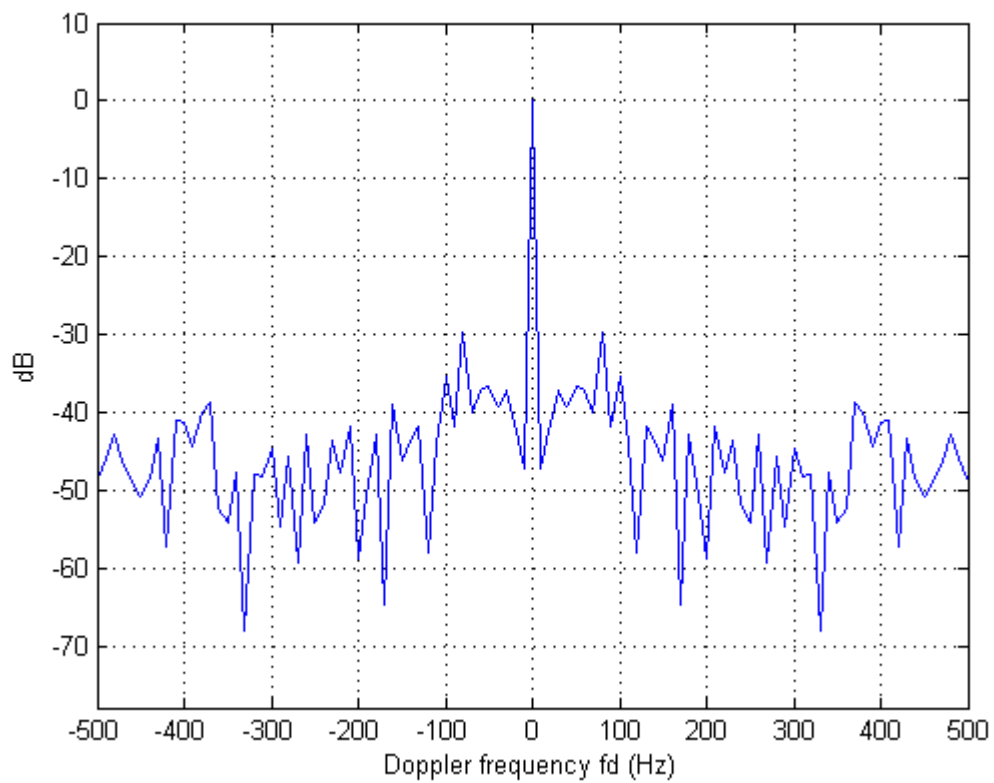


Figure A.1 b: Zero delay cut through ambiguity plot

Table A.1: Bandwidth variation of Radio 2000 waveform

Time (s)	Bandwidth (kHz)
0.1	20
0.2	6
0.3	25
0.4	10
0.5	18.5
0.6	31
0.7	14
0.8	5
0.9	19
1.0	15
1.1	33
1.2	0.5
1.3	0.5
1.4	18
1.5	35
1.6	23
1.7	50
1.8	5
1.9	8
2.0	16
Average Bandwidth (kHz)	18.97

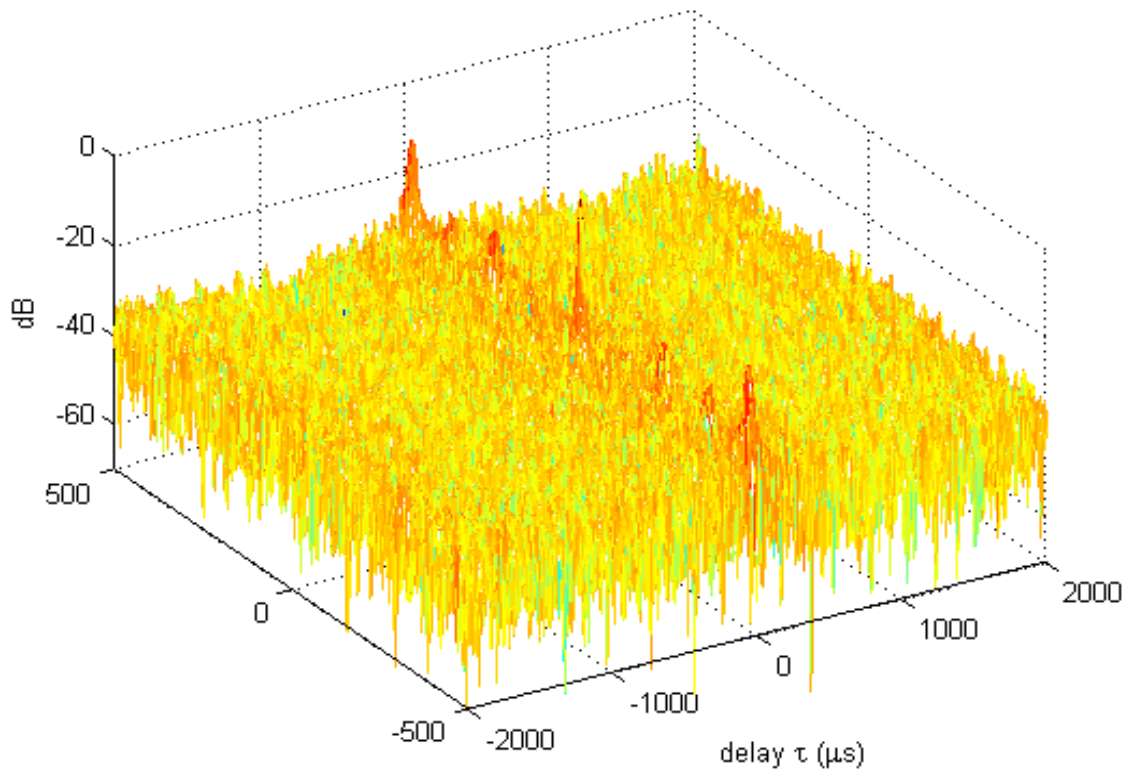


Figure A.2: Ambiguity plot of Classic FM transmission

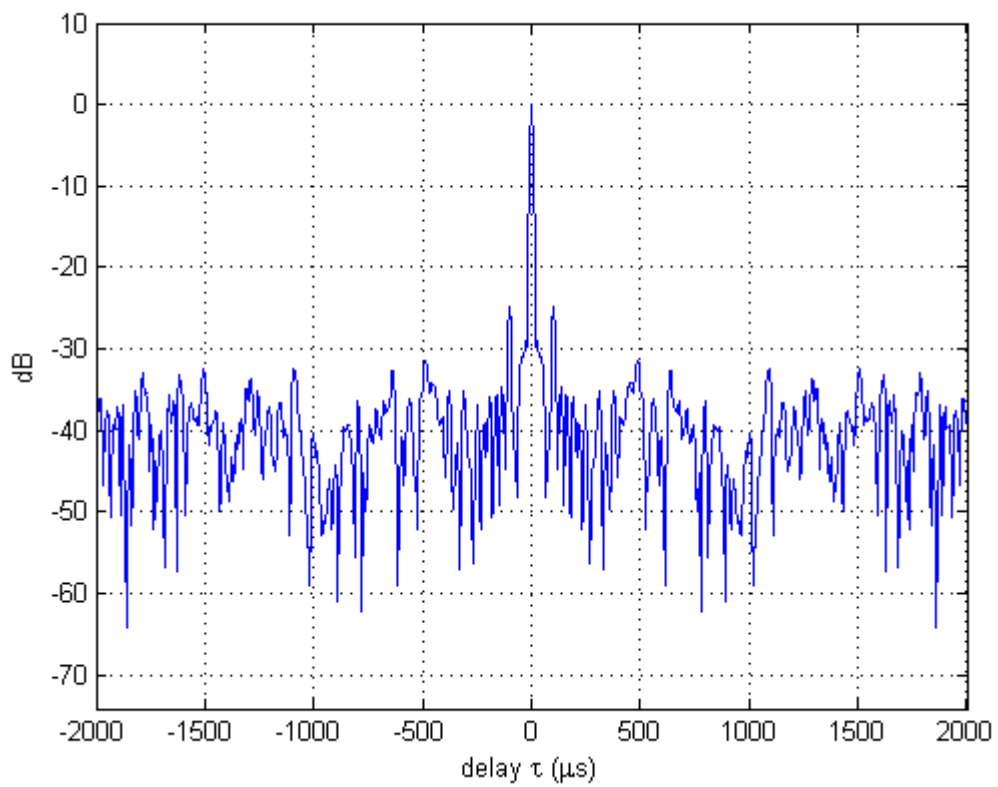


Figure A.2 a: Zero doppler cut through ambiguity plot

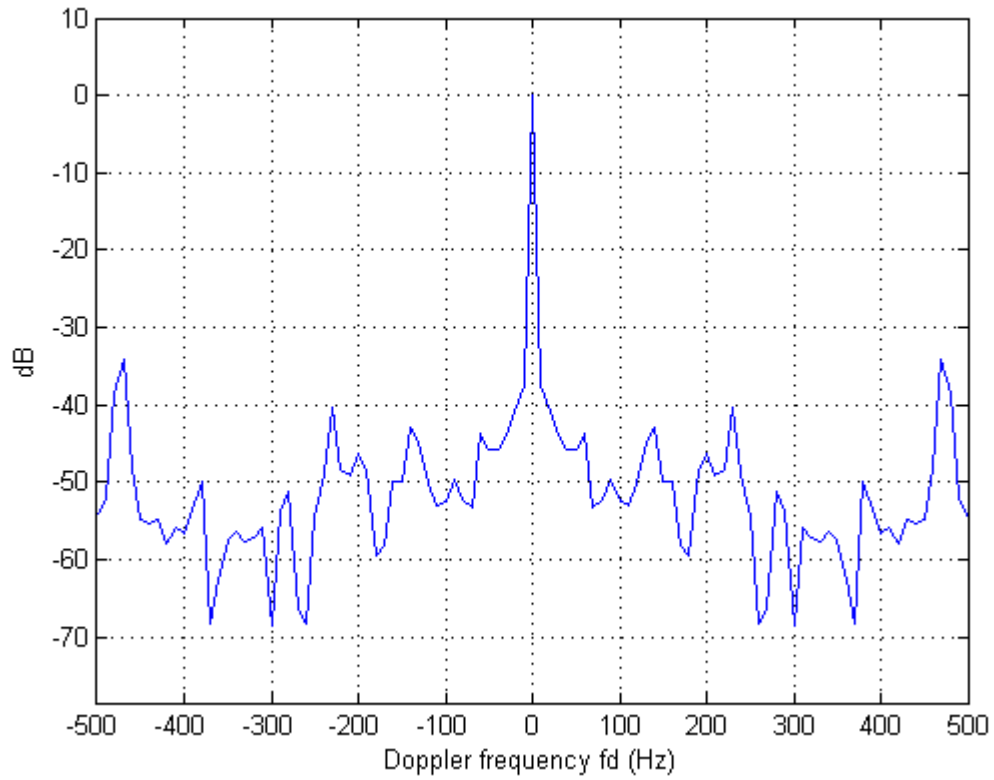


Figure A.2 b: Zero delay cut through ambiguity plot

Table A.2: Bandwidth variation of Classic FM waveform

Time (s)	Bandwidth (kHz)
0.1	9
0.2	7
0.3	20
0.4	25
0.5	25
0.6	15
0.7	24
0.8	22
0.9	9
1.0	32.5
1.1	45
1.2	13
1.3	24
1.4	48

1.5	41
1.6	13
1.7	4.5
1.8	0.6
1.9	5
2.0	4.5
Average Bandwidth (kHz)	18.81

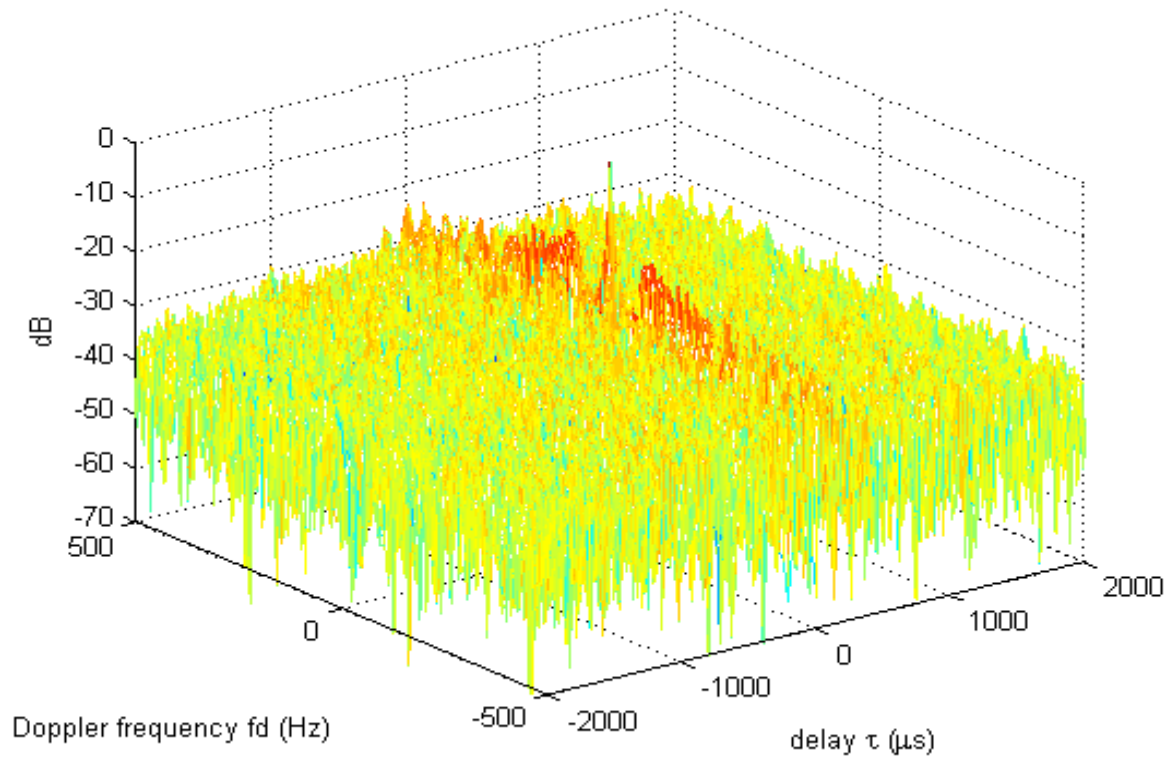


Figure A.3: Ambiguity plot of UmhloboFM transmission

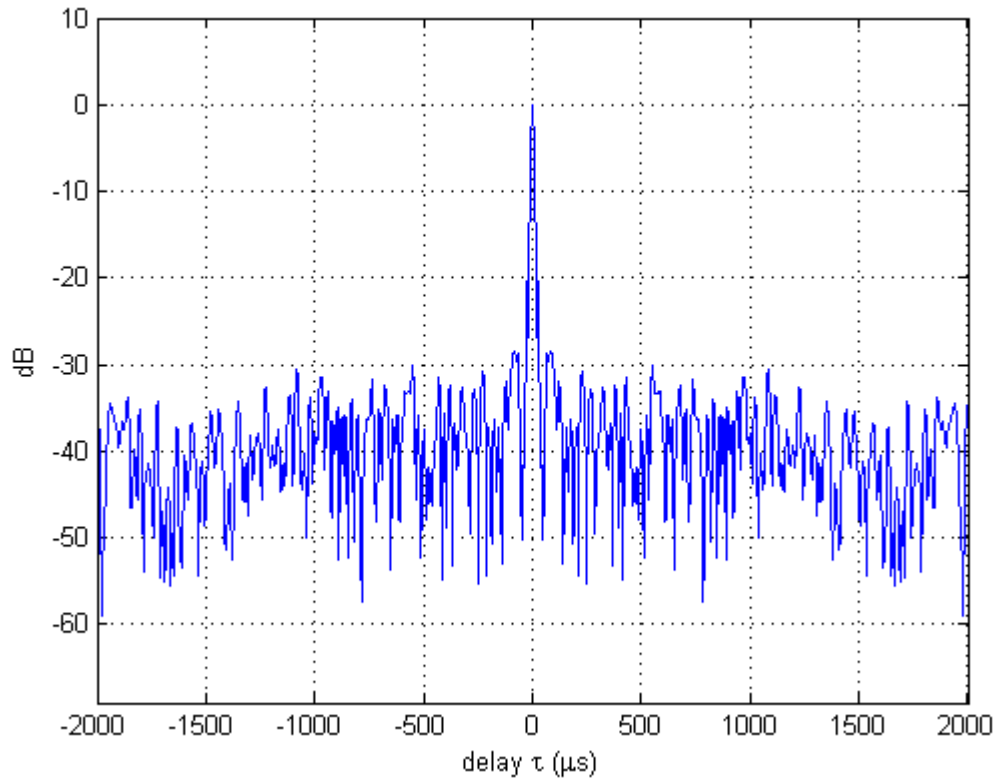


Figure A.3 a: Zero doppler cut through ambiguity plot

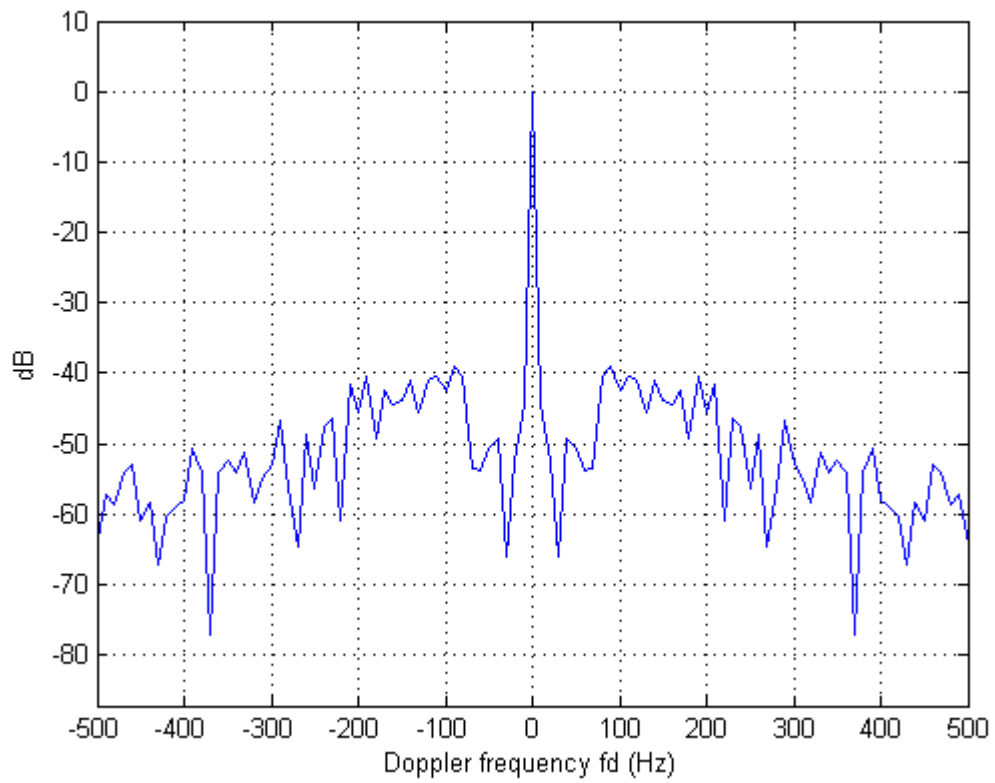


Figure A.3 b: Zero delay cut through ambiguity plot

Table A.3: Bandwidth variation of Umhlobo FM waveform

Time (s)	Bandwidth (kHz)
0.1	41
0.2	70
0.3	75
0.4	35
0.5	53
0.6	52
0.7	36
0.8	40
0.9	45
1.0	39
1.1	42.5
1.2	65
1.3	28
1.4	51
1.5	35
1.6	44
1.7	23
1.8	67
1.9	68
2.0	55
Average Bandwidth (kHz)	45

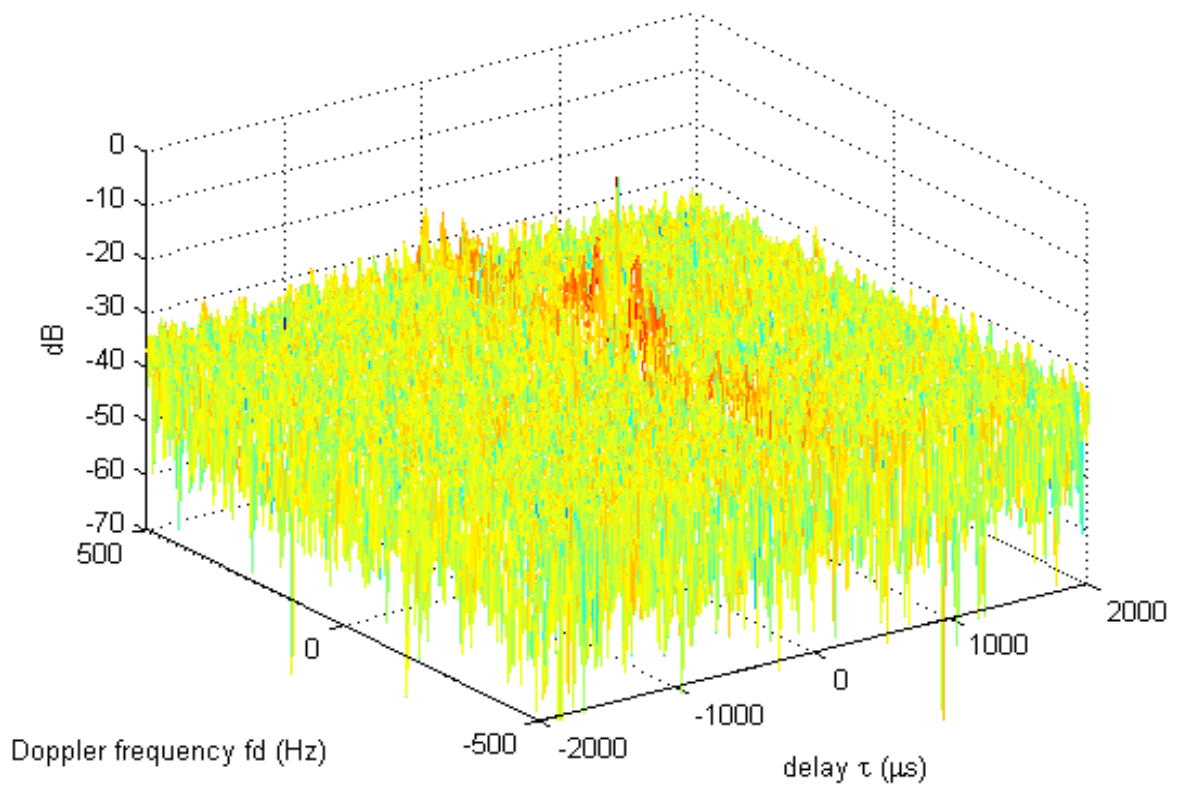


Figure A.4: Ambiguity plot for RGHP transmission

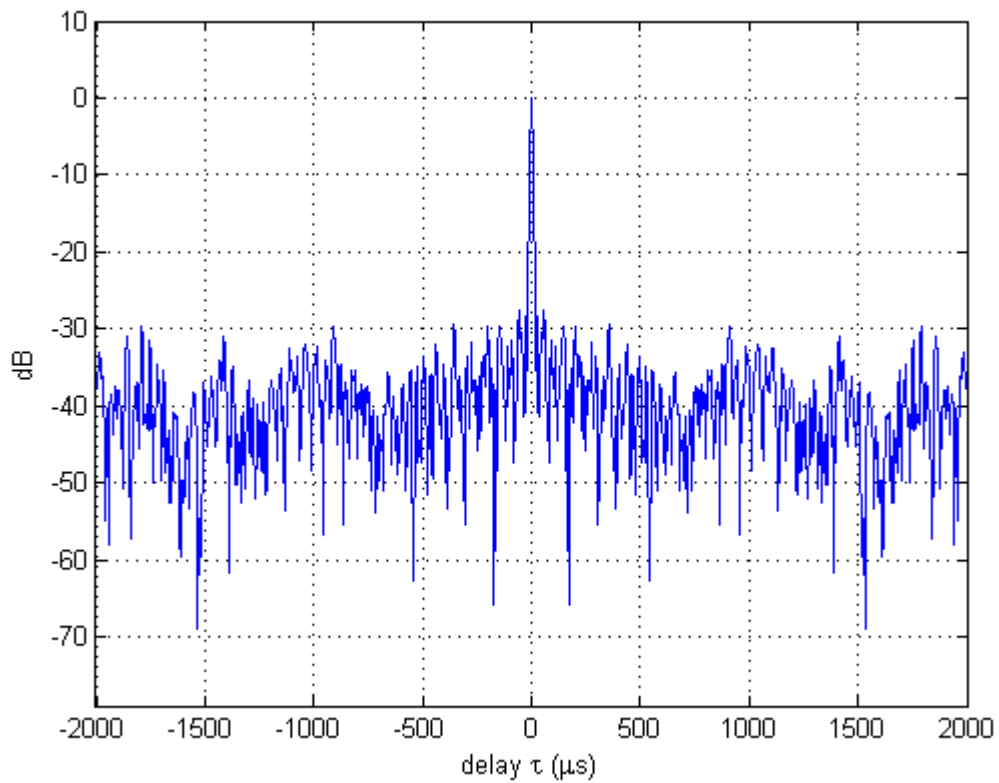


Figure A.4 a: Zero doppler cut through ambiguity plot

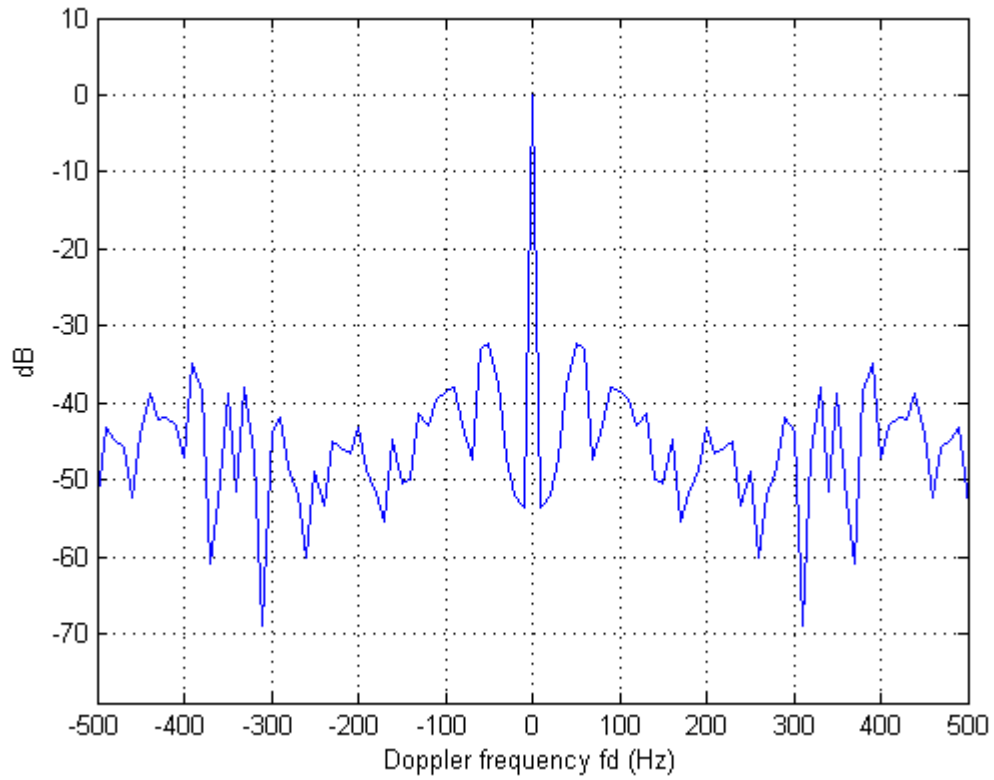


Figure A.4 b: Zero delay cut through ambiguity plot

Table A.4: Bandwidth variation of RGHP waveform

Time (s)	Bandwidth (kHz)
0.1	39
0.2	115
0.3	73
0.4	52
0.5	38
0.6	57
0.7	46
0.8	60
0.9	53
1.0	55
1.1	107
1.2	48
1.3	49
1.4	42
1.5	59

1.6	30
1.7	63
1.8	62
1.9	50
2.0	118
Average Bandwidth (kHz)	63.6

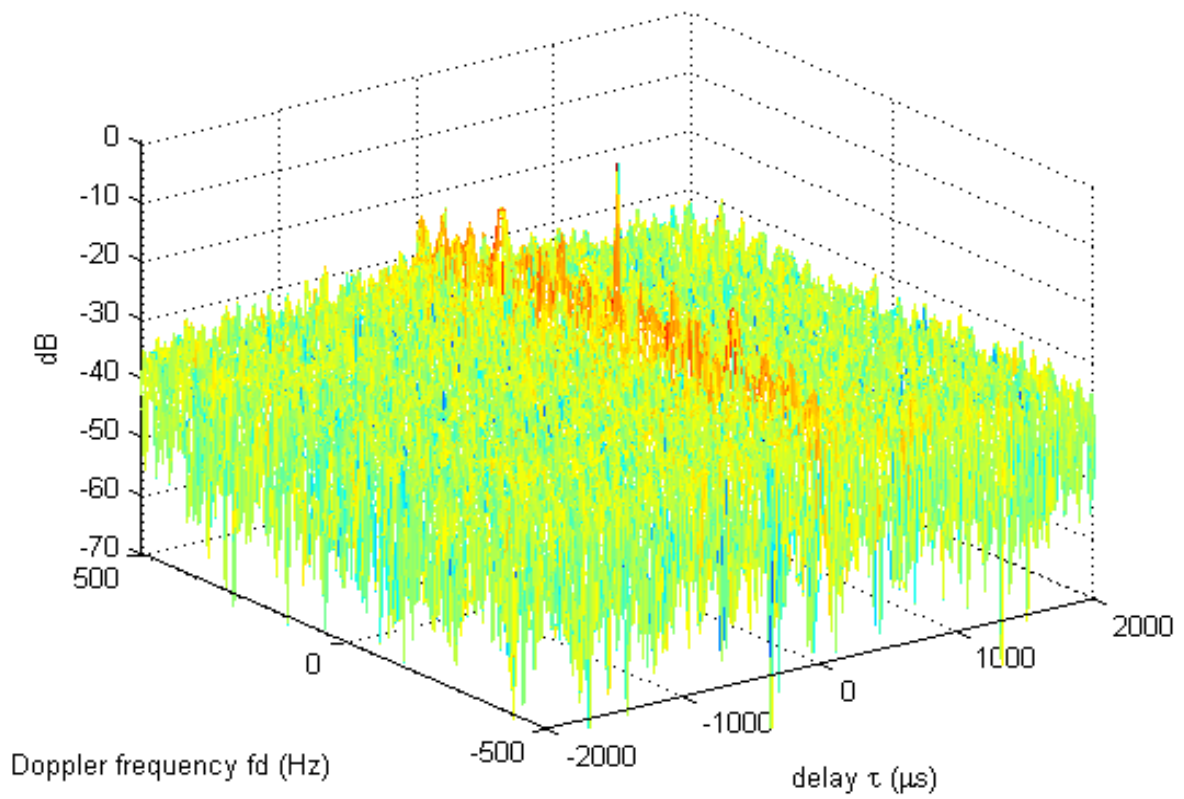


Figure A.5: Ambiguity plot of RSGR transmission

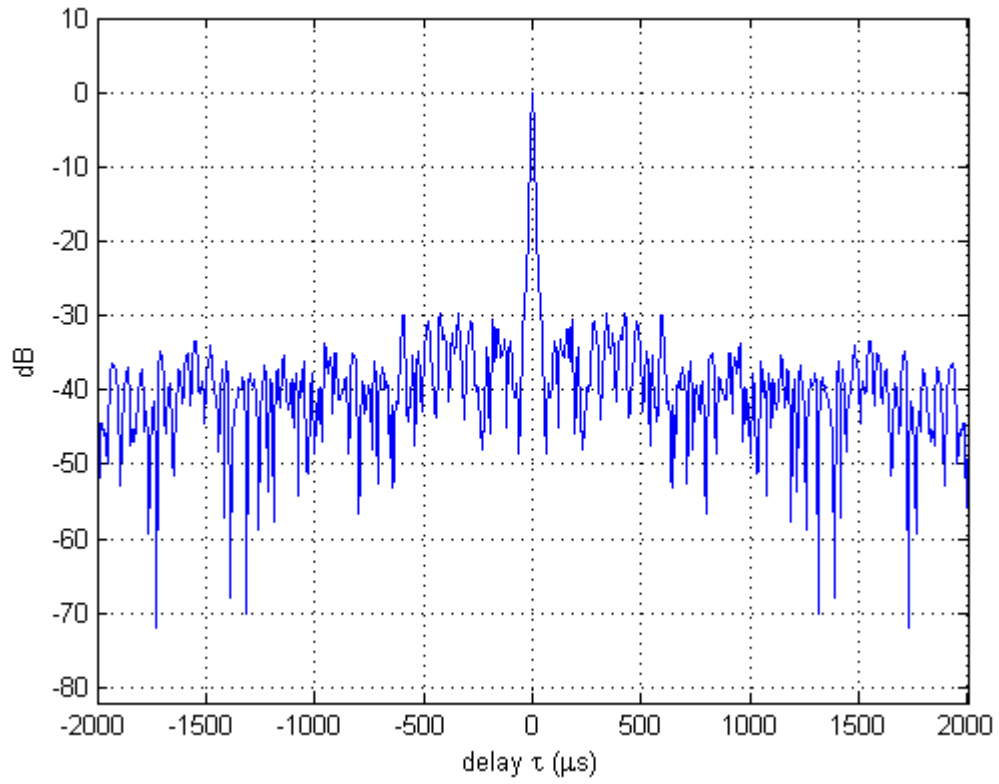


Figure A.5 a: Zero doppler cut through ambiguity plot

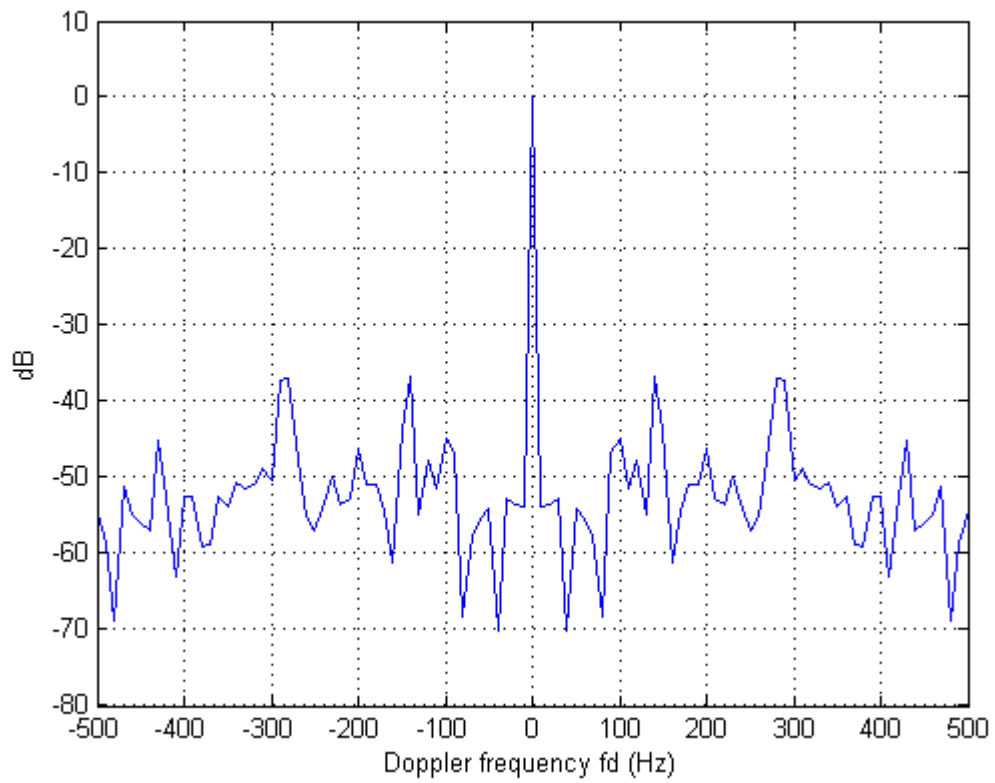


Figure A.5 b: Zero delay cut through ambiguity plot

Table A.5: Bandwidth variation of RSGR waveform

Time (s)	Bandwidth (kHz)
0.1	3.5
0.2	0.3
0.3	4
0.4	30
0.5	9
0.6	35
0.7	40
0.8	21
0.9	18
1.0	1.5
1.1	55
1.2	20
1.3	50
1.4	1.2
1.5	4.5
1.6	7.5
1.7	5.5
1.8	14
1.9	5.5
2.0	13
Average Bandwidth (kHz)	16.1

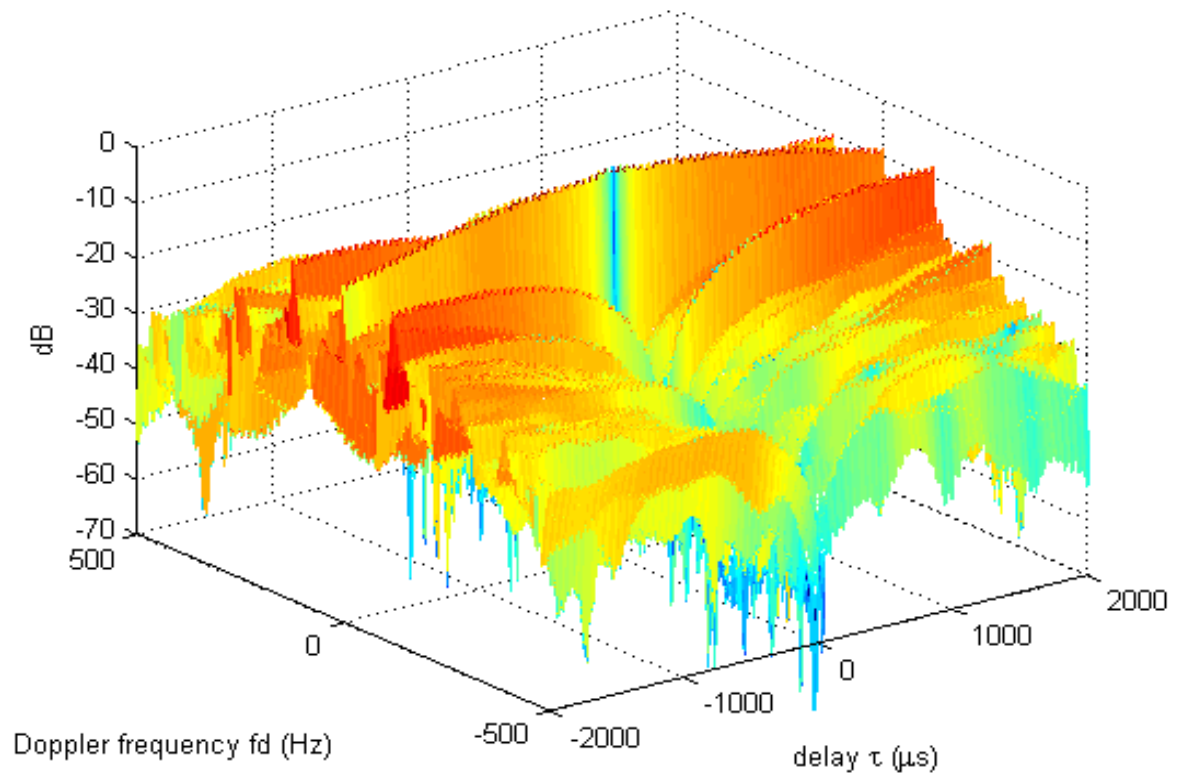


Figure A.6: Ambiguity plot of SAFM transmission

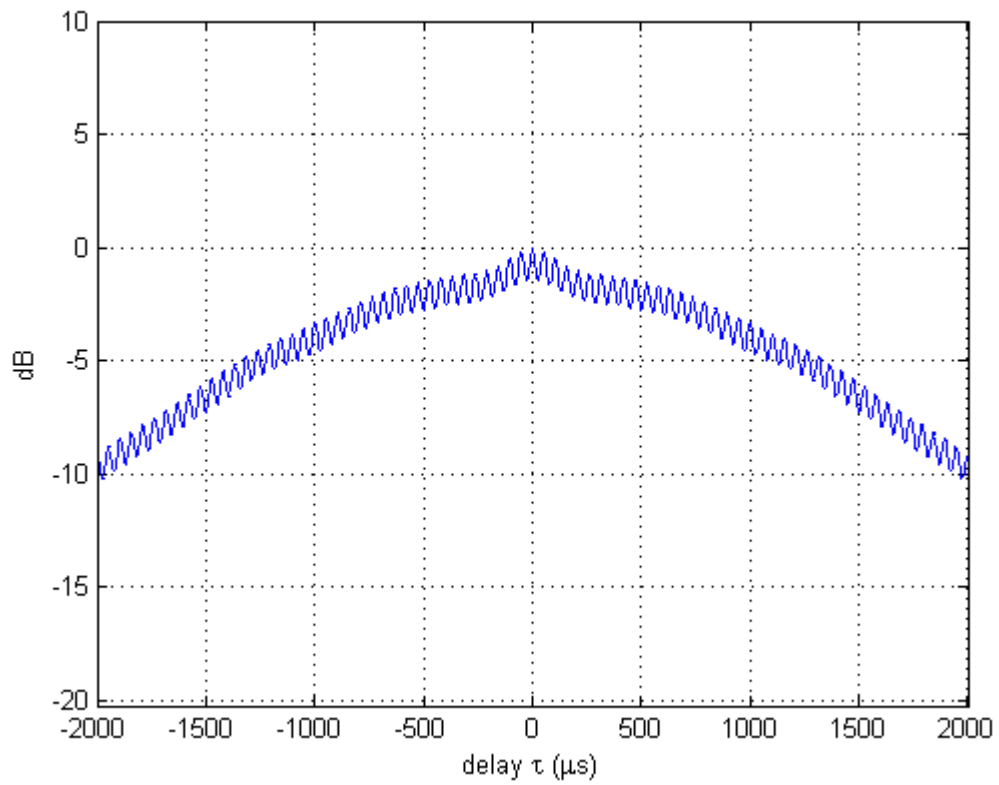


Figure A.6 a: Zero doppler cut through ambiguity plot

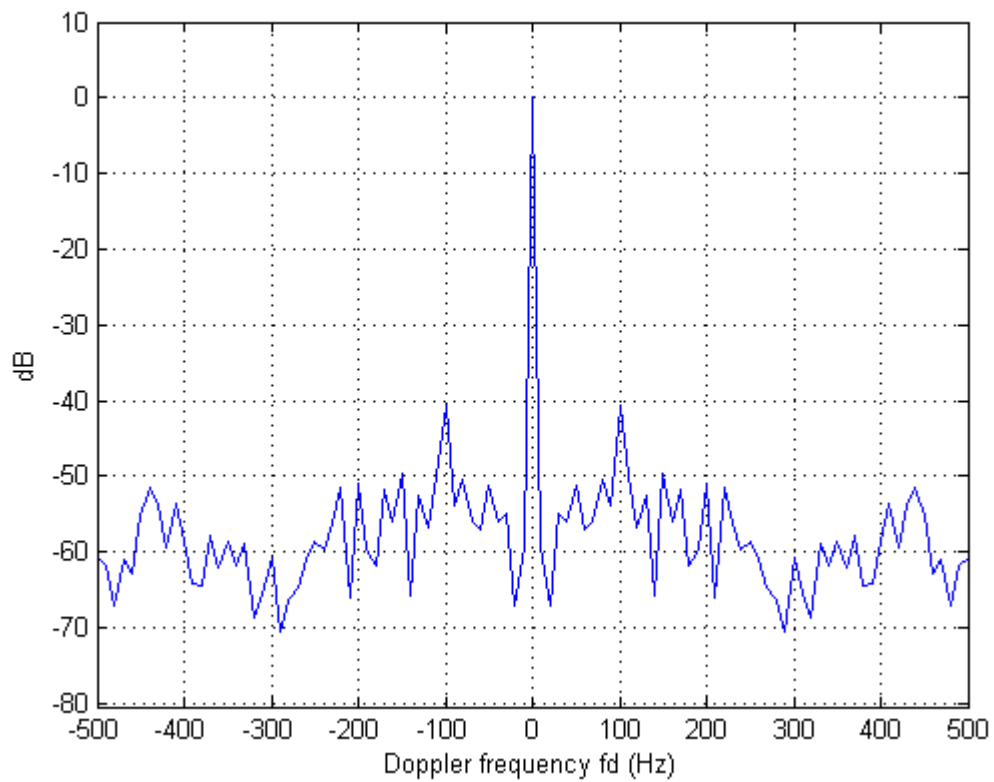


Figure A.6 b: Zero delay cut through ambiguity plot

Table A.6: Bandwidth variation of SAFM waveform

Time (s)	Bandwidth (kHz)
0.1	40
0.2	40
0.3	47.5
0.4	30
0.5	47
0.6	13
0.7	17
0.8	38
0.9	2.5
1.0	1.4
1.1	2.5
1.2	6
1.3	18
1.4	40
1.5	6
1.6	7.5
1.7	1.4
1.8	3.5
1.9	1.6
2.0	27.5
Average Bandwidth (kHz)	19.9

# **Appendix B**

## **Data Sheets and Sentech Table**

Sentech Station Information  
(First Page Only)

STATION NAME	STATION CODE	LAT DEG	LAT MIN	LAT SEC	LONG DEG	LONG MIN	LONG SEC	MAP NUMBER	SITE HEIGHT	MAST HEIGHT	SERVICE CODE	TX FREQ	TX OUT PWR	ERP SPEC	FREQ BAND	ANT GAIN	ANT FACE	ANT TIER
CAPE TOWN	C1	-34	-3	-15	18	23	15	3418AB	902	154	RAD5	89	1	10	FM	10	4	6
CAPE TOWN	C1	-34	-3	-15	18	23	15	3418AB	902	154	LOBO	92.1	1	10	FM	10	4	6
CAPE TOWN	C1	-34	-3	-15	18	23	15	3418AB	902	154	RGHP	95.3	1	10	FM	10	4	6
CAPE TOWN	C1	-34	-3	-15	18	23	15	3418AB	902	154	2000	98.6	1	10	FM	10	4	6
CAPE TOWN	C1	-34	-3	-15	18	23	15	3418AB	902	154	RSGR	102.1	1	10	FM	10	4	6
CAPE TOWN	C1	-34	-3	-15	18	23	15	3418AB	902	154	SAFM	105.7	1	10	FM	10	4	6
CAPE TOWN	C1	-34	-3	-15	18	23	15	3418AB	902	154	SBC1	183.25	1	15.85	TVV	12	4	3
CAPE TOWN	C1	-34	-3	-15	18	23	15	3418AB	902	154	SBC2	207.25	1	15.85	TVV	12	4	3
CAPE TOWN	C1	-34	-3	-15	18	23	15	3418AB	902	154	MNET	231.25	1	15.85	TVV	12	4	3
CAPE TOWN	C1	-34	-3	-15	18	23	15	3418AB	902	154	CSN	735.25	0.1	0.25	TVU	4	4	1
CAPE TOWN	C1	-34	-3	-15	18	23	15	3418AB	902	154	ETV	767.25	1	6.76	TVU	8.3	4	4
CAPE TOWN	C1	-34	-3	-15	18	23	15	3418AB	902	154	SBC3	799.25	1	6.76	TVU	8.3	4	4
TABLE MOUNTAIN	C1.1	-33	-57	-25	18	24	13	3318CD	1067	14	METR	88.6	0.02	0.02	FM	0	1	1
TABLE MOUNTAIN	C1.1	-33	-57	-25	18	24	13	3318CD	1067	14	RAD5	89.9	0.02	0.02	FM	0	1	1
TABLE MOUNTAIN	C1.1	-33	-57	-25	18	24	13	3318CD	1067	14	LOBO	92.5	0.02	0.02	FM	0	1	1
TABLE MOUNTAIN	C1.1	-33	-57	-25	18	24	13	3318CD	1067	14	RGHP	95.8	0.02	0.02	FM	0	1	1
TABLE MOUNTAIN	C1.1	-33	-57	-25	18	24	13	3318CD	1067	14	2000	99.1	0.02	0.02	FM	0	1	1
TABLE MOUNTAIN	C1.1	-33	-57	-25	18	24	13	3318CD	1067	14	RSGR	102.6	0.02	0.02	FM	0	1	1
TABLE MOUNTAIN	C1.1	-33	-57	-25	18	24	13	3318CD	1067	14	SAFM	106.2	0.02	0.02	FM	0	1	1
TABLE MOUNTAIN	C1.1	-33	-57	-25	18	24	13	3318CD	1067	14	SBC2	495.25	0.1	0.5	TVU	7	2	1
TABLE MOUNTAIN	C1.1	-33	-57	-25	18	24	13	3318CD	1067	14	SBC1	527.25	0.1	0.5	TVU	7	2	1
TABLE MOUNTAIN	C1.1	-33	-57	-25	18	24	13	3318CD	1067	14	MNET	591.25	0.1	0.5	TVU	7	2	1
TABLE MOUNTAIN	C1.1	-33	-57	-25	18	24	13	3318CD	1067	14	SBC3	751.25	0.1	0.59	TVU	7.7	2	1
TABLE MOUNTAIN	C1.1	-33	-57	-25	18	24	13	3318CD	1067	14	CSN	783.25	0.05	0.29	TVU	7.7	2	1
TABLE MOUNTAIN	C1.1	-33	-57	-25	18	24	13	3318CD	1067	14	ETV	815.25	0.1	0.59	TVU	7.7	2	1
AURORA	C1.10	-33	-49	-39	18	38	29	3318DC	176	23	SBC2	487.25	0	0	TVU	4.2	3	1
AURORA	C1.10	-33	-49	-39	18	38	29	3318DC	176	23	SBC3	551.25	0	0	TVU	4.2	3	1
AURORA	C1.10	-33	-49	-39	18	38	29	3318DC	176	23	MNET	583.25	0	0	TVU	4.2	3	1
AURORA	C1.10	-33	-49	-39	18	38	29	3318DC	176	23	SBC1	727.25	0	0	TVU	4.2	3	1
AURORA	C1.10	-33	-49	-39	18	38	29	3318DC	176	23	ETV	759.25	0	0	TVU	4.2	3	1
GRABOUW	C1.11	-34	-6	-5	18	58	3	3418BB	1181	30	RHLD	93.6	0.1	0.1	FM	0	1	1
GRABOUW	C1.11	-34	-6	-5	18	58	3	3418BB	1181	30	RKFM	94.9	0.01	0.01	FM	0	1	1
GRABOUW	C1.11	-34	-6	-5	18	58	3	3418BB	1181	30	RSGR	101.7	0.01	0.01	FM	0	1	1
GRABOUW	C1.11	-34	-6	-5	18	58	3	3418BB	1181	30	SAFM	105.3	0.01	0.01	FM	0	1	1
GRABOUW	C1.11	-34	-6	-5	18	58	3	3418BB	1181	30	HART	107.8	0	0.01	FM	4	1	1
GRABOUW	C1.11	-34	-6	-5	18	58	3	3418BB	1181	30	SBC2	615.25	0.05	0.5	TVU	10	3	4

**4937 DI5 RF TUNER MODULE**  
**3x8899 (3x7702)**  
**ADVANCE DATA SHEET**

**CABLE MODEM APPLICATIONS**

**1 APPLICATIONS**

The 4937 DI5 Tuner Module is specifically designed for subscriber-side cable modem applications.

**2 FEATURES**

- DOCSIS compatible
- VHF, Hyperband, and UHF
- Band selection and tuning controlled by I<sup>2</sup>C bus
- Downstream frequency range from 50 MHz to 860 MHz
- Upstream frequency range from 5 MHz to 42 MHz
- Single 5V power supply

**3 INTRODUCTION**

The receiver uses a single-conversion approach to 43.75 MHz with the reception frequency range divided into VHF low, VHF high, and UHF. A second conversion to 5.75 MHz is available for QAM demodulators requiring a lower center frequency (3x7702); alternately, the output frequency is 43.75 MHz (3x8899).

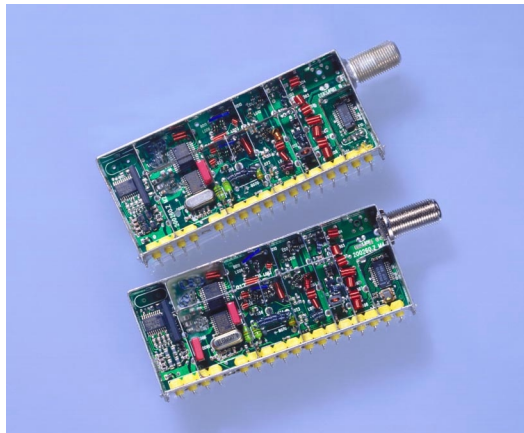


**Figure 1** 4937 DI5 RF Tuner Modules

Band selection and tuning is done via the I<sup>2</sup>C-bus, while a separate three-wire bus and transmit enable control the upstream amplifier.

The common cable input/output is realized by an F-connector (75Ω) per [IPS-sp-406].

Two automatic gain control (AGC) inputs are available to level the signal into an external demodulator. The tuner's intermediate frequency (IF) output is designed to drive a low-pass image reject filter prior to the QAM demodulator IC.

A DC/DC converter is built in, so that only a single supply voltage of 5V is required.

#### 4 MECHANICAL SPECIFICATIONS

This section contains mechanical specifications for the 4937 DI5 RF Tuner Module.

##### 4.1 MECHANICAL DRAWING

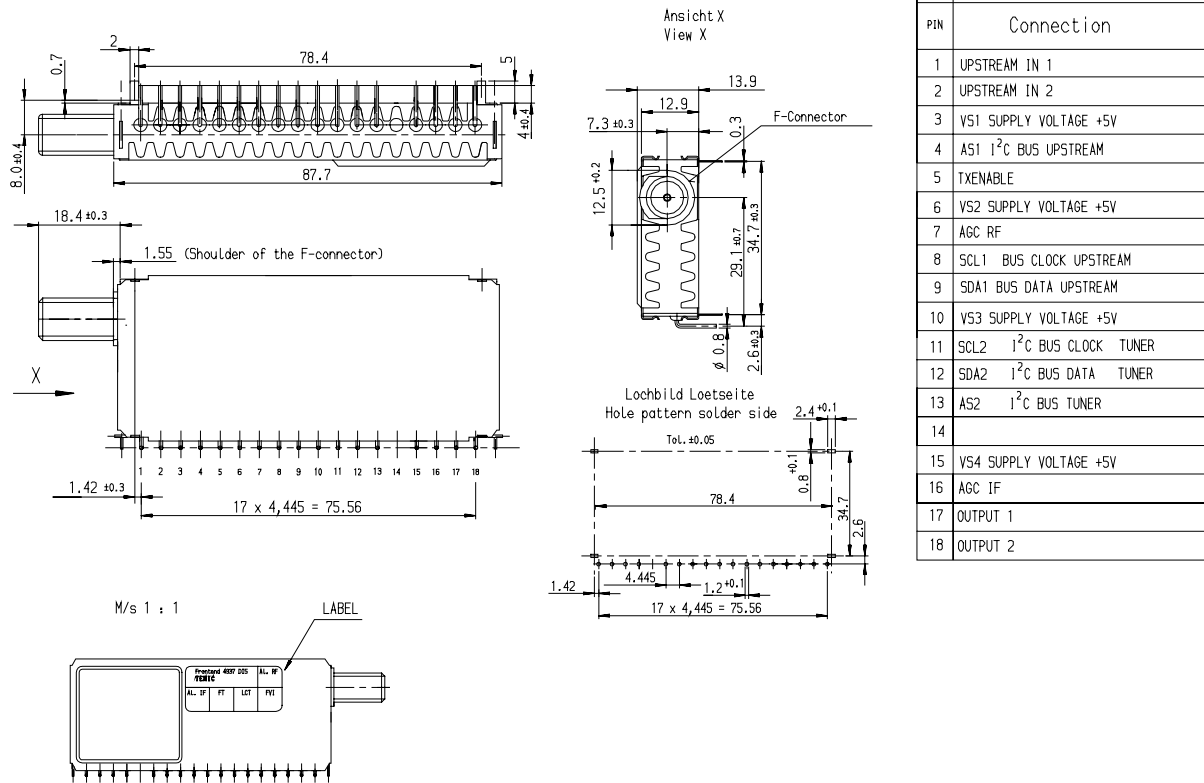


Figure 2 Mechanical Drawing

Preliminary



## 4.2 MECHANICAL CHARACTERISTICS

**Table 1 Mechanical Characteristics**

CHARACTERISTIC	DIMENSIONS
Dimensions	According to the drawing in Figure 2
Weight	Approximately 56g
Plug holding strength	Plug according to SCTE spec. IPS-sp-407
Tuner connection	The tuner provides four pins at bottom cover for horizontal mounting and grounding
Screw fixing of F-connector*	Absolute maximum torque strength: 3.39 Nm / only once Absolute maximum cantilever strength: 3.39 Nm Absolute maximum axial strength: 8.99N

\* If the tuner is not mounted on the chassis, the frame may be bent during the test. Regardless of mounting, the F-connector will not be pulled out of the frame.

## 5 FUNCTIONAL SPECIFICATIONS

### 5.1 ABSOLUTE MAXIMUM RATINGS

Stresses greater than those listed in Table 2 may cause permanent damage to the device. These are stress ratings only; functional operation of the device under conditions other than those listed in Table 3 is not recommended or implied. Exposure to any of the absolute-maximum rating conditions for extended periods of time may affect reliability.

**Table 2 Absolute Maximum Specifications**

PARAMETER	MIN	MAX	UNIT
Supply voltage		6	V
AGC voltage		6	V
Storage temperature	-30	+70	°C



## 5.2 OPERATING CHARACTERISTICS

The operating characteristics listed in Table 3 reflect the conditions necessary for optimal performance and operating reliability.

**Table 3 Operating Characteristics**

PARAMETER	MIN	TYP	MAX	UNIT	CONDITIONS OR LOCATION
Frequency range					
VHF Low	50		162	MHz	
VHF High	156		469	MHz	
UHF	463		860	MHz	
Frequency range, referenced to center frequency of 6 MHz bandwidth					
VHF Low	53		159	MHz	
VHF High	159		466	MHz	
UHF	466		857	MHz	
Tuning resolution					
Standard tuning increment (see Table 8)		62.5		kHz	
Recommended takeover frequencies, referred to center frequency					
VHF Low / VHF High		158		MHz	
UHF		464		MHz	
Output Frequency					
3x7702		5.75		MHz	± 0.05 MHz
3x8899		43.75		MHz	± 0.05 MHz
Input impedance					
VHF/UHF Common		75		Ω	Unbalanced
AGC voltage for maximum gain					
RF			4	V	± 0.1V
IF			4	V	± 0.1V
Power supply voltage					
Voltage $V_{S1}$		5	± 0.3	V	Pin 3
Voltage condition $V_{S1}$			150	mA	
Voltage $V_{S2}$		5	± 0.25	V	Pin 6
Voltage condition $V_{S2}$			200	mA	
Voltage $V_{S3}$		5	± 0.25	V	Pin 10
Voltage condition $V_{S3}$			200	mA	
Voltage $V_{S4}$		5	± 0.3	V	Pin 15
Voltage condition $V_{S4}$			100	mA	
Permissible ripple voltage (20 Hz to 100 kHz)			20	mVpp	

Preliminary



PARAMETER	MIN	TYP	MAX	UNIT	CONDITIONS OR LOCATION
Temperature					
Operating temperature	0		60	°C	

## 6 TUNER DOWNSTREAM DATA

**Table 4 Electrical Characteristics**

PARAMETER	TEST CONDITIONS	MIN	TYP	MAX	UNIT
Frequency range		55		860	MHz
Input signal level		40		80	dB $\mu$ V
Voltage gain	Measured between antenna input and IF output (pins 17 and 18). The input is loaded with 75 $\Omega$ and the IF output is loaded with a test circuit (see Figure 5).	60	80	95	dB
Output level at 1 k $\Omega$	The output impedance is about 220 $\Omega$ . Pins 17 and 18 are not DC decoupled.		1		V <sub>pp</sub>
Noise figure	VHF Low		8	10	dB
	VHF High		8	10	dB
	UHF		8	10	dB
VSWR	Antenna input			3	
IF Rejection [Rejection of CW Signal at highest possible IF (46.75 MHz) fed into the tuner input relative to a CW at desired channel center frequency measured at the IF mixer output. Both signals must have the same level at F-connector input.]	VHF Low	50	70		dB
	VHF High	60	80		dB
	UHF	60	80		dB
Upstream rejection	Isolation between upstream output (5 MHz to 42 MHz) and IF mixer out (40.75 MHz to 46.75 MHz)	75			dB
Image rejection	VHF Low	60	70		dB
	VHF High	55	65		dB
	UHF	55	60		dB
RF Tilt	For all AGC settings and over a 6 MHz bandwidth around center frequency			2.5	dB
Signal level for 1 dB gain compression	AGC deactivated with AGC = 4V (pins 7 and 16) for maximum gain	72			dB $\mu$ V
Phase noise					
VHF Low	Measured at 1 kHz distance from carrier		-71	-55	dBc/Hz
VHF High			-60	-55	dBc/Hz
UHF			-58	-55	dBc/Hz

Preliminary



PARAMETER	TEST CONDITIONS	MIN	TYP	MAX	UNIT
VHF Low	Measured at 10 kHz distance from carrier		-95	-80	dBc/Hz
VHF High			-85	-80	dBc/Hz
UHF			-85	-80	dBc/Hz
VHF Low	Measured at 20 kHz distance from carrier		-102	-90	dBc/Hz
VHF High			-92	-85	dBc/Hz
UHF			-90	-85	dBc/Hz
VHF Low	Measured at 100 kHz distance from carrier		-109	-100	dBc/Hz
VHF High			-106	-100	dBc/Hz
UHF			-103	-100	dBc/Hz
Oscillator voltage	F-connector terminated with 75Ω				
<860 MHz				15	dBμV
<1740 MHz				40	dBμV
Intermodulation	With a fully loaded multi-tone signal generator (129 channels), with carrier levels at +15 dBmV, and with AGC set for a 44 dBmV first IF level, distortion levels shall not exceed these limits.				
Composite triple beat				-50	dBc
Composite second order beat				-50	dBc
Group delay	Over any 6 MHz bandwidth centered about the tuned frequency, and for AGC over the range from maximum gain down to -25 dB below maximum gain, the group delay variation as measured between the antenna terminal and the output terminal (Pins 17 and 18) shall not exceed these limits.				
55 MHz to 860 MHz			100	200	ns p-p
PLL Setting time	Charge pump current high		40	100	ms
AGC Range					
RF AGC range (Pin 7)	By varying AGC voltage from +4V to +0.5V, this gain reduction must be possible	40	50		dB
IF AGC range (Pin 16)		26	33		dB

Preliminary



### 6.1 INFLUENCE OF AGC

The curves in Figure 3 and Figure 4 are measured at +25°C with an input level of 45 dBμV. The values are typical values and can vary within the guaranteed limits.

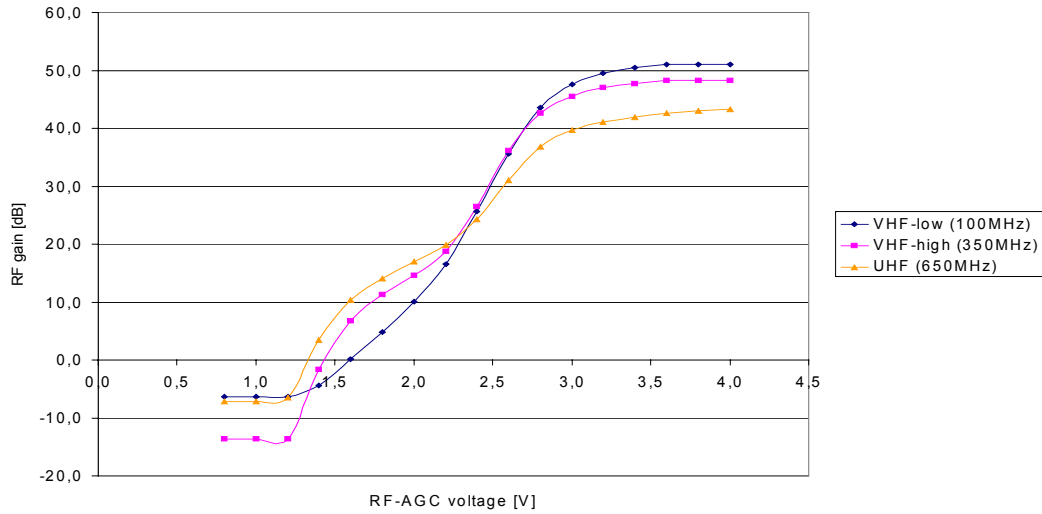


Figure 3 RF Gain vs. AGC Voltage

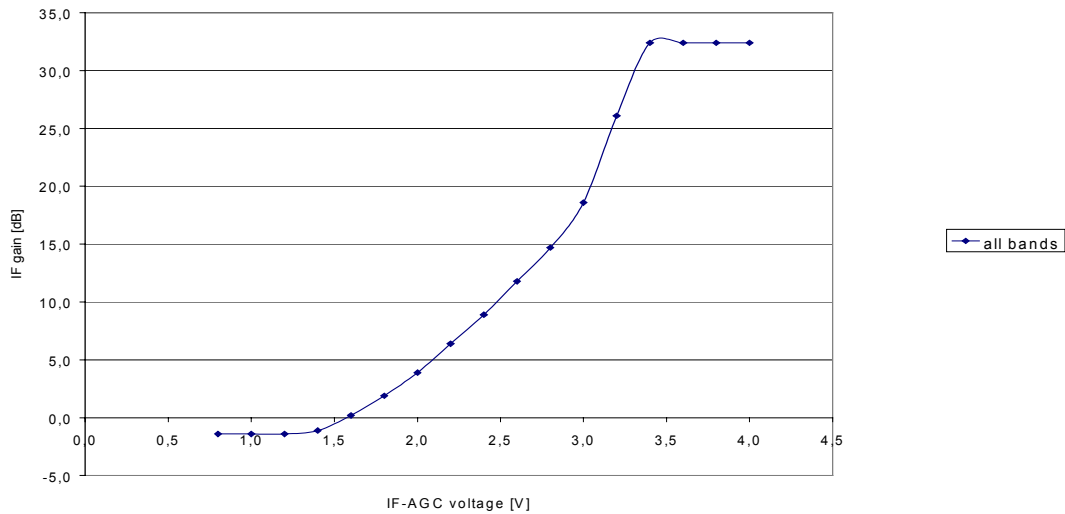


Figure 4 IF Gain vs. AGC Voltage

The noise figure shall not increase by more than the corresponding AGC gain reduction. The input return loss shall be maintained within the specified limits over the entire range of AGC voltage.

Preliminary



## 7 TUNER UPSTREAM DATA

All data is measured according to the test circuit shown in Figure 6 on page 9. The input impedance between Pins 1 and 2 for this tuner is 50 ohms.

Table 5 Tuner Upstream Data

PARAMETER	TEST CONDITIONS	MIN	TYP	MAX	UNIT
Input level	Source impedance 75Ω sym		33	35	dBmV
Voltage gain	Gain control word = maximum gain	25	27	29	dB
Gain steps		0.7	1	1.3	dB
Gain range		59			dB
Group delay variation	5 MHz to 42 MHz (3.2 MHz bandwidth)			60	nsec
Amplitude ripple variation					
5 MHz to 42 MHz	1.28 MHz bandwidth			± 0.2	dB
Absolute accuracy of transmitted power	5 MHz to 42 MHz			± 2	dB
TX Transient Spurs					
Gain setting = maximum gain				16	mVp-p
Gain setting < (maximum gain -12)				8	mVp-p
TX Transient duration	TXEN rise/fall time < 0.1 μs			2	μsec
Reverse channel harmonic distortion	V <sub>out</sub> = +58 dBmV				
5 MHz to 42 MHz	2 <sup>nd</sup> harmonic level, single tone	-53			dBc
5 MHz to 42 MHz	3 <sup>rd</sup> harmonic level, single tone	-54			dBc
54 MHz to 60 MHz			-40	-35	dBmV
60 MHz to 88 MHz			-50	-40	dBmV
88 MHz to 860 MHz			-50	-45	dBmV
Noise floor	Input terminated with 75Ω				
Transmit mode noise	Voltage gain 24 dB		131	150	nV / √Hz
Transmit disable mode noise	TXEN low, voltage gain 24 dB		810		pV / √Hz

Preliminary

## 8 TUNER MEASUREMENT TEST CONDITIONS

All tuner data are held under the following conditions unless otherwise noted:

- Measurement tolerance 10% or 1 dB
- Ambient temperature + 25°C ± 3°C
- Supply voltages + 5V ± 2%
- AGC voltage + 4V ± 2%



## 8.1 TEST CIRCUITS

### 8.1.1 VOLTAGE GAIN, TILT, AND NOISE FIGURE

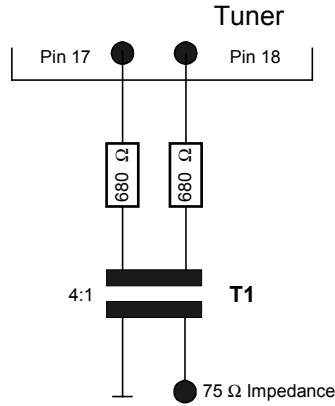


**Figure 5** Test Circuit for Voltage Gain, Tilt, and Noise Figure

For the voltage gain, tilt, and noise figure test circuit:

- Loss of test-dummy: 22.6 dB
- T1 = RF – Transformer (ohms - ratio = 1:4)
- Type: MCL T4-1 or equivalent

### 8.1.2 UPSTREAM CHANNEL

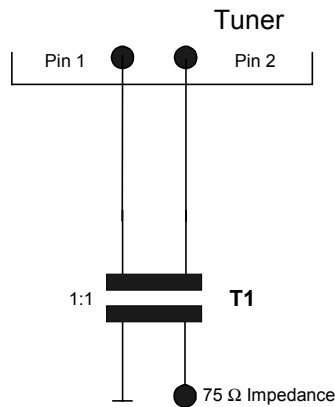


**Figure 6** Test Circuit for Upstream Channel

For the upstream channel test circuit:

- Loss of test-dummy: < 1 dB
- T1 = RF – Transformer (ohms - ratio = 1:1)
- Type: MCL T1-1 or equivalent

Preliminary



## 9 CONTROL

### 9.1 WRITE DATA FORMAT FOR I<sup>2</sup>C BUS

Table 6 Write Data Format

	MSB							LSB	ACK
Address byte	1	1	0	0	0	MA1	MA0	R/W <sup>1</sup>	A <sup>2</sup>
Divider byte 1	0	N14	N13	N12	N11	N10	N9	N8	A
Divider byte 2		N7	N6	N5	N4	N3	N2	N1	N0
Control byte 1	1	CP	T2	T1	T0	RSA	RSB	OS	A
Control byte 2		P7	P6	P5	P4	P3	P2	P1	P0

<sup>1</sup> R/W = 0 is write mode

<sup>2</sup> A = Acknowledge

### 9.2 ADDRESS SELECTION FOR I<sup>2</sup>C BUS

Table 7 Address Selection

MA1	MA0	ADDRESS	VOLTAGE AT PIN 11
0	0	C0	(0 to 0.1) V <sub>S3</sub>
0	1	C2	Open circuit or (0.2 to 0.3) V <sub>S3</sub>
1	0	C4	(0.4 to 0.6) V <sub>S3</sub>
1	1	C6	(0.9 to 1) V <sub>S3</sub>

### 9.3 OSCILLATOR FREQUENCY AND DIVIDER BYTE CALCULATION

Table 8 Oscillator Frequency and Divider Byte Calculation

RSA	RSB	REFERENCE DIVIDER	MINIMUM TUNING STEP	F <sub>REF</sub>
1	1	512	62.5 kHz	7.8125 kHz
X	0	640	50.0 kHz	6.25 kHz
0	1	1024	31.25 kHz	3.90625 kHz

Use the following formula to calculate oscillator frequency and divider byte.

$$f_{osc} = f_{ref} \times 8 \times SF$$

Preliminary



Where:

$f_{osc}$  = Local oscillator frequency

$f_{ref}$  = Crystal reference frequency / 512 = 4 MHz / 512 = 7.8125 kHz

SF = Programmable scaling factor

Scaling factor is  $SF = 16384 \times n14 + 8192 \times n13 + 4096 \times n12 + 2048 \times n11 + 1024 \times n10 + 512 \times n9 + 256 \times n8 + 128 \times n7 + 64 \times n6 + 32 \times n5 + 16 \times n4 + 8 \times n3 + 4 \times n2 + 2 \times n1 + n0$

## 9.4 CONTROL BYTE (I<sup>2</sup>C)

Table 9 Control Byte 1 Settings (Default)

	MSB							LSB	ACK
Control byte 1	1	0	0	0	1	1	1	0	A

Table 10 Control Byte 1 Settings Default Descriptions

CODE	DESCRIPTION	SETTINGS
CP	Charge pump current	1 = Fastest tuning 0 = Better phase noise for distance < 10 kHz to the carrier
OS	Tuning voltage	0 = On 1 = Off
RSA, RSB	Reference divider	See Table 8 on page 10
T0, T1, T2	Test mode bit	See Table 11

Table 11 Test Mode Bit Settings

T2	T1	T0	DEVICE OPERATION
0	0	1	Normal mode
0	1	x	Charge pump is off
1	1	0	Charge pump is sinking current
1	1	1	Charge pump is sourcing current
1	0	0	Internal test mode
1	0	1	Internal test mode

Table 12 Control Byte 2 (Band Selection)

BAND	ACTIVE PORT	P7	P6	P5	P4	P3	P2	P1	P0
UHF	P0	0	X	1	1	X	X	X	X
VHF High	P2	1	X	0	1	X	X	X	X
VHF Low	P1	1	X	1	0	X	X	X	X

Note: X = not used, P3 = used for upstream shutdown (see section 9.6)

Preliminary



## 9.5 READ DATA FORMAT (I<sup>2</sup>C)

**Table 13 Read Data Format (I<sup>2</sup>C)**

	MSB							LSB	ACK
Address byte	1	1	0	0	0	MA1	MA0	R/W	A
Status byte	POR	FL	I2	I1	I0	A2	A1	A0	A

*Note: MSB is transmitted first.*

**Table 14 Read Data Format Descriptions**

CODE	DESCRIPTION
R/W	1 = Read mode
POR	Power on reset flag (POR = 1 at power on)
FL	In lock flag (FL = 1 when PLL is locked)
I2, I1, I0	Digital levels for I/O ports P0, P1, and P2
A2, A1, A0	Digital output of 5-level ADC for AFC function. Values for correct tuning: A2 = 0, A1 = 1, A0 = 0

## 9.6 PROGRAMMABLE-GAIN AMPLIFIER CONTROL (THREE-WIRE BUS)

**Table 15 Pin Map (Three-Wire Bus)**

PIN	SYMBOL	DESCRIPTION
4	AS1	Active low enable
5	TXEnable	Hardware shutdown
8	SCL1	Serial clock
9	SDA1	Serial data

A serial data interface controls the programmable-gain amplifier (PGA). It has an active-low enable (AS1) to sample the data, with data clocked in MSB (D7) first on the rising edge of SCL1. Data is stored on the rising edge of AS1. The gain is determined by a 6-bit word (D5 – D0).

**Table 16 Data Register (3-Wire Bus)**

BIT	MNEMONIC	DESCRIPTION
MSB 7	D7	Software shutdown
6	D6	Test bit
5	D5	Gain control, bit 5
4	D4	Gain control, bit 4
3	D3	Gain control, bit 3
2	D2	Gain control, bit 2
1	D1	Gain control, bit 1



BIT	MNEMONIC	DESCRIPTION
0	D0	Gain control, bit 0

Setting PLL-Port 3 low shuts down the PGA. Port 3 is controlled over the I<sup>2</sup>C bus (SDA2; SCL2). Control byte 2 (P3) has to be 1 for shutdown or 0 for normal mode. Hardware shutdown overrides software shutdown (D7) and stored gain settings will be lost. In normal active mode, port 3 must be held high. To bias only the differential output-power-amp between bursts, TXEnable (Pin 5) must be held low. TXEnable must be held high for transmit mode.

Table 17 State Diagram (3-Wire Bus)

SHDN PORT 3	TXEN PIN 5	D7	D6	D5	D4	D3	D2	D1	D0	STATE
1	0	X	X	X	X	X	X	X	X	Shutdown mode
0	0	0	X	X	X	X	X	X	X	Software shutdown mode
0	0	1	X	X	X	X	X	X	X	Transmit disable mode
0	1	1	X	X	X	X	X	X	X	Transmit mode
0	1	1	X	0	0	0	0	0	0	Maximum gain – 63 dB = minimum gain
0	1	1	X	0	0	0	0	0	1	Maximum gain – 62 dB
0	1	1	X	-	-	-	-	-	-	-
0	1	1	X	1	0	0	0	0	1	Maximum gain – 30 dB
0	1	1	X	-	-	-	-	-	-	-
0	1	1	X	1	1	1	1	1	0	Maximum gain – 1 dB
0	1	1	X	1	1	1	1	1	1	Maximum gain

Preliminary

### 9.7 SERIAL INTERFACE TIMING

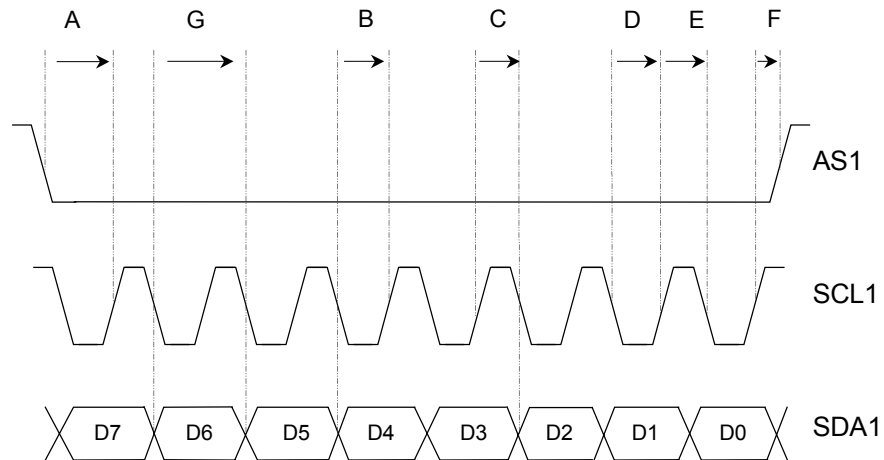


Figure 7 Serial Interface Timing



**Table 18 Timing Characteristics**

PARAMETER	SYMBOL	MIN	TYP	MAX	UNITS
AS1 to SCL1 rise setup time	A	10			ns
AS1 to SCL1 rise hold time	F	20			ns
SDA1 to SCL1 setup time	B	10			ns
SDA1 to SCL1 hold time	C	20			ns
SDA1 pulse width high	G	50			ns
SDA1 pulse width low	G	50			ns
SCL1 pulse width high	E	50			ns
SCL1 pulse width low	D	50			ns

## 10 SAFETY AND RELIABILITY

### 10.1 ELECTROSTATIC DISCHARGE (ESD) PROTECTION



**WARNING:** The 4937 DI5 Tuner Module contains components that can be damaged by electrostatic discharge.

Observe these precautions:

- Ground yourself before handling the tuner.
- Do not touch the tuner connector pins without ESD protection.

### 10.2 HIGH VOLTAGE

The tuner meets specifications IEC 801.2 level 2.

### 10.3 HUMIDITY

**Table 19 Local Oscillator Drift**

PARAMETER	DRIFT	UNIT	PROCEDURE
VHF Low	± 15	kHz	1. Run 60 hours at 55°C and 20% relative humidity. 2. Run 1 hour at 23°C and 50% relative humidity. 3. Take first measurement. 4. Run 65 hours at +40°C and 95% relative humidity. 5. Take second measurement.
VHF High	± 45	kHz	
UHF	± 75	kHz	

Preliminary



## 10.4 VIBRATION TEST

After applying vibration of 1.5 mm amplitude, frequency of 10 - 55 -10 Hz (1 minute) each X, Y, Z direction for 2 hours (total 6 hours), tuner shall not have any rattling or loosening and shall comply with the variation to its initial value as listed in Table 20.

**Table 20 Vibration Test**

PARAMETER	MEASUREMENT	UNIT
Gain variation	< $\pm 3$	dB
Wave variation	< $\pm 30$	%

## 10.5 MICROPHONY

The microphony test is made with a TV set. The resolution is optimal. With maximum AF output of the TV set, the tuner is free of microphonic effects, provided the unit is installed in a professional manner.

## 10.6 LOOSE CONTACT TEST OF TUNER ALONE

The test pattern is a color bar. The resolution is 3 MHz. To test, there must be no interruption effects when the edge of the tuner is knocked, provided it is fastened with a ground contact.

## 10.7 SOLDER LIMITS

See application note APN001.

## 10.8 NATIONAL REGULATIONS

The tuner meets the requirements of VDE 9872/7.72 and Amtsblatt DBP 069/1981 (FTZ), EN 55013, EN 55020 (if properly mounted into TV set, VCR, or converter).



**11 ORDERING INFORMATION**

The 4937 DI5 Tuner Modules may be ordered in the packaging units and quantities shown in Table 21 and Table 22. For packaging options and quantities other than those shown, contact one of the offices listed on the last page of this document.

**Table 21 Packaging Units**

PACKAGING UNITS	4937 TUNER MODELS	
	3x8899	3x7702
Number of Tuner Modules Per Box	72	72
Number of Boxes Per Master Box	40	40

**Table 22 Order Quantities**

NUMBER OF MASTER BOXES	TOTAL NUMBER OF TUNERS PER MASTER BOX	
	3x8899	3x7702
0.5	1,440	1,440
1.0	2,880	2,880
1.5	4,320	4,320
2.0	5,760	5,760
2.5	7,200	7,200
3.0	8,640	8,640
3.5	10,080	10,080
4.0	11,520	11,520
4.5	12,960	12,960
5.0	14,400	14,400

Preliminary

**12 REVISION HISTORY**

NAME	DESCRIPTION	ECN No.	DATE	REV
Hennig			24.11.00	M1
Hennig		011/01	20.02.01	01
Hennig	Change 3x7702 (3x8899) to 3x8899 (3x7702)	050/01	10.07.01	02



## NOTICES

NOTICE - The information in this document is believed to be accurate and reliable. Microtune assumes no responsibility for any consequences arising from the use of this information, nor from any infringement of patents or the rights of third parties which may result from its use. No license is granted by implication or otherwise under any patent or other rights of Microtune. The information in this publication replaces and supersedes all information previously supplied, and is subject to change without notice. The customer is responsible for assuring that proper design and operating safeguards are observed to minimize inherent and procedural hazards. Microtune assumes no responsibility for applications assistance or customer product design.

NOTICE - The devices described in this document are not authorized for use in medical, life-support equipment, or any other application involving a potential risk of severe property or environmental damage, personal injury, or death without prior express written approval of Microtune. Any such use is understood to be entirely at the user's risk.

TRADEMARKS - Microtune, MicroTuner, and the Microtune logo are trademarks of Microtune, Inc. All other trademarks belong to their respective companies.

PATENTS - Microtune's products are protected by one or more of the following U.S. patents: 5,625,325; 5,648,744; 5,717,730; 5,737,035; 5,739,730; 5,805,988; 5,847,612; 6,100,761; 6,104,242; 6,144,402; 6,163,684; 6,169,569; 6,177,964; 6,218,899 and additional patents pending or filed.

COPYRIGHT - Entire contents Copyright © 2001 Microtune, Inc.

### World Headquarters

Microtune, Inc.  
2201 Tenth Street  
Plano, TX 75074  
USA

Telephone: 972-673-1600  
Fax: 972-673-1602  
Email: sales@microtune.com  
Website: www.microtune.com

### European Headquarters

Microtune GmbH and Co. KG  
Marie Curie Strasse 1  
85055 Ingolstadt / Germany

Telephone: +49-841-9378-011  
Fax: +49-841-9378-010  
Sales Telephone: +49-841-9378-020  
Sales Fax: +49-841-9378-024

### Pan-Asian Headquarters

Microtune, Inc. - Hong Kong  
Silvercord Tower 1, Room 503  
30 Canton Road  
Kowloon, Hong Kong

Telephone: +852-2378-8128  
Fax: +852-2302-0756

For a detailed list of current sales representatives, visit our Web site at [www.microtune.com](http://www.microtune.com).

Preliminary

